PERTURBATION STUDIES IN A PLASMA CONFINED BY MULTI-POLE LINE-CUSP MAGNETIC FIELD

By

MEENAKSHEE SHARMA

PHYS06201304002

Institute for Plasma Research, Gandhinagar

A thesis submitted to the

Board of Studies in Physical Sciences

In partial fulfillment of requirements

for the Degree of

DOCTOR OF PHILOSOPHY

of

HOMI BHABHA NATIONAL INSTITUTE

March, 2021

Homi Bhabha National Institute[1]

Recommendations of the Viva Voce Committee

As members of the Viva Voce Committee, we certify that we have read the dissertation prepared by Meenakshee Sharma entitled **"Perturbation Studies in a Plasma Confined by Multi-pole Line-cusp Magnetic Field"** and recommend that it may be accepted as fulfilling the thesis requirement for the award of Degree of Doctor of Philosophy.

Chairman – Prof. P. K. Chattopadhyay	P.K.C.
Guide – Dr. N. Ramasubramanian	N Raman
Examiner - Dr. Ramesh Narayanan	Ramesh Narayanan
Member 1- Dr. Joydeep Ghosh	J Ghosh
Member 2- Dr. L. M. Awashti	L Awasthi
Member 3- Dr. Pintu Bandhyopadhyay	
Technical Advisor – Prof. Y. C. Saxena	

Final approval and acceptance of this thesis is contingent upon the candidate's submission of the final copies of the thesis to HBNI.

I hereby certify that I have read this thesis prepared under my direction and recommend that it may be accepted as fulfilling the thesis requirement.

Date: 12/Mar/2021

Place: Gandhinagar

Signature N Raman

Guide N. Ramasubramanian

[1] This page is to be included only for final submission after successful completion of viva voce.

STATEMENT BY AUTHOR

This dissertation has been submitted in partial fulfillment of requirements for an advanced degree at Homi Bhabha National Institute (HBNI) and is deposited in the Library to be made available to borrowers under rules of the HBNI.

Brief quotations from this dissertation are allowable without special permission, provided that accurate acknowledgement of source is made. Requests for permission for extended quotation from or reproduction of this manuscript in whole or in part may be granted by the Competent Authority of HBNI when in his or her judgment the proposed use of the material is in the interests of scholarship. In all other instances, however, permission must be obtained from the author.

Meenakshee Sharma

DECLARATION

I, hereby declare that the investigation presented in the thesis has been carried out by me. The work is original and has not been submitted earlier as a whole or in part for a degree / diploma at this or any other Institution / University.

मीनाक्षी

Meenakshee Sharma

List of Publications arising from the thesis

Journal

(a) Published

1. "Evidence for neutrals carrying ion-acoustic wave momentum in partially ionized plasmas", **Meenakshee Sharma**, A. D. Patel, Z. Shaikh, N. Ramasubramanian, R. Ganesh, P. K. Chattopadhyay, and Y. C. Saxena, *Physics of Plasmas*, **2020**, *27*, 022120.
2. "Role of Multi-cusp magnetic field on plasma confinement", **Meenakshee Sharma**, A. D. Patel, N. Ramasubramanian, Y. C. Saxena, P. K. Chattopadhyay, and R. Ganesh, *Plasma Research Express*, **2020**, 2, 045001.
3. "A New Multi-Line Cusp Magnetic Field Plasma Device (MPD) with Variable Magnetic Field", A. D. Patel, **M. Sharma**, N. Ramasubramanian, R. Ganesh, and P. K. Chattopadhyay, *Review of Scientific Instruments*, 2018, **89**, 043510.
4. "Experimental Observation of Drift Wave Turbulence in an Inhomogeneous Six-Pole Cusp Magnetic Field Of MPD", A. D. Patel, **M. Sharma**, R. Ganesh, N. Ramasubramanian, and P. K. Chattopadhyay, *Physics of Plasmas*, 2018, **25**, 112114.
5. "Characterization of Argon plasma in a variable multi pole line cusp magnetic field configuration", A. D. Patel, **M. Sharma**, N. Ramasubramanian, J. Ghosh, and P. K. Chattopadhyay, *Physica Scripta*, 2020, **95**, 035602.

(b) To be submitted

1. "Effect of oblique cusp magnetic field on IA wave propagation", **Meenakshee Sharma**, A. D. Patel, N. Ramasubramanian, R. Ganesh, P. K. Chattopadhyay, and Y. C. Saxena.

2. “Leak Width In A Multi-Cusp Field Configuration: A Revisit with a Versatile Experimental device”, **Meenakshee Sharma**, A. D. Patel, N. Ramasubramanian, R. Ganesh, and P. K. Chattopadhyay.

Conferences

1. “Design of Cesium Oven for a Multi-cusp Plasma Device”, **Meenakshee Sharma**, A. D. Patel, and N. Ramasubramanian, Plasma Scholar's Colloquium (PSC-2015), Kolkata, India.
2. “Design and Characterization of Cesium Oven for a Multi-cusp Plasma Device”, **Meenakshee Sharma**, A. D. Patel, and N. Ramasubramanian, Asian Plasma Fusion Association 2015, Ahmedabad, India.
3. “Study of Electron Temperature and Density in Multi-cusp Plasma Device”, **Meenakshee Sharma**, A. D. Patel, N. Ramasubramanian, and P. K. Chattopadhyay, Frontiers in Plasma Physics and Science (FPPS-2016), Ujjain, India.
4. “Imaging of Argon Plasma in Multi Cusp Plasma Device”, **Meenakshee Sharma**, A. D. Patel, N. Ramasubramanian, and P. K. Chattopadhyay, Plasma Science Society of India (PSSI-2017), Gandhinagar, India.
5. “Study of Effect of Multi-line Cusp Magnetic Field on Plasma Parameters”, **Meenakshee Sharma**, A. D. Patel, N. Ramasubramanian, and P. K. Chattopadhyay, Plasma Science Society of India (PSSI-2017), Gandhinagar, India.
6. “Effect of multi-line cusp geometry on confined plasma parameters”, **Meenakshee Sharma**, A. D. Patel, and N. Ramasubramanian, 28th Symposium Plasma Physics and Technology (SPPT-2018), Prague, Czech Republic.

7. "Study of propagation of ion acoustic soliton in multi-cusp plasma", **Meenakshee Sharma**, A. D. Patel, N. Ramasubramanian, 45th European Physical Society Conference on Plasma Physics (EPS-2018), Prague, Czech Republic.
8. "Study of Ion Acoustic Wave in Inhomogeneous Magnetic Field of Multi-cusp Plasma Device", **Meenakshee Sharma**, A. D. Patel, N. Ramasubramanian, 2nd Asia-Pacific Conference on Plasma Physics (AAPPS-DPP 2018), Kanazawa, Japan.
9. "Leak Width in A Multi-Cusp Field Configuration: A Revisit with a Versatile Experimental device", **Meenakshee Sharma**, A. D. Patel, N. Ramasubramanian, R. Ganesh, and P. K. Chattopadhyay, 27th IAEA Fusion Energy Conference (FEC 2018).

Meenakshee Sharma

त्वदीयं वस्तु गोविन्दः तुभ्यमेव समर्पये

ACKNOWLEDGEMENTS

This thesis has been kept on track and been seen through to completion with the support and encouragement of numerous people, friends, well-wishers and colleagues. At the end of my thesis, I would like to thank all those people who made this thesis possible and an unforgettable experience for me. First of all I would like to express deep gratitude to my thesis supervisor, Dr. N. Ramasubramanian for his guidance, encouragement and gracious support throughout this research work. I am eternally grateful to him for his supportive and friendly nature. His constant encouragement, critical comments were really boosting my interests and made me to explore in new directions as well. I admired and learned the art of precise expression of ideas, patience to listen from him. I specially thank him for the freedom that he has given me to do research and his availability for discussion at any time. I am thankful to him for encouraging me during difficult personal circumstances and remembering these moments, words fail me in thanking him for his support.

I am also thankful to Prof. Y. C. Saxena, he has always been there to listen and give advice. His insightful comments and constructive criticisms at different stages of my research were thought provoking and they helped me focus my ideas. I humbly appreciate their motivating ideas and fruitful discussions.

I want to acknowledge my Doctoral committee chairman Prof. P. K. Chattopadhyay and members, Dr. Lalit Mohan Awasthi, Prof. R. Ganesh, Dr Joydeep Ghosh, and Dr. Pintu Bandhopadhyay whose help and sympathetic attitude at every point during my research helped me to work in time. I would like to express my warm thank to late Prof. P. K. Kaw and Prof. S. K. Matoo for their ideas, help and support in initial stage of my PhD.

I would also like to thank Prof. S. K. Mattoo, Prof. Y.C. Saxena, and Prof. A. Sen for their special lectures. These lectures have introduced me to the advances of plasma physics covering the domains of theoretical, simulation and experimental realization of plasma physics. I am also grateful to other faculty members Prof. R. Ganesh, Dr. S. Sengupta, Dr. M. Ramasubramanian, Dr. R Goswami, Dr. M. Kundu, Dr. A. K. Chattopadhyay, Dr. V. P. Anitha, and others, who have taught me during the pre- Ph.D. course work.

It is my pleasure to thank Dr. AmitKumar Patel, a colleague and senior, we worked, discussed and argued together. He helped me to understand various technical and physical aspects of several diagnostics developed and used in MPD.

There were several instances during the experimental or other activities, when I needed equipment or information. I always got warm support from my colleagues in the BETA lab, Basic lab and MEL lab, Umesh, Zubin, Sayak Bose, Hirel, Pankaj, Amulya, Ganguli, Priya Vandana, Surabhi, Garima, Lavkesh, Manu, Yeole, Pratibha, Raval, Bhoomi, Neeraj, Sonu. I would like to convey my sincere thanks to all of them.

I am also grateful to a staff members from the workshop, stores, electronics lab, computer centre, library, purchase section, administration, drafting section, air and water cooling section, canteen and security at Institute for Plasma Research for their co-operation and help during the entire duration of my PhD. I would like to thank Mr. Pankaj Shrivatava for the invaluable help in designing and developing the necessary electronic circuits, he not only helped me but also taught me every small parts and working of circuits. I would like to thank Mukesh and Rajni for working with me to make and install Multi-pole line cusp plasma Device.

I am greatly thankful to my seniors and friends in the hostel for their unconditional support and company. My warm regards to Aswin, Soumen, Sayak, Aditya, Sanat, Kshitish, Deepak, Ujjwal, Manjit, Gurudatt, Vikram Sagar, Satya, Rameswar, Sushil, Pravesh, Vikram Dharodi, Veda Prakash, Rana, Sandeep Rimza, Dushyant, Vara, Bhibhu, Neeraj, Roopendra, Chandrashekhar, Mangilal, Vidhi, Akanksha, Deepa, Meghraj, Harish, Samir, Narayan, Sonu, Debraj, Umesh, Ratan, Amit, Surabhi, Bhumika. I am very much thankful for my batchmates Alam, Atul, Jervis, Deepak, Chetan, Sagar, Sandeep, Harshita, Pallavi, making this journey so fabulous and enjoyable. My special thanks go to Hiral, Sneha and Roopendra da to stand with me all the time. I heartily thanks to Pallavi and Deepa ma'am, for being here as a close friend to listen to me, the time spend with them always comforted me and widen my horizons. I am also very much thankful to all my juniors, Shivam, Avanish, Rupak, Arun, Neeraj, Garima, Srimanta, Mayank, Devshree, Nidhi, Ayushi, Swapanali, Pawandeep, Satadal, Sanjeev, Tanmay, and other scholars and TTPs for taking me to grow with you all together in IPR hostel, a delightful natural ambient inside the campus.

Family is kind of backbone in a person's life so at last I would like to thank, my family. I am greatly indebted to my parents, especially to my father, for their unconditional love, support, motivation and everything in my life. They are the reason, whatever, I am today. I would like to thank my younger sister Niru for her unconditional love and support, my younger brother Pawan, it was delightful to see him as grown up responsible son and brother. I specially want to thank my younger sister Sandhya and brother-in-law Karunakar for taking the responsibility of an elder and because of their support; I could focus on PhD without worrying about my family. In the end, I would like to thank Prabhakar, for being a supportive friend and family member, who always stands with me, criticized and encouraged me. Without him I might not have been completed the PhD.

Contents

List of Figures

List of tables

Chapter 7

Conclusion and Future Scope

Surprises are galore when quiescent plasma is perturbed by a small periodic voltage. Usually it is desired to have perturbations to be periodic as well as to be small enough so that the basic characteristics of plasma are not changed irreversibly. The achievable quiescence level in plasma is very important to start with. Because it would be easy to track the effect of those perturbations, if the agitations/fluctuations are too small before the perturbation. Though it is very hard to achieve quiescent plasma, to improve it further is quite demanding. The invention and development of the Q-machine in the early 1960s changed the experimental landscape by providing a quiet plasma source. Further studies took advantage of a major improvement in low temperature plasma sources. Multi-pole cusp configuration is believed to be an ideal configuration in which the field is B~0 in the center, as well as the boundary field curvature is also good for the plasma confinement [32,35,154,156,176–178]. In 1973, Limpaecher and Mackenzie [32] developed a multi-dipole plasma device and produced extremely quiet plasma. They surrounded unmagnetized plasma with a multi-dipole magnetic field created by permanent magnets with alternating polarities facing the plasma. Plasma confined in this multi-dipole cusp magnetic field geometry resulted in uniform, quiescent plasmas with density fluctuations $(\delta n/n) \approx 0.03\%$.

7.1 Summary and Conclusions

The Multi-pole line cusp Plasma Device (MPD) [58,67,142] is described in detail. It contains a main cylindrical chamber of 150 cm length, 40 cm diameter, and 0.6 cm wall thickness and it is used for all experiments presented in this thesis. The whole chamber is pumped down to a pressure 10^{-6} mbar using a Turbo Molecular Pump (TMP) backed by a rotary pump, while a combination of the Ionization and Pirani gauges are used for pressure measurement. The Argon gas is filled for plasma production. The plasma discharge is created between a 2D vertical array of tungsten filament-based cathode source and grounded chamber wall. The filamentary source is centered at R=0 cm, field free region of cusp magnetic field. The emphasis is given on the development of diagnostics. The major contributions are namely, the development of 1) single Langmuir probe and its measurement circuits, 2) probe array for the azimuthal measurement, 3) directional probe to measure the IA wave propagation, 4) Emissive probe for the measurement of plasma potential (ϕ_p), and 5) Mach probe for plasma flow velocity and flux measurement. The techniques used for measurements, method of operation, and estimation of local plasma parameters are discussed. Some MATLAB routines are written for processing the Langmuir probe I-V characteristics to estimate the mean plasma parameters and for frequency power spectrum to analyze the fluctuations data obtained.

In MPD, the magnetic field to confine the plasma is produced using six electromagnets integrated with profiled core material to mimic permanent magnets, but the pole strengths can be varied by varying the current [58,67,142]. The filamentary produced argon plasma confined in this device is found to be very quiescent (<0.1%). This is expected due to the good curvature of the plasma, which is the center of curvature of the confining field is outside the confined volume. With this setup, it would be prudent to study the reaction of the quiescent plasma to small perturbations.

In a quest for more quiescent plasma, experiments were done in the MPD set up with various configurations of line-cusp fields by changing the current direction in the electromagnets appropriately. In one of such configurations, 12 poles could be produced using the six electromagnets. This is achieved by making all the magnets of same pole type by passing current in the same direction in all six magnets. The six virtual poles in between those magnets add to give 12 pole cusps. The plasma confined in this twelve pole with six magnets (TPSM) is rigorously compared with that of produced by the six poles with six magnets (SPSM) with same current in both configurations. Various plasma parameters such as plasma density, electron temperature, plasma potential, floating potential, plasma quiescence level, and axial plasma flow is compared for these two cusp configurations. Plasma parameters are measured using Langmuir probe, emissive probe, and Mach probe. The plasma confined in TPSM has larger field free volume (cylindrical volume of radius $\sim$ 10 cm and length 100 cm) than SPSM (cylindrical volume of radius $\sim$ 4 cm and length 100 cm) because of the geometrical sizes of the magnet. The peak density (typically $2 \times 10^{16} \backslash m^3$ at R=0 cm) and temperature value (typically 4.5 eV at R=0 cm) of the plasma is found to be nearly the same in both configurations. But the radial extend of plasma with nearly flat density is found to be larger in TPSM (radius of $\sim$ 10 cm) compared to SPSM (radius of $\sim$ 4 cm), thus providing a larger volume of plasma with nearly flat density in the field free region. The net axial plasma flow (V_d/C_s), measured using the Mach probe is found to be negligible < $0.1C_s$ at the centre of the device for both cusp configurations. As we move radially outboard the axial flow increases in SPSM (it is 0.3 C_s at R=10 cm) and while for TPSM it is negligible <$0.02C_s$ throughout the radial extent. The absence of both density gradient and field free region along with negligible axial flow makes the plasma to be more quiescent and uniform as well in TPSM. The presence of uniform plasma upto about a radius of ~10 cm and, absence of drift wave modes, negligible axial flow and absence of reasonable fluctuations makes TPSM the ideal plasma background to excite any wave mode or perturbation. Because of this, TPSM is selected to do perturbation studies in the field free region.

For perturbing the plasma with periodic voltage pulses, the range of Ion-Acoustic frequencies are selected, since they are the well documented frequency ranges and to see how the waves behave for the different levels of ionization. When the frequency of the perturbing voltage is low much below the ion–plasma frequencies, (ω_{pi}) the ions form regions of compression and rarefaction just as in ordinary sound waves [21]. While the compression is due to the perturbing voltage, the rarefaction is due to the ion thermal motions as well as imperfect shielding by the thermal energy of the electrons and the wave propagates with both the electrons and ions oscillating almost in phase.

To launch IA waves, a grid of 5 cm diameter (< 20 cm diameter of uniform field free plasma in TPSM) is placed inside the vacuum chamber with outside controls through appropriate vacuum interfaces. The plane of the grid is kept normal to the z-axis, 65 cm away from the plasma source at middle plane of the device, z=75 cm. The IA wave is usually launched below ion plasma frequency($\omega_{pi}/2\pi, \omega_{pi} = \sqrt{n_e e^2/\epsilon_0 m_i}$). In this experiment, a window of operating argon gas pressure range has been varied from 2×10^{-4} mbar to 30×10^{-4} mbar which gives a plasma density (n_e) in the range $1.5 \times 10^{15} - 3 \times 10^{16}$ m^{-3}. For this background plasma condition, the ion plasma frequency $\omega_{pi}/2\pi$ varies from $1.3 \times 10^{6} - 5.8 \times 10^{6}$ Hz. Therefore, the frequency of the IA wave propagation has been chosen to be 10^5 Hz and the nature of perturbation is sinusoidal with appropriate perturbation potential. The perturbation potential is chosen such that it penetrates the sheath voltage appeared across the exciter grid and can make the fluctuations in plasma density. The propagation of this potential perturbation / IA wave is recorded at different axial locations using a movable receiver directional probe (of 8 mm diameter) away from the exciter grid (moving opposite to the plasma source) up to 20-30 cm. The basic characteristic of IA wave in plasma are also described in detail. The dispersion relation of IA wave, experimentally obtained $\omega - k$ curve shows a straight line as theoretically predicted. The phase reaction between perturbed normalized density and perturbed plasma potential normalized with electron temperature, demonstrates the same phase behavior as described for IA wave. The frequency spectrum of ion-saturation fluctuation shows a sharp peak at 100 kHz when the IA wave of 100 kHz is excited in plasma. The IA wave is also excited with various perturbation voltages to ensure the absence of pseudo-waves in plasma along with IA wave. The IA wave propagation in plasma depends on many factors and properties of plasma, and there are various mechanisms to damp such as, Landau damping, damping due to geomertical spread of wave packet, collisional damping or gas damping, damping due to plasma density gradient, two-electron temperature, magnetic field obliqe to propagation of wave, which are all discussed in detail.

While the Ion acoustic waves have been mostly observed to be propagated by the charged particles, the role of the neutral particles has been reported only to dampen the wave [89,91,104,105], for the regime where, ion-neutral collision frequency (ν_{in}) is greater than the ion-acoustic wave frequency ω ($\nu_{in} > \omega$). The versatility of the MPD makes it possible to set the wave frequency and the ion-neutral collision such that $\omega \geq \nu_{in}$. When the IA wave excited with this condition and without any applied magnetic field, it is observed that the neutral particles are carrying part of the wave momentum, thus helping the wave propagation. The experimental results show that, for a given perturbation magnitude of said frequency, the observable propagation length of IA wave increases with the neutral density. The propagation length is the distance from the grid to the point along the z-axis, where the wave amplitude ($\delta n/n$) signal is distinctly above the detection level. This phenomenon of neutrals carrying IA momentum has been observed in the pressure window of 2×10^{-4} mbar to 30×10^{-4} mbar in MPD without any magnetic field. While the propagation length for 2×10^{-4} mbar is around 5.8 cm, it is more than 14 cm for $30 \times$

10^{-4} mbar of gas pressure. The increase in neutral density leads to an increase in the ion-neutral collision frequency, thus decreasing the ion-neutral collision mean free path. When a perturbed ion imparts momentum to a neutral in a wave front, the neutral in-turn gives the momentum further to another ion /neutral traversing the mean free path. If the next wave front is present within that mean free path, the momentum is carried forward one wave front to another. This is possible when the wavelength of the IA wave and the ion-neutral collision mean-free path are comparable. For the experiments presented here, the two lengths are comparable and hence the wave momentum is carried forward for longer distances. This is the first time this observation has been reported. The wave amplitude ($\delta n/n$) is also found to increase with the increase in the background neutral pressure.

In these experiments, the IA is launched in the field free region where the ions are unmagnetized. Hence the IA propagation is expected not to be affected by the magnetic field in the cusp regions. But since the electrons also participate in the IA wave propagations and the cusp magnetic field affects them. Hence there is a need to study the effect of the cusp magnetic field on the propagation of IA waves. Since the MPD experimental set up has electromagnets, the studies on the effect of cusp magnetic field on the propagation of IA waves have been taken up. For this, many IA wave experiments are studied with varying field values at the cusp region. It is observed, as the cusp magnetic field strength increases from 10G – 300 G, after a certain value of cusp magnetic field (certain current value in electromagnets), the IA gets heavily damped, and its propagation ceases to exist in plasma. Since the cusp magnetic field has r and θ component of the magnetic field no z-component is present in this configuration and the wave excited at a perpendicular to the field lines, along the z-axis. The oblique nature of cusp magnetic field restricts the free motion of electrons along the wave propagation and the restoring force provided by electrons becomes weak. As the cusp magnetic field strength increases the wave propagation ceases away in absence of the required restoring force. Another reason of heavy IA wave damping with cusp magnetic field can be presence of two temperature electron specie. Since the cusp magnetic field confines hot primary electrons by mirror effect, the increase in the cusp field value alters the local plasma parameters before the wave is even launched. Hence, the exact segregation of data for comparisons with different cusp field values is not possible. To do this, more diagnostics and control are needed to keep as much as variables (plasma parameters) constant and allow the rest to change for said studies.

7.2 Future Work

The future work primarily aimed for the better understanding of IA wave damping with increasing cusp magnetic strength, it needs further more detail experiments. The thesis work can be extended for the following research work;

- In this thesis we have discussed the excitation of IA eave at R=0 cm along z-axis, so this study can be extended to the wave excitation at some other radial locations like R=10 cm along z-axis and observe the effect of curvature of magnetic field IA wave. It is a plan of future research in MPD. As reported in literature it is expected that we can have an IA wave in z-axis, and in radial direction we can observe an Ion-cyclotron wave as well.
- The IA wave solitons can be excited in the field free regimes of cusp magnetic field. The effect of variation of pole magnetic field (magnet current in coils) on IA solition properties can be studied.
- Interaction of two IA wave solitons in the field free regimes of cusp magnetic field and effect of cusp strength variation on their interaction can also be studied. This study is being carried out presently in MPD.

- Apart from electrostatic IA wave, electromagnetic waves can also be excited and studied in MPD plasma.

Summary

The thesis is summarized as follows:

- Perturbation studies need field free and quiescent plasma because the presence of magnetic fields triggers Drift waves, many other instabilities, and fluctuations.
- Plasma confined in Multi-pole line-cusp magnetic field has field free region. This region is characterized in this thesis and found to be quiescent as well.
- In a quest for more quiescent plasma, experiments were done with two different configurations of the Multi-pole line-cusp field using the electromagnets of the device.
- The Twelve Pole Six Magnet (TPSM) configuration is identified to confine the larger volume of quiescent and uniform for perturbation study in Multi-pole line-cusp Plasma Device (MPD).
- The Ion Acoustic (IA) wave is successfully exited in MPD; its basic characteristics and dispersion relation is established and validated experimentally.
- The effect of neutrals on IA wave is observed to enhance the propagation length of IA wave as with increasing neutral density, the neutrals also carry the momentum of IA wave and help in the increase in propagation length.
- The experimental result of effect of cusp magnetic field on the IA wave propagation is presented. The role of oblige cusp magnetic field and two electron temperature on wave damping with increasing magnetic field strength is discussed.

Chapter 1
Introduction

Structured systems have binding energies larger than the ambient thermal energy. Placed in a sufficiently hot environment, they decompose. At temperatures exceeding atomic ionization energies, atoms decompose into negatively charged electrons and positively charged ions. These charged particles are strongly affected by each others' electromagnetic fields. Nevertheless, because the charges are no longer bound, their assemblage becomes capable of collective motions of great vigor and complexity. Such an assemblage is termed as plasma. Plasmas resulting from ionization of neutral gases generally contain equal numbers of positive and negative charge species. The oppositely charged particles are strongly coupled, and tend to electrically neutralize one another on macroscopic length-scales. Such plasmas are termed quasi-neutral.

The 95% of the baryonic content of the Universe consists of plasma such as stars, nebulae, interstellar space, the solar system in the form of the solar wind, and the earth ionosphere are filled with plasma. Although naturally occurring plasma is rare on earth (e.g. a lightning strike) but there exists a long list of man-made plasmas such as sparks, arcs, fluorescent lamp, plasma torches, plasma-displays, plasma thrusters, fusion plasmas etc.

1.1 Brief History of Plasma

Irving Langmuir first used the word plasma to describe an ionized gas in 1927. Langmuir and Tonk were investigating the physics and chemistry of tungsten-filament light-bulbs. In the process, they discovered various plasma phenomena such as plasma sheath and plasma oscillations and developed theories also. After Langmuir, plasma research gradually spread in many directions, of which five are most significant, 1) Earth ionosphere: development of radio broadcasting theory of EM waves propagation through non-uniform magnetized ionosphere. 2) Astro Physics: The pioneer in this field was Hannes Alfven, who developed the theory of magnetohydrodynamics (MHD) in 1940. The two topics of particular interest in MHD theories are magnetic reconnection and dynamo theory. 3) Controlled thermonuclear fusion: The development of hydrogen bomb in 1952 leads scientists' interest towards controlled thermonuclear fusion as a promising power source for the future. 4) Van Allen's belt: Discovery of Van Allen's belt in 1958 leads to space plasma physics. 5) High power lasers: The development of high-power lasers in 1960 led to laser plasma physics and inertial confinement fusion.

Plasma is complex temporally and spatially, characterized by the excitation of an enormous variety of collective dynamical modes. Plasma deals with the complex interaction of many charged particles with external or self-generated electromagnetic fields. Which leads to the motivation of this thesis.

1.2 Motivation of Thesis

Plasma, if not confined is subject to losses over a period of time. Even after the confinement (like applying external magnetic field), plasma loss is an ubiquitous phenomenon prevalent in the laboratory, space, and astrophysical systems [1–3]. It continues to remain a core problem for magnetically confined fusion plasmas [4–7]. It hence motivates us to continue the efforts in theoretical, computational and experimental investigations to develop the better understanding of the physical phenomena responsible for the loss of plasma particles. The losses are mostly due to the presence of fluctuations excited in the plasma system and/or various instabilities which are inherently present in the system. These fluctuations can be of electrostatic and or electromagnetic nature [8–12].

In plasma, any source of free energy can drive fluctuations and instabilities. Therefore, plasmas are unstable to the slightest of perturbations. The understanding of the plasma response to a controlled repetative perturbation is the main ingredient of this thesis work.

Desirable features of the plasma for perturbation studies are listed as follows:

a) **Uniformity**: Radially and axially uniform plasma with radius of the uniform plasma greater than equal to the wavelength of the wave to be excited is preferred.

b) **Reproducibility**: The plasma should exhibit the same physical characteristics under the identical operating conditions. This is a necessity for studying the different aspects of the wave phenomena in a controlled manner.

c) **Quiescence**: Ideally, one would require plasma with background fluctuation level $\delta n_{noise}/n$ much less than the perturbation level that is going to be excited. The quiescence level in plasma is most important for perturbation studies.

1.3 Quiescent Plasma

The suitability of a plasma source has been judged, keeping in mind the required plasma features as described in the previous section. In order to identify a potential plasma source for carrying out the proposed experiments for perturbation study, a number of laboratory plasma sources such as DC glow discharge, Radio frequency (RF) discharge, electron cyclotron resonance (ECR) discharge, contact ionization discharge, and multi-filamentary discharge have been reviewed.

1.3.1 Q-Machine

In the Q machine, plasma is produced by contact ionization [13] of an alkali earth metal vapour on a hot metal plate, and in this way, both electrons and ions have the same temperature as that of the hot plate ~ 0.2 eV. Plasmas over a wide range of densities [14–

17] $10^{7} - 10^{13}\ cm^{-3}$ have been produced in Q machines. The plasma produced by contact ionization is mostly fully ionized and radially uniform. Long plasma column (> 1 m) can be easily produced by confining the plasma using an axial magnetic field. The plasma produced in Q machines is generally very quiescent as most of the free energy sources which can excite instabilities are avoided. In Q-machine, drift wave turbulence [18–20] is observed in presence of an axial magnetic field. In the presence of drift waves, we will not be able to understand the plasma response purely due to the imposed perturbation.

The desired plasma should be as quiescent as in a Q-machine but without a magnetic field to avoid self-excited wave modes and instabilities in the plasma. However, the external magnetic field cannot be avoided, as it is essential for plasma confinement. In this context, cusp magnetic field configuration comes into the picture, where the central region of the magnetically confined plasma has $B = 0$ value.

1.3.2 Multi-dipole devices

An External Magnetic field, in the confinement of laboratory plasmas has several causes, from thermo-nuclear fusion [21,22] to fundamental plasma studies to the field of plasma applications. Many different geometries of the magnetic field are tried for plasma confinement for several decades. Of particular interest is the cusp magnetic configuration, in which the centre of the radius of curvature of the magnetic field lines is outside the confined region. Confined plasma is virtually free from the magnetic field [23]. The cusp configuration has nearly zero magnetic field (null field) in the centre of the confining region and the maximum magnetic field at the magnet poles. In this configuration, the centre of curvature of the confining magnetic field does not exist in the region of confined plasma. The plasma confined is in the good curvature region of the magnetic field [24]. The principal advantage of cusps confinement systems is MHD stability.

Initially, the cusp Magnetic field was proposed for plasma confinement in thermonuclear fusion [25–30]. Cusp magnetic field have various geometries like Spindle-cusp [27], Picket-fence cusp [31], Spherical cusp [28], multi-dipole cusp [32] etc. The principle of plasma confinement by magnetic "wall" originated with the fusion effort, where some large devices use multipole orders up to the octopole [33]. For confinement studies a multipole device described by Sadowski [34] uses a spherical arrangement of 32 electromagnets. The multipole principle, however, has apparently not been applied to the problem of containment of large volume quiescent uniform plasma for basic studied in plasma physics. Such fields are found to reflect ions and electrons in these ordinary laboratory discharge plasmas to such extent that ionizing source requirements are reduced by three orders of magnitude [32].

These low temperature discharge devices employing multi-pole cusps have been studied since 1973, when R. Limpaecher and K. R. MacKenzie [32] first showed that they could be used to confine large volume, uniform, and quiescent plasmas with densities much higher than other linear plasma devices. Limpaecher and Mackenzie [32] developed a multi-dipole plasma device and surrounded unmagnetized plasma with a multi-dipole magnetic field created by permanent magnets with alternating polarities facing the plasma. Plasma confined in this multi-dipole cusp magnetic field geometry resulted in uniform, quiescent plasmas with density fluctuations $(\delta n/n) \approx 3 \times 10^{-4}$. The confinement of primary electrons is the dominant factor in the large increase of plasma densities. Multidipole device represents an improvement in plasma density over conventional devices (linear cylindrical devices with axial magnetic field) by about a factor of 10, whereas the direct density measurements in the steady state at 5×10^{-6} Torr indicate an improvement by about 1000. Presumably this difference is due to the increased electrostatic confinement for ions in the steady state, and an increase in the plasma production by a factor of 2-3 [32]. The plasma lost to the wall is shown to present a minimum for a certain magnet space [35]. Plasma confinement by three different cusp geometries has been studied by Lenug et al. and full-line cusps have been shown to give the highest plasma density [36] and maximum confinement of hot electrons [35,37].

The multi cusp magnetic field is widely used in plasma ion sources [26,38–40] and reported as very promising candidates for the production of intense uniform ion beams, used in fusion plasmas. Cusp configuration is also used in ion thruster, which is suited for deep space missions and orbit station-keeping for satellites due to their high efficiency and long life time [41].

The Multipole uniform and quiescent plasmas are widely employed in several applications including particle sources [42–44], plasma deposition [22,45], plasma implantation [46], plasma etching [47], production of precursors [48], plasma wall interaction for material selection for plasma facing component in ITER [49], and thermonuclear fusion due to the favorable magnetohydrodynamic stability [25,34,50,51] etc. Radial and axial uniformity in plasma parameters plays a crucial role in the above mentioned applications of plasma. As discussed by Mukherjee and John [45], the larger the volume of uniform plasma is produced, the larger size of material for plasma implantation can be used and more uniform distribution can be achieved.

Optimization of the number of poles (magnets) and cusp configurations in multipole cusp magnetic field has remained a topic of research ever since this configuration has been proposed. It includes various motivations, to achieve the maximum confinement of hot electrons [52–55], minimize the plasma loss along cusp lines [56–58], vary the field free volume [57,59,60] etc.

The plasma leak is crucial in the cusp magnetic field since it governs the efficiency of the confined plasma [61]. Lots of plasma containment studies through magnetic cusp focused on quantifying the leak width at the magnet pole have been performed [52,62–66]. The exact scaling for the amount of plasma leaking is not well known, though many scaling exists ranging from ion gyro-radius (ρ_i) to electron gyro-radius (ρ (ρ_e) to hybrid gyroradius ($\sqrt{\rho_e \rho_i}$).

The Multi-pole line cusp Plasma Device (MPD) has adopted cusp magnetic field geometry for plasma confinement, produced using six electromagnets. Electromagnets facilitate the production in a MPD of various cusp geometries and a wide range of magnetic field strength. Patel et al. [67] discussed the versatility of the MPD system, like controlling the number and position of null regions, varying the high beta volume, controlling the number of poles, varying the cusp configurations etc [67,68]. The experiments addressed in rest of the thesis are performed in MPD.

1.4 Plasma Perturbation

Plasma supports several modes, and understanding of these various modes is crucial for understanding of basic plasma physics. Plasma oscillations are one of the fundamental modes of plasma and it is observed when the plasma is perturbed locally. In the presence of finite temperature, these oscillations propagate and constitute a wave.

1.4.1 Ion Acoustic Wave

Ion acoustic (IA) waves are low-frequency pressure waves in plasma. If the ion plasma frequency (ω_{pi}) dramatically exceeds the wave frequency, both the electrons and ions oscillate almost in phase. IA wave is a longitudinal wave. In the propagation of ion waves, electrons provide the restoring force for ion inertia. Some of the characteristics of the ion waves are similar to those of ordinary sound waves; therefore, they are called Ion Acoustic

Waves (IAW). In 1929, Lewi Tonks and Irving Langmuir provided details of their experiments on oscillations in plasmas as well as a derivation of the phase velocity of ion-acoustic waves associated with the oscillations [69]. In 1933, J. J. Thomson provided a derivation of ion-acoustic waves from ion fluid equations and the Boltzmann relation for electrons . Thomson's derivation has been the basis of all fluid derivations of ion-acoustic waves ever since. The first measurements of standing waves were reported by Revans [70] in 1933 four years after the prediction of IAW. Direct observations of propagating ion-acoustic waves took 33 years, and it was reported by Wong et al. [71] in the Q machine in 1962. Excitation of IAW and their propagation in plasma has been studied by many researchers in past decades [72–81]. Several other phenomena of IAW, like diffraction [82–84], reflection [85,86], and damping [71,87–91] of the wave, have also been topics of attraction for many researchers over the years.

Ion acoustic wave frequency, wavelength, and phase velocity data have been the basis of valuable plasma diagnostics. In single species plasmas with cold ions of known mass, IA wave phase velocity provides the electron temperature, T_e. The phase velocity of IA waves provides a simple alternative to measure the relative ion concentrations of two ion species in plasma [92]. Negative and positive ion plasmas are another example of two ion species plasmas for which IA waves can provide ion number density ratios [93–96]. In the presence of plasma drift, the IA phase velocity provides a technique to determine the drift velocity in sheath-presheath plasma [92,94,97,98].

The Ion-acoustic (IA) wave has been observed in astrophysical plasmas also like, solar wind [99], Saturn ring [100], Comets, Neutrinos [101,102], Magnetosphere as well as in fusion plasmas. IA wave has also been used as a diagnostic tool for plasma studies [73,103]. After many decades when Langmuir and Tonk [69] first identified this IA wave, it is still an evolving and exciting subject. However, the interaction of neutral particles with plasma species in IA wave propagation has not been sufficiently addressed in research community. A very few works reported on the effect of neutral collisions on ion-acoustic wave propagation argued the strong damping of wave for higher neutral collisions [104,105]. Those studies are based on the condition of $\omega < \nu_{in}$, where ω is ion-acoustic mode frequency and ν_{in} is ion-neutral collision frequency.

Neutrals are an important component of plasma; planetary ring system, asteroid zone, comets, Magnetosphere, and the low-attitude ionosphere are a few examples of weakly ionized plasma in the space environment. In most of the laboratory plasmas, the influence of neutrals can be observed. The application of gas puffing or gas modulation as plasma diagnostic is recognized as a powerful tool in Tokamaks to determine the neutral density or neutral density fluctuations [106,107]. The use of energetic neutral atom (ENA) imaging to remotely study various global plasma objects in space [108–114] are few mentions. The influence of the neutral is very complex, and the details are not known yet.

Since the study of influence of neutrals on plasma phenomena is a useful to understand better partially ionized plasmas, therefore, in partially ionized plasma, the role of neutrals in IA wave propagation is explored in this thesis.

The experiments are performed in Multi-pole line cusp Plasma Device to explore the effect of neutral on IA wave propagation for $\omega \geq \nu_{in}$. The observations suggest that the collisions can support the wave to propagate for longer distances for high neutral pressure, contrary to other reported work [89,91,104,105].

1.5 Scope and Outline of the Thesis

This thesis is organized in seven chapters, briefly described in the following text.

Chapter-1: *Introduction and Motivation*. Detailed literature survey and current status of the research work on perturbations in quiescent plasma is presented in this chapter, followed by the motivation of the thesis.

Chapter-2: *Experimental Setup and Diagnostics.* In this chapter, the Multi-pole line cusp Plasma Device (MPD) has been described in detail. The emphasis is given on the development of diagnostics. The major contributions are namely, the development of 1) single Langmuir probe and its measurement circuits, 2) probe array for the azimuthal measurement, 3) Triple probe to measure the real time fluctuation of electron temperature, 4) Emissive probe for the measurement of plasma potential (ϕ_p), and 5) Mach probe for plasma flow velocity and flux measurement. The techniques used for measurements, method of operation, and estimation of local plasma parameters are discussed in detail.

Chapter-3: Plasma characterization in different cusp configurations. In this chapter, we discuss the investigations of plasma characterization in two different cusp configurations namely Six Pole Six Magnets (SPSM) and Twelve Pole Six Magnets (TPSM) cusp configuration. The radial variation in plasma parameters, as well as their dependence on experimental conditions are discussed here.

Chapter-4: *Basic Ion Acoustic Wave Perturbation*. In this chapter, after a brief about the requirements for a reasonable potential perturbation characteristics of the IA wave, like the frequency, the voltage magnitude, the voltage required for overcoming the sheath etc. have been given. Then the IA wave exciter used in MPD and its essential characteristics like the size and opacity of the exciter grid, etc. have been given in detail. The IA wave exciter circuit and signal receiver directional probe are also added in this chapter. The basic launching and detection and the method to infer the required information like wave velocity, propagation length etc. are given here.

Chapter-5: *Role of Neutrals in IA Wave Propagation*. In this chapter, the results related to the role of neutrals in IA wave propagation are discussed in detail with the required physics to understand the phenomena.

Chapter-6: *Effect of Cusp Field on IA Wave Propagation*. In this chapter, the observed effects of cusp magnetic field on the propagation of IA wave in the field free central region are given in detail along with possible physics explanations and the shortcoming for a complete understanding.

Chapter-7: *Conclusions and Future Scope*. The thesis is concluded with the observations and experiments performed with future work. **The future work** primarily aimed for the better understanding of IA wave damping with increasing cusp magnetic strength, it needs further more detail experiments.

Chapter 2

Experimental Setup and Diagnostics

The device was developed to investigate the basic physics of plasma confined in a cusp magnetic field geometry. This experimental device has been designed and fabricated to study the space plasma physics (viz. magnetic reconnection, magnetosonic waves), plasma turbulence in inhomogeneous magnetic field, ion acoustic wave, soliton wave interaction, electron plasma wave, Landau damping, non-linear coherent structure, wave-particle trapping and un-trapping etc. in a quiescent plasma. In this Chapter, the Multi-pole line-cusp Plasma Device (MPD) is described. The details of the vacuum vessel, plasma source, production, diagnostics developed, and measurement methods are discussed.

2.1 Vacuum Chamber

The vacuum vessel of **M**ulti-pole line cusp **P**lasma **D**evice (MPD) [67,68,115] is made up of non-magnetic stainless steel (SS-304L).

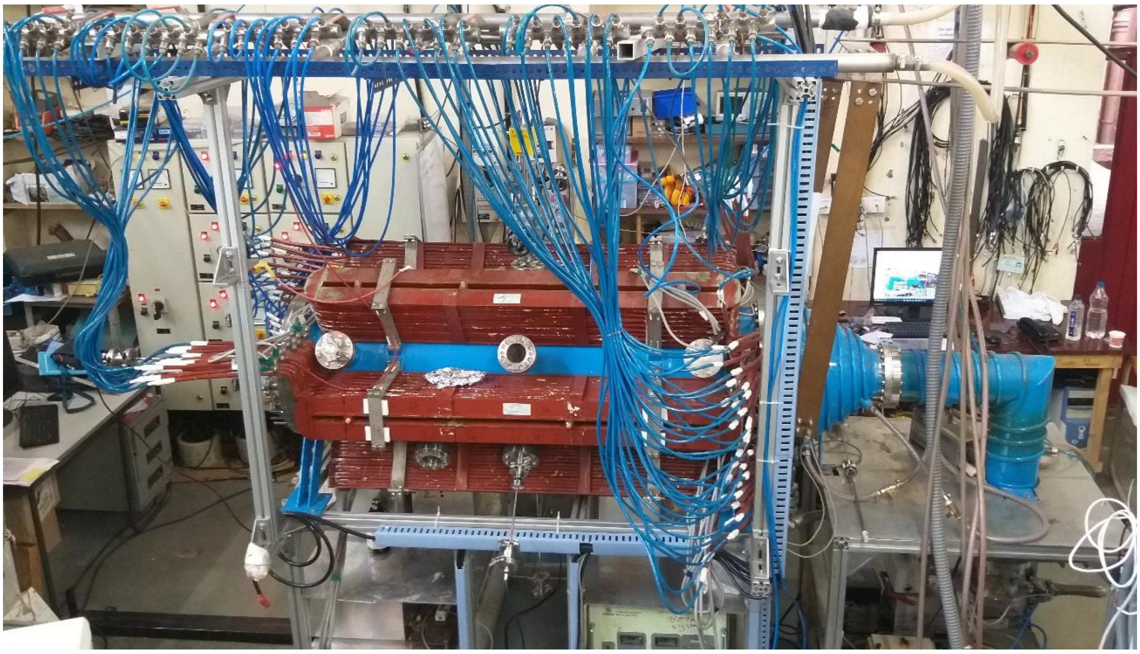

*Figure 2.1: photograph of the **M**ulti-pole line cusp **P**lasma **D**evice (MPD), front view of the chamber.*

The figure 2.1 shows an image of the integrated multi-pole cusp magnetic field plasma device (MPD), and figure 2.2 shows a 3D view/schematic of the device without magnet system. It consists of three parts: a) L-shape baffle b) conical chamber and c) main cylindrical chamber. The L-shape baffle is a connector in between conical reducer and pumping station.

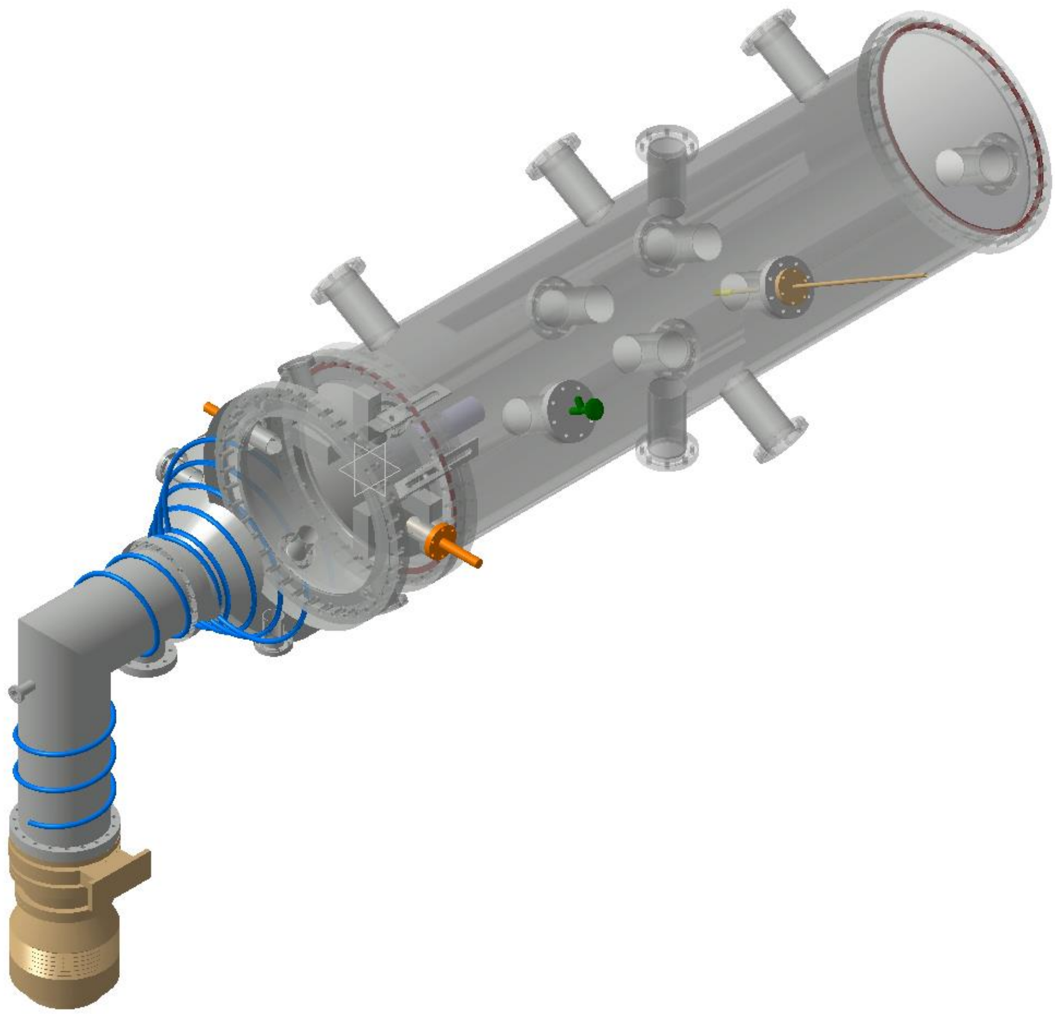

Figure 2.2:Isometric 3-D view of device without electromagnets.

The conical reducer chamber is developed to hold the plasma source and it has the provision to move the source along the axis in the main cylindrical chamber. The conical chamber has four DN 35 CF ports distributed azimuthally 90^{o} apart for current feedthroughs to provide the electrical connections to the plasma source. The smaller end of the conical chamber is connected to a pumping system using L shaped baffle via a DN 160 CF joint. The other end of the conical chamber is connected to the main cylindrical chamber with through DN 400 CF joint. The cylindrical chamber of the device is the main chamber to produce plasma and used to perform the related studies. The main cylindrical vacuum vessel has 0.6cm wall thickness, 150 cm length and 40 cm diameter, and it is made up of non-magnetic stainless steel (SS-304). Figure 2.3 shows the isometric 3D view of the device, including all three parts of the device. It has a total 12 radial ports of DN 63 CF standard welded at various axial locations and distributed azimuthally as shown in figure 2.3. These ports have been used for feedthroughs of electrical connections, to view inside the chamber and can be used for radially movable diagnostics probes as shown in figure 2.2.

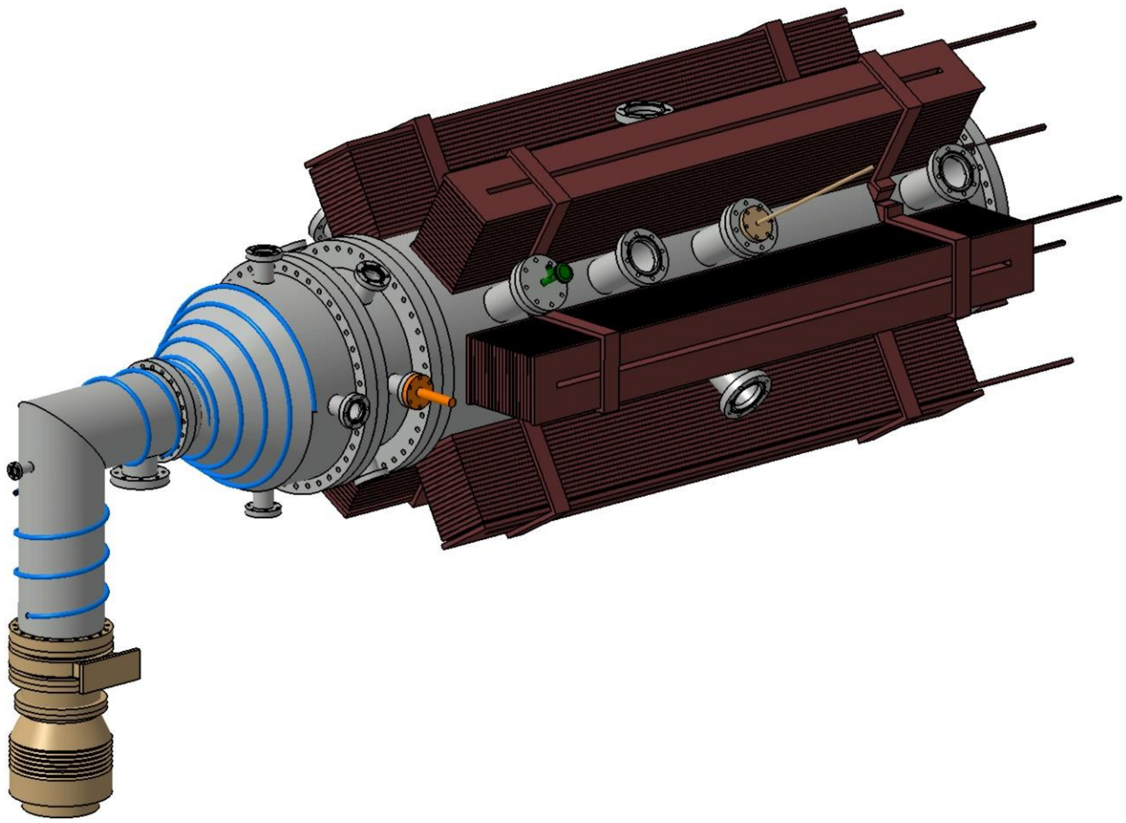

Figure 2.3: Isometric 3D view of MPD.

The one end of the main chamber is closed with a DN 400 CF flange consisted with different DN 63 CF port and DN 35 CF port for plasma viewing and for plasma diagnostics particularly for axial measurements. To evacuate the system, a pumping system is required. The pumping system used for MPD, consists of a turbo molecular pump TMP (having speed 440 l/s and model TPH 521 PC) backed by a rotary pump (having speed 12 m^3/h and model DUO 10 MC). This pumping system smoothly takes the system to a base pressure of 1×10^{-6} mbar within 3 hours. The conventional Pirani gauge, and a hot cathode ionization gauge (Hornet IGM-402 model) are employed to monitor the pressure of the device. All the gauges have been placed away from the magnetic field using a suitable extension to reduce the effect of magnetic field on the filament.

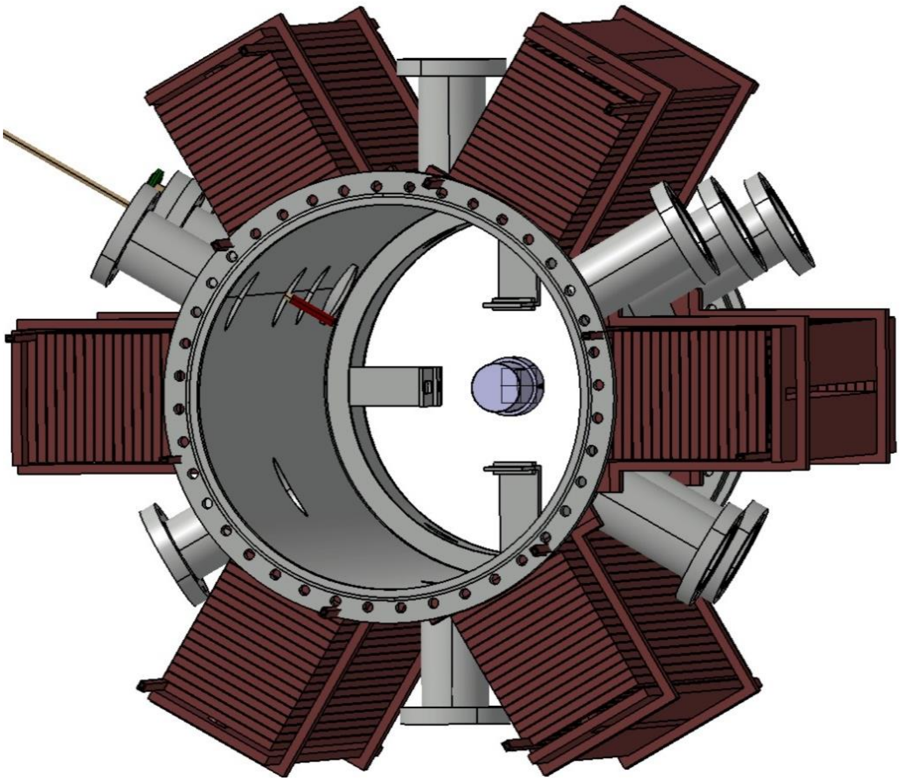

Figure 2.4: Cross-sectional view of the MPD, showing the arrangement of electromagnets and centered plasma source located at the one end of the device.

The pumping system and gauge are controlled by the DCU controller. The automatic pressure controller is used for gas feeding during plasma discharges. All joints and ports in the system are CF standard and copper gaskets are used for vacuum sealing. The whole vacuum system is mounted on a non-magnetic stand made up of aluminum square bars. The stand containing the conical chamber and pumping system can be moved axially. The L shape connector and conical chamber has been brazed with hollow copper pipe for cooling the wall.

In MPD, a multi-pole cusp magnetic field configuration is adopted to confine the Argon plasma. The multi pole cusp magnetic field is usually created by placing rows of magnets along the length of the cylindrical plasma chamber, over its periphery. The main chamber also has slots over the periphery to firmly support the magnets by non-magnetic C-clamps as shown in figure 2.3. The electromagnets have been used in the MPD to produce the cusp magnetic field. The figure 2.4 shows the sectional 3D view of the main chamber, to show the arrangement of electromagnets. The details of electromagnets and cusp magnetic field configurations produced by these magnets are discussed in Chapter 3.

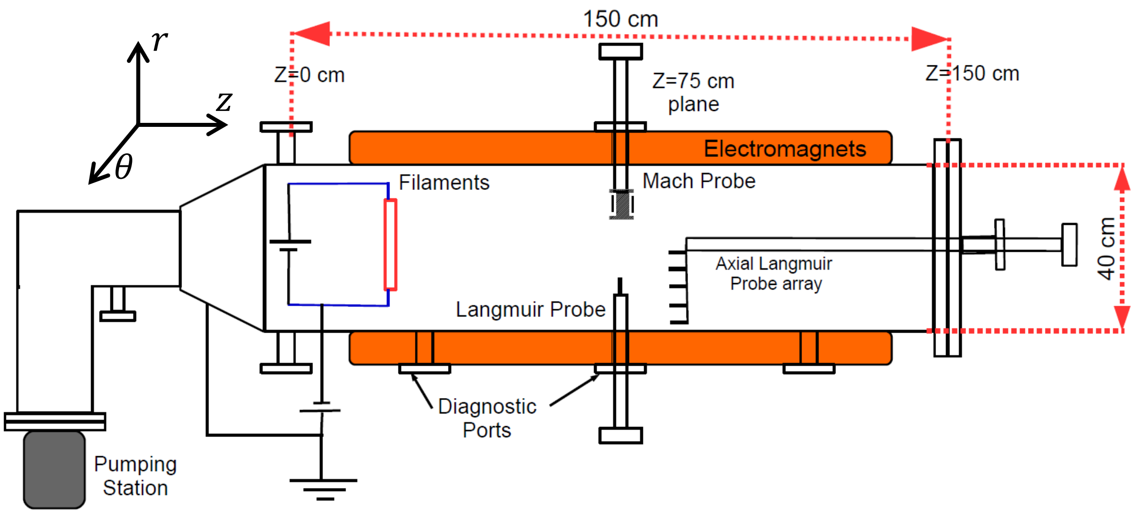

Figure 2.5: Schematic of the MPD device, electromagnet, and its diagnostics, inset of the figure shows the opted coordinate system of the device.

The schematic of the MPD and coordinate system is shown in figure 2.5. The figure shows the location of plasma source in main cylindrical chamber, dimensions of the chamber along with the implemented plasma diagnostics, the radial Langmuir probe, Mach probe, and axial probe array etc.

2.2 Plasma Source

Hot cathode plasmas produced using the tungsten filaments are generally quiescent [32]. Studying fundamental plasma phenomena such as Landau damping, non-linear coherent structure, wave-particle trapping and un-trapping etc., requires reasonably quiescent plasma of finite volume while the plasma, being in a field free region is an added advantage. It is generally observed that the ratio of *me/mi* crucially controls the finite beta effects [2]. Hence, it is desirable to have a source which can produce plasma of gas species with different masses, especially with inert gases like Argon, Krypton and Xenon etc. With these desired considerations, a tungsten filament based source has been designed and fabricated. A two-dimensional array of joule heated filaments is mounted on the conical source chamber. The multi-filamentary source consists of five filaments arranged in the form of a rectangular array. This two-dimensional vertical array has five filaments of tungsten wires of 8 cm length and 0.5 mm diameter. The filaments are arranged with a 2 cm spacing, which is less than twice the Larmor radius of the primary electrons near the filaments. The filaments are attached to SS-316 rectangular frames. This source is held inside the conical reducer such that the filaments are inside the main chamber. The source is placed at a distance of 20 cm from the inner wall of the main cylindrical chamber as shown in figure 2.5.

(a)

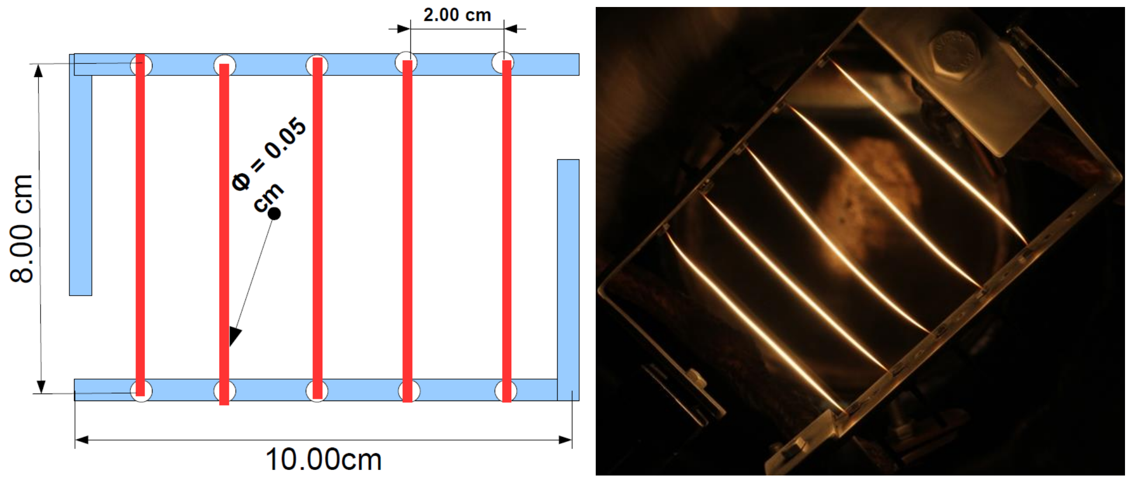

Figure 2.6: (a) Schematic of filamentary plasma source (b) picture of source while heating.

The source is pushed well inside the main chamber to keep it away from the edge effects of the electromagnets. It is centered at R=0 cm, where the cusp magnetic field due to electromagnets is negligible, as the central regime is nearly field free in this cusp configuration. All filaments are electrically connected in parallel for the electron emission with equal energy distribution. A floating power supply of 15V/500A is used to heat the filaments with a typical filament current of 80 -100 A, such that 16-20 A current passes through per filament. The electrical connections are shown in figure 2.7. The lighting photo of rectangular plasma source inside the vacuum chamber is shown in figure 2.6.

2.3 Plasma Production

Plasma is produced by electron impact ionization of neutral gas. The schematic illustration of plasma production circuit used in MPD is shown in figure 2.7.

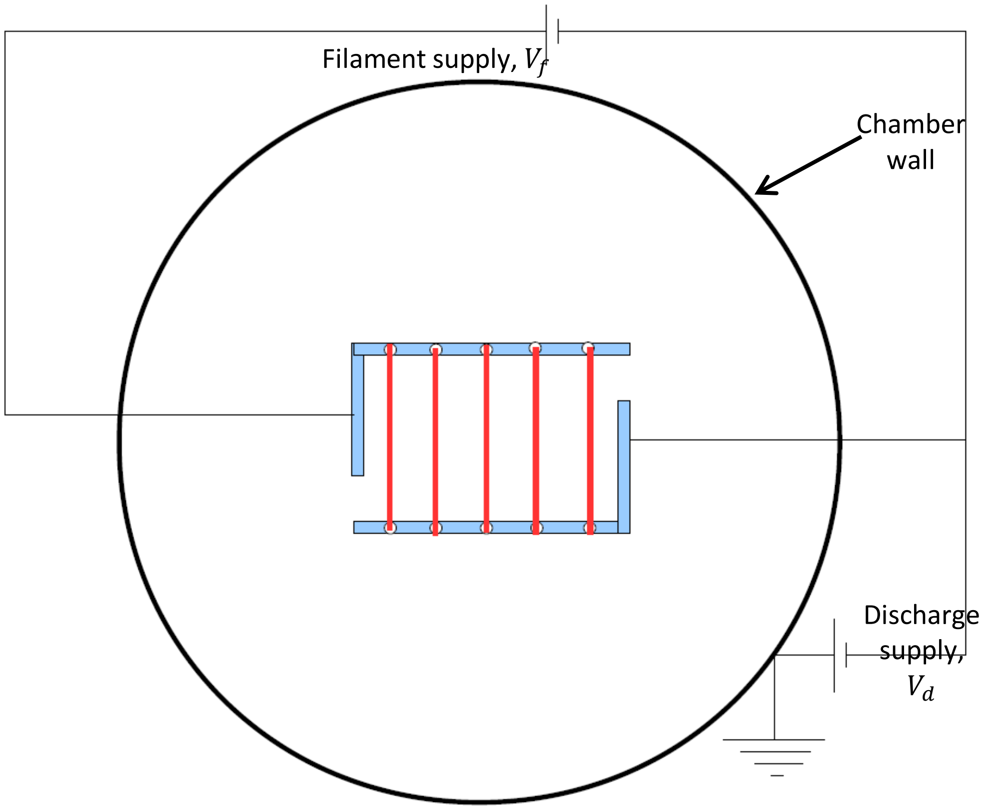

Figure 2.7: Schematic of plasma discharge mechanism, showing the discharge circuit.

As shown in the schematic circuit of plasma discharge, the negative leg of the filament power supply is connected to the negative leg of the discharge power supply (of 128 V, 25 A). The positive leg of the discharge power supply is connected to grounded vacuum vessel. The heating current for each filament for daily operation is maintained at ~18-20 A, for thermionic emission of electrons and the voltage drop across the filaments is 7.5 V. The filaments are biased with a voltage of -50 V with respect to the grounded chamber walls using the discharge power supply. Regulated power supplies have been deployed for magnets, the filaments and the discharge supplies, ensuring stability. The primary electrons emitted from the filaments travel in the electrical field directions towards chamber wall anode, while they are confined by the cusp magnetic field lines. The chamber is filled with Argon gas through a needle valve many times before the plasma discharge and maintained at a certain required operating pressure during the discharge. The filamentary Argon discharge plasma is struck between the hot filament based cathode source and the grounded vessel wall. With this configuration of plasma production, discharge current of 2 to 6 A is achieved. The accelerated electrons produce plasma of density ~10^{15}-10^{16} m^{-3} by impact ionization and electron temperature, T_e =3-5 eV. The diagnostics are used to measure, plasma parameters such as plasma density (n_e), electron temperature (T_e), plasma potential (ϕ_p), and floating potential (ϕ_f), fluctuations in these parameters and other plasma parameters to estimate the plasma behavior and characteristic is discussed in detail in next section.

2.4 Diagnostic technique

In this thesis work, Langmuir probe-based diagnostics are used to measure various plasma parameters, like plasma density (n_e), electron temperature (T_e), floating potential (V_f) and plasma potential (V_p). Conventional emissive probes are also used to measure the plasma potential. Directed plasma flow is measured using Mach probe. The density and potential fluctuations are measured with Langmuir probe. Directional probe is used to measure the plasma perturbation along the z-axis.

The Langmuir probe (LP) is probably the simplest plasma diagnostics known but it is an intrusive diagnostic. Hence, the dimension of the wire should be chosen in such a way that it should in principle NOT perturb the plasma or alter plasma properties. The Langmuir probe is easy to fabricate but challenging to understand and interpret. The Langmuir probes have the advantage to provide local measurements of plasma properties. The probe diagnostics used in this Thesis work consist of cold collecting probes and hot emissive probes. The cold collecting probes used are single and triple Langmuir probes, an array of Langmuir probes and Mach probe.

2.4.1 Langmuir Probe

The Langmuir probe (LP) diagnostics is being used since it was first introduced by Irvin Langmuir in 1926 [116] for the measurement of basic plasma parameters [117–121]. The LP is a small conducting electrode of any shape (sphere, cylinder or planer) immersed in plasma and it allows local measurement of plasma parameters. It is a conventional diagnostic for investigating plasma parameters using fundamental techniques.

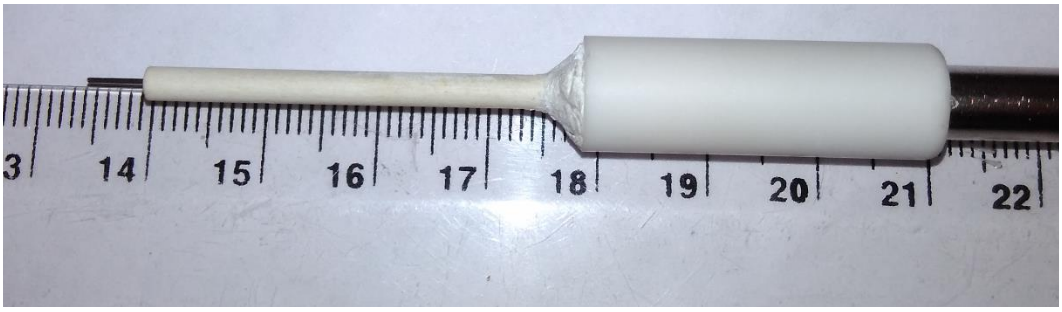

Figure 2.8: Picture of Langmuir probe

The Langmuir probes used in MPD are made up of the cylindrical tungsten wire of 1 mm diameter and 5 mm length. The probe is mounted through a ceramic tube and ceramic holder as an insulator as shown in figure 2.8. The entire probe assembly is mounted on a movable shaft and inserted from the radial ports using feedthrough for easy radial movement. When the Langmuir probe is immersed in plasma and biased with respect to a reference electrode or the grounded vessel, it draws currents from plasma, noted as plasma current, I_p. This probe current depends on the applied bias voltage, V_b on the probe, therefore, varying the voltage V_b over a wide range provides an I-V characteristic of LP [122]. The typical Langmuir probe current voltage characteristics are shown in figure 2.9.

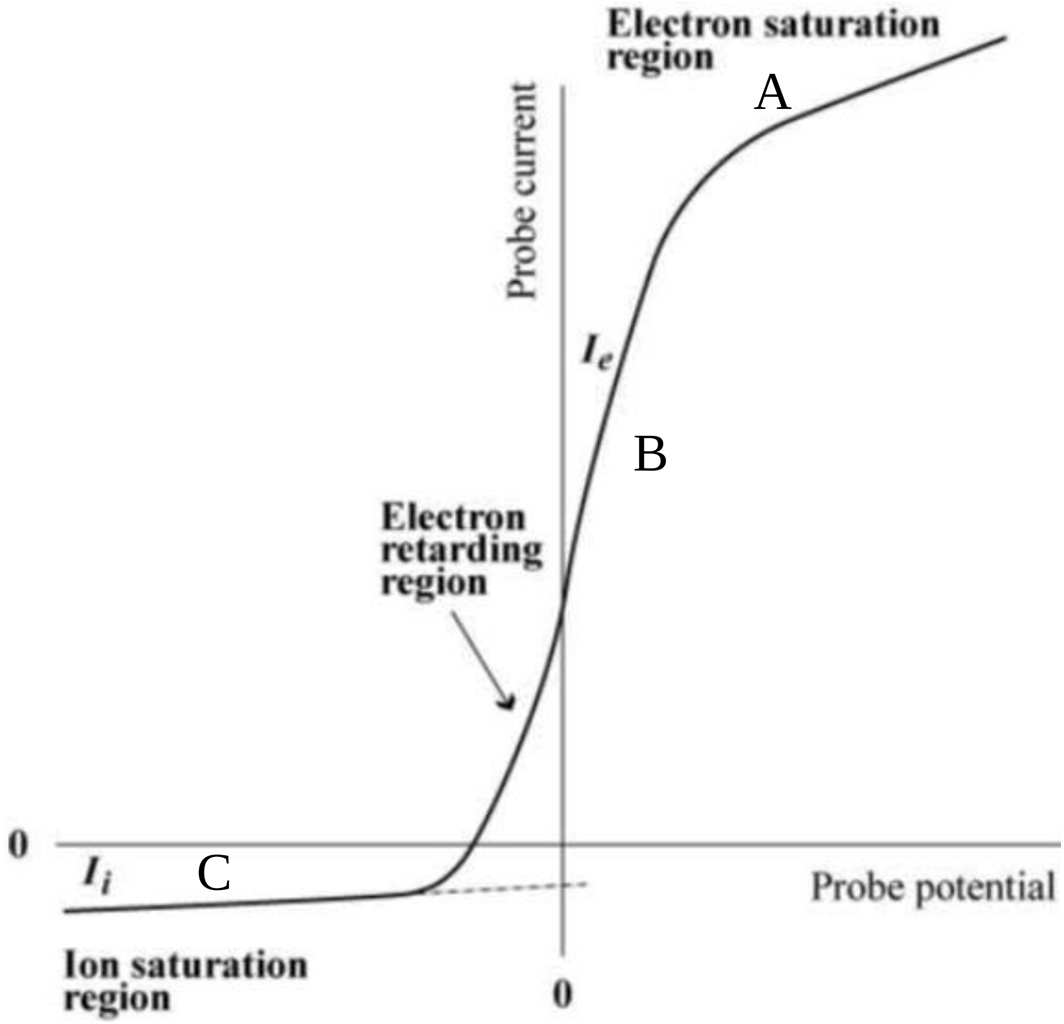

Figure 2.9: Ideal I-V characteristic of Langmuir probe.

When the biased voltage at the probe is equal to the plasma potential, there is no electric field between the probe tip and the plasma; hence electrons and ions are collected by the probe surface with their thermal velocities. If the bias voltage (V_b) at the probe tip is increased above the plasma potential (V_p), a sheath is formed around the probe and thus the probe area increases with biased voltage. As a result, the probe current slowly increases with probe potential above the plasma potential as shown in the region **A** of figure 2.9. Now, decreasing the bias voltage to the probe lower than the plasma potential, the probe becomes negative with respect to the surrounding plasma thus plasma electron is reflected from the probe tip and entering in region **B,** which is known as bulk electron region. The probe current is zero when the electron current is equal to the ion current at the floating potential (V_f). Decreasing the bias voltage further, all the electrons repel and only ions are collected by the probe surface. The ion current changes slowly with the bias voltage and this region is known as the ion saturation region (region **C**).

Conventionally, the electron current collected by the probe has been considered to be positive and the ion current to be negative. The probe current of ideal Langmuir probe I-V characteristic can be written as the follows,

$$I_p = I_{es} e^{(V_b - V_p)/kT_e} - I_{is} \qquad \textit{2-1}$$

where, I_p is the probe current at biased potential V_b, I_{es} is the electron saturation current at the plasma potential $V_p = V_b$ and I_{is} is the ion saturation current.

The typical plasma parameters such as electron temperature, plasma density, plasma potential and floating potential can be obtained as follows.

2.4.1.1 Estimation of electron temperature

As shown in equation 2.1, the plasma current drawn using Langmuir probe is the sum of electron current and ion current. For estimation of electron temperature [123,124] from the I-V characteristic, the ion saturation current (I_{is}) should be subtracted from probe current, $I_e = I_p - I_{is}$. The linear extrapolation of I_{is} is followed to get the electron current (I_e), shown in figure 2.10 (b). For $V_b > V_f$, $I_{is} \ll I_e$, on taking the natural log of the equation 2.1, we get

$$ln\left(\frac{I_e}{I_{es}}\right) = \frac{e}{kT_e} V_b - \frac{eV_p}{kT_e} \qquad \textit{2-2}$$

It can be compared to the equation of straight line, $Y = mX + C$, here $m = \frac{e}{kT_e}$. Hence, the temperature can be determined from inverse of the slope from linear region of logarithmic plot of electron current, which can be written as, $T_e = \left[\frac{\ln I_e(2) - \ln I_e(1)}{V(2) - V(1)}\right]^{-1}$.

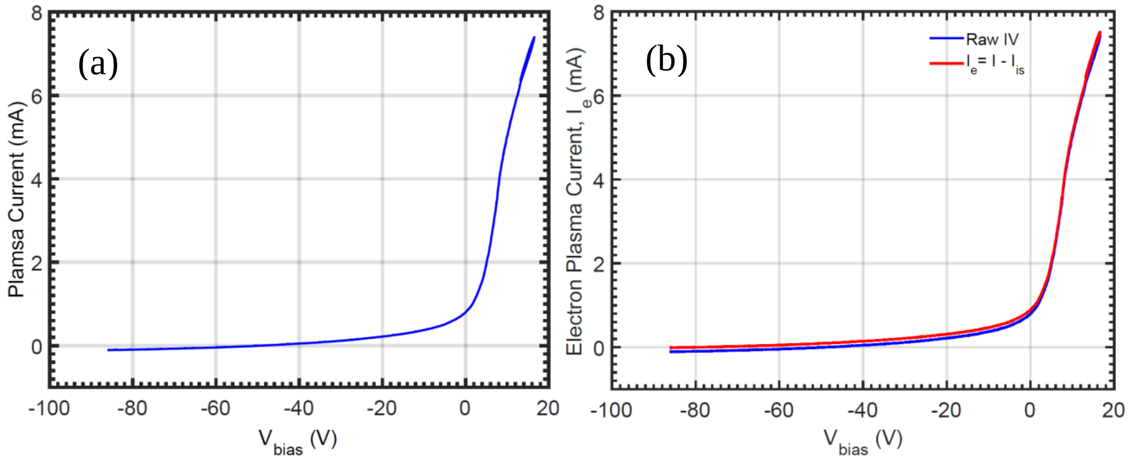

Figure 2.10: (a) Measured Langmuir probe V-I characteristic of plasma and (b) V-I with subtraction of ion saturation current, ($I_e = I - I_{is}$).

The variation of probe current, I_p with bias voltage, V_b, the raw I-V curve is shown in figure 2.10 (a) and variation of electron current, I_e with V_b, after subtraction of ion saturation current is shown figure 2.10 (b). The variation of $\ln I_e$ is shown in figure 2.11 (a). This curve of $\ln I_e - V_b$, shows two slopes, which indicates the presence of two electron temperature distribution in plasma. The lower slope shown in figure 2.11 (a) provides the hot electron temperature, T_{eh}. When we extrapolate the lower slope upto its intersections with V_p, this value of current is hot electron saturation current, I_{ehs}. To estimate the cold electron or bulk electron temperature, the hot electron saturation current is subtracted from electron current.

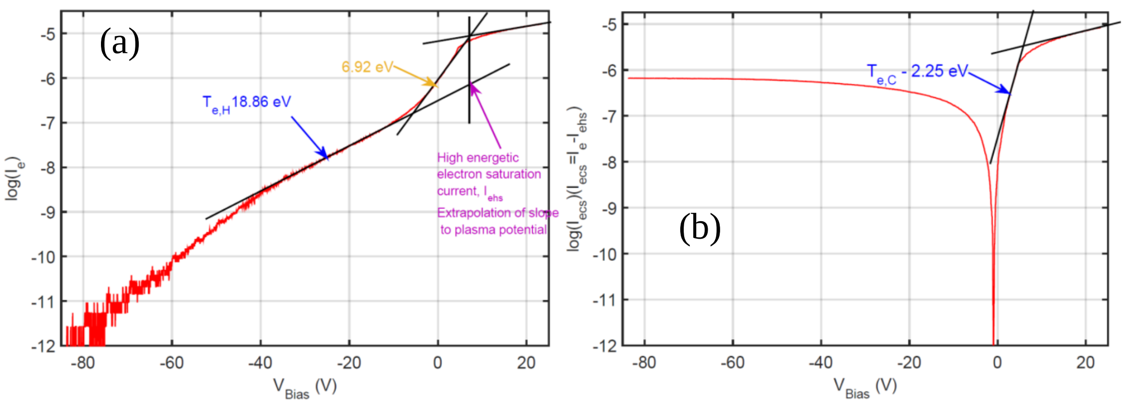

Figure 2.11: Variation of (a) $ln(I_e)$ with probe bias voltage, (V_b) to estimate hot electron temperature and (b) $ln(I_e - I_{ehs})$ with probe bias voltage, (V_b) to estimate cold electron temperature for 2×10^{-4} mbar neutral pressure and -50 V discharge voltage at R=0 cm.

The variation of $\ln(I_e - I_{ehs})$ with V_b is shown in figure 2.11 (b). The slope of linear regime of $\ln(I_e - I_{ehs}) - V_b$, provides the cold or bulk electron temperature, T_{ec}, shown in figure 2.11 (b).

2.4.1.2 Estimation of Plasma Potential

Theoretically, the plasma potential is defined as the potential where electron probe current gets saturated (does not depend on bias potential, V_b) but this is not observed in most of the experimental I-V characteristics.

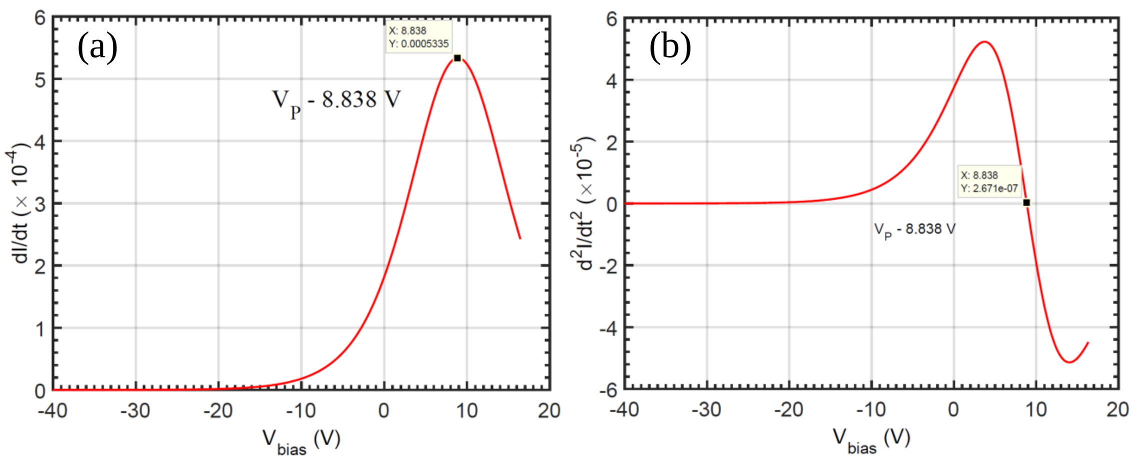

Figure 2.12: Variation of (a) first derivative, (I) and, (b) second derivative of probe current with probe bias voltage (V_b) to determine the plasma potential, (V_p).

The typical plasma potential can be obtained from the intersection of two lines in the logarithmic plot of electron current as shown in figure 2.11 (a) and 2.11 (b). The intersection point is obtained by expanding the straight line on the linear region of and saturated part of the curve. The more precisely plasma potential V_p, can be determined by differentiating I_e corresponding to maximum of dI_e/dV as shown in figure 2.12 (a) or where $d^2I_e/dV^2 = 0$, as shown in figure 2.12 (b). It is also to be noted that the plasma potential is measured from the inflection point of first derivative of *V-I* characteristics of Langmuir probe (as shown in figure 2.12 (a)). The second derivative of *V-I* characteristics is used to check whether its value becomes zero at plasma potential 2.12 (b).

2.4.1.3 Estimation of Floating Potential

The floating potential is the voltage, where probe draws no net current, it happens when probe draws same amount of electron and ion current $I_e = I_i$. In general, where I-V characteristic of Langmuir probe shows zero current is defined as floating potential of plasma i.e., $I_p(V_b = V_f) = 0$. In this way the floating potential can be estimated directly from I-V characteristic. On other hand it can be obtained by substituting $I_p = 0$ in equation 2.1. This gives $I_{es} \exp \frac{e(V_f - V_p)}{kT_e} - I_{is} = 0$; $\frac{e(V_f - V_p)}{kT_e} = \ln \frac{I_{is}}{I_{es}})$ and $V_f = V_p + \frac{kT_e}{e} \ln \frac{I_{is}}{I_{es}}$. On substitution of required values, we obtain the expression of floating potential in terms of plasma potential and electron temperature for Argon plasma as $V_f = V_p - 5.5\, T_e$. For MPD plasma, the floating potential is measured by using high impedance unbiased Langmuir probe.

2.4.1.4 Estimation of Plasma Density

The plasma density is calculated from the ion saturation current. In a collisionless single ion species plasma the ion saturation current to the probe is given by the below equation [125–127],

$$I_{is} = 0.6\, n\, e\, c_s A_p, \qquad n = \frac{I_{is}}{0.6\, e\, c_S\, A_p} \qquad \text{2-3}$$

where, e is electronic charge, A_p is probe area and c_s is Bohm velocity. The Bohm velocity is defined by $c_s = \sqrt{T_e/m_i}$ where T_e is electron temperature and m_i is ion mass. The electron temperature obtained after hot electron temperature correction is used in the Eq. 2.3, to determine the plasma density. For error calculation in density the below equation is considered,

$$\frac{\delta n}{n} = \sqrt{\left(\frac{\delta I_{is}}{I_{is}}\right)^2 + \left(\frac{1}{2}\frac{\delta T_e}{T_e}\right)^2 + \left(\frac{\delta n}{n}\right)_s} \qquad \text{2-4}$$

where $\delta I_{is}/I_{is}$ error in ion saturation current, $\delta T_e/T_e$ error in electron temperature measurement, $(\delta n/n)_s$ is the statistical variation in density [128].

2.4.1.5 Developed electronic circuit for LP measurement

For the measurement of plasma parameters of plasma confined in MPD, a sweeping circuit (as shown in the figure 2.13) of frequency 1 Hz and a voltage sweep from -80 V to +20 V is developed. This circuit consists two parts (1) ramp voltage generator circuit and (2) current measurement circuit. A triangular waveform is generated using MAX038 CPP IC and this is amplified using PA85, as shown in figure 2.13 (Ramp voltage generator). The typical range of ion saturation current is determined from discharge voltage V_D. To repeal the total electrons, the applied bias voltage should be more negative than V_D. Hence, the lower limit of sweeping voltage is decided to be -80 V. As the typical floating potential for the hot cathode plasma varies in the range of -5 V to -45 V and the plasma potential is typically around 10 V, therefore, typical range of sweep voltage is chosen to -80 V to +20 V. Output voltage is the sum of bias voltage and the voltage proportional to the probe current. The differential amplifier at the second stage subtracts the bias voltage from the first stage output and provides voltage proportional to probe current.

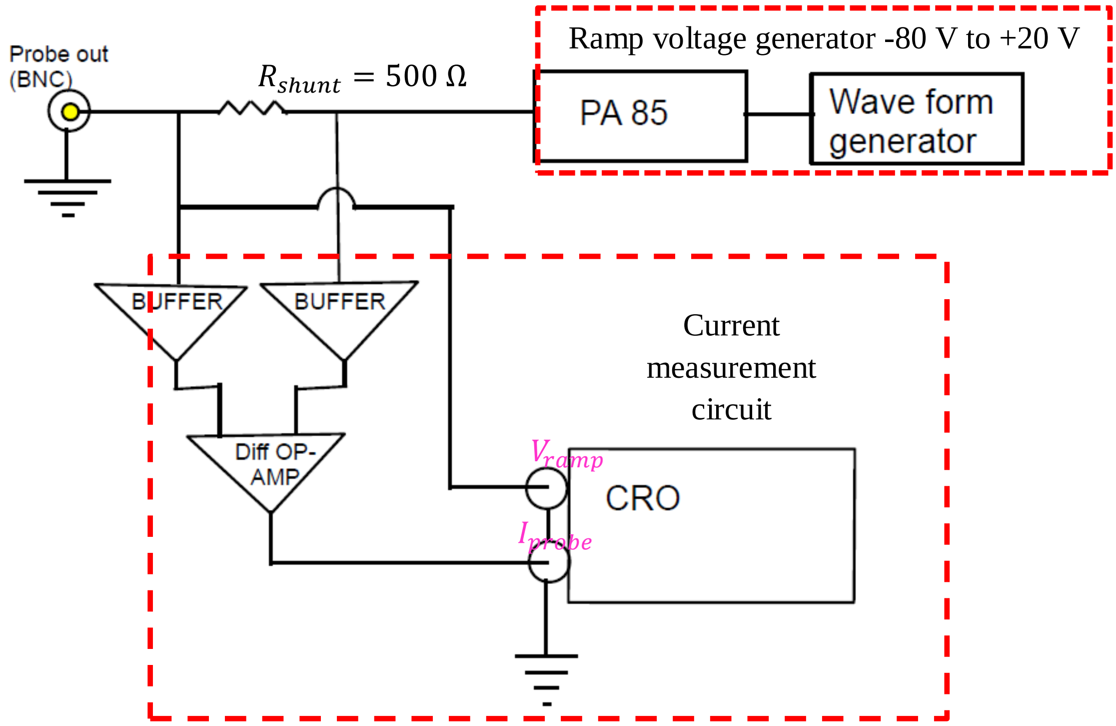

Figure 2.13: Schematic of wave form generator and current measurement circuit, measure the current drawn from plasma using Langmuir probe across a resistance.

The figure 2.14 shows the photograph of sweeping circuit used in this thesis. The Langmuir probes may not need to be compensated, for DC filamentary discharge plasma [22].

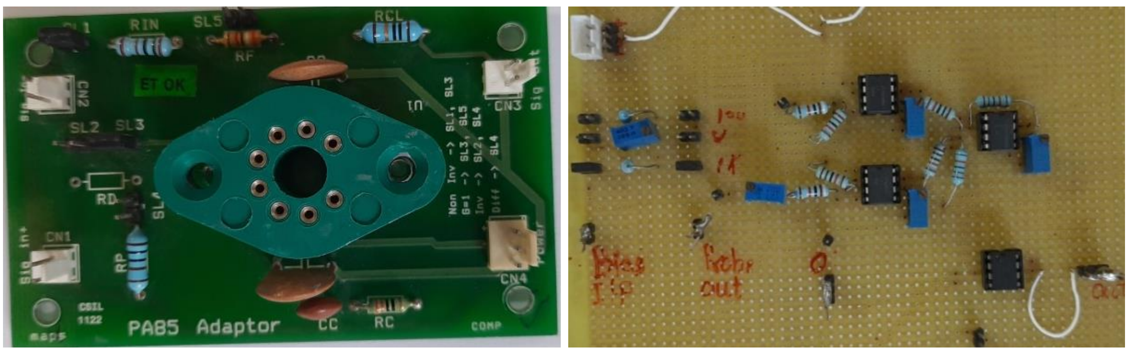

Figure 2.14: Picture of (a) Voltage amplification circuit using PA85 and (b) current measurement circuit using LF356.

2.4.2 Directional Langmuir Probe

A directional Langmuir probe is an ordinary Langmuir probe with shielding provided by insulating structure. The shielding restricts the solid angle through which the probe collects particles. The directional Langmuir probe is useful in direct measurement of particle flux in any particular direction [129,130].

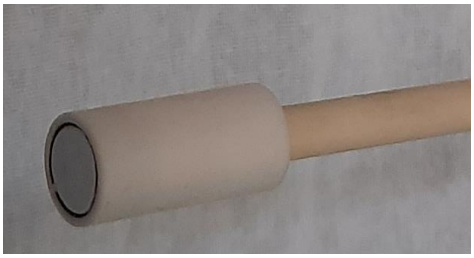

Figure 2.15: Picture of directional Langmuir probe.

For the measurement of ion current, it collects the component of ion-saturation current along the particular direction of the flow velocity. In this thesis, the directional probe is used to measure the IA wave propagation along the Z-axis of the cylindrical system.

2.4.3 Probe Array

A linear array of five single Langmuir probes is used for a 2-d measurement of plasma parameters on the r-θ plane. The radial separation between consecutive probe tips is 4 cm, length of each tip is 5 mm and probe tips are aligned horizontally as shown in figure 2.16.

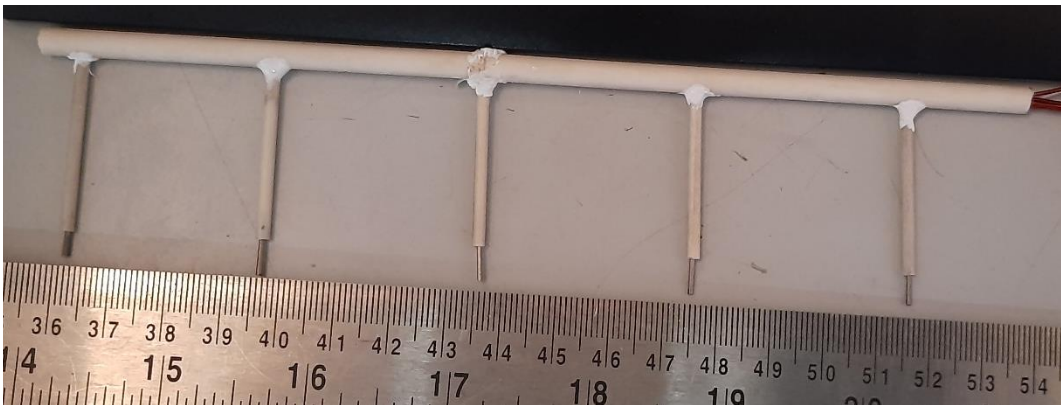

Figure 2.16: Schematic of (a) Mach probe, (b) five radial probe array integrated with a rotatable axial shaft, (c) 2-d measurement in $\boldsymbol{r}-\boldsymbol{\theta}$ plane.

This array consists of 5 probes placed at five radial locations with an interval of 4 cm i.e., at R=2, 6, 10, 14, and 18 cm, as shown in figure 2.16. The array is mounted on a rotatable axial shaft and the shaft itself is fitted from the endplate of the vacuum chamber such that the shaft is at the center of the device at R=0. The important application of this diagnostics is in the estimation of azimuthal uniformity in plasma parameters as well as measuring the radial variation of plasma parameters, which will be discussed in Chapter 3.

2.4.4 Emissive Probe

As discussed in Sec. 2.4.1.2, theoretically plasma potential can be determined by sweeping the voltage across the Langmuir probe and “knee” around (see figure 2.11) the electron saturation region determines the plasma potential. However, during experimental measurements particularly in a magnetized plasma, electron saturation does not occur and the “knee” cannot be easily identified and values obtained are erroneous.

Emissive probes are commonly used in plasma devices to measure the plasma potential. In 1923, the intention of emitting probe was first proposed by Langmuir [131]. Electron emission from the probe provides an opportunity for direct measurement of plasma potential. Usually the probe is heated to emit electrons and the electron emission current depends upon the potential surrounding it. Thus, if the current in the emissive probe circuit is measured for a given probe temperature, one can estimate the potential around the probe locally. Emissive probe is particularly useful for the measurement of spatial gradient in plasma potential for determining electric field. The complete operation of emissive probe is as follows: When a probe is biased more positive than the local plasma potential, electrons emitted from the probe are reflected back to the probe. When the probe is biased negative with respect to the plasma potential, electrons from the emitting probe escape to the plasma and appear as an effective ion current. This process is not sensitive to plasma flow and beams because it directly depends on the plasma potential rather than electron kinetic energy.

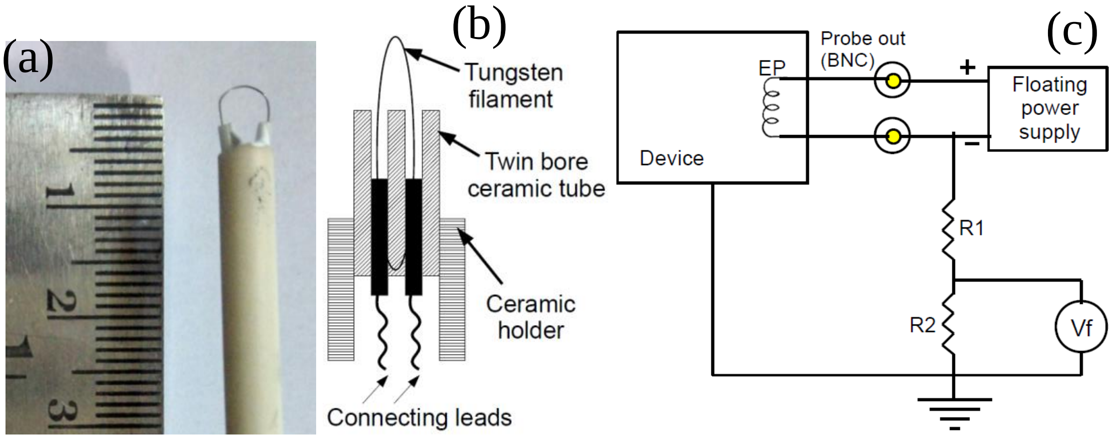

Figure 2.17: (a) Picture of emissive probe, (b) schematic of emissive probe and, (c) schematic of probe connections to measure plasma potential, (V_p).

There are three methods for determining plasma potential using the emissive probe, a) floating potential method, b) Inflection point method, c) separation point method. In the present work, the floating point with large emission method is used [132].

2.4.4.1 Floating potential method

It is based on the fact that as emission increases, the floating potential of an emissive probe approaches the plasma potential [133]. Different methods are used to heat the probe viz. Ohmic heating using a floating power supply, using a laser beam, or Ohmic heating through collection of electron current from the plasma itself. The emissive probes are known to work best for densities in the range $10^5 - 10^{12}\ cm^3$ and space charge effects are known to be insignificant for magnetic fields when the average electron Larmor radius r_{L_e} is larger than the probe radius r_P [132–134]. The only major source of error while using emissive probe is of the order $T_{w/e}$ where T_w is the temperature of the heated probe [134]. A picture and schematic view of the emissive probe is provided in figure 2.17 (a) and (b) respectively.

A thin 0.125 mm tungsten wire has been used to make the emissive probe. The two ends of this half-loop are pulled through the two bores of a double-bore ceramic tube and are at the other end connected by feedthroughs to an external floating power supply (7 A, 32 V).

Thus, the loop can be heated to the required temperature (white glow ≅ 2500 K). Contact between the leads of the wires connected to the power supply and the tungsten filament is made by squeezing the filament and the connecting wire into the bore of the ceramic tube as shown in figure 2.17 (b). The filament is heated by passing current through it using a floating power supply. The emissive probe circuit is shown in figure 2.17 (c). The emissive probe loop is heated by passing DC current across its terminals with a floating DC power supply. Typically, 1-2 V potential drop is observed across at the heating DC supply, depending upon the contact resistance of emissive probe connections. Therefore, measurements have been performed across a potential divider applied between two terminals. The loop of the emissive probe is held perpendicular to the magnetic field lines to minimize the magnetic field effects on the electron emission from the probe.

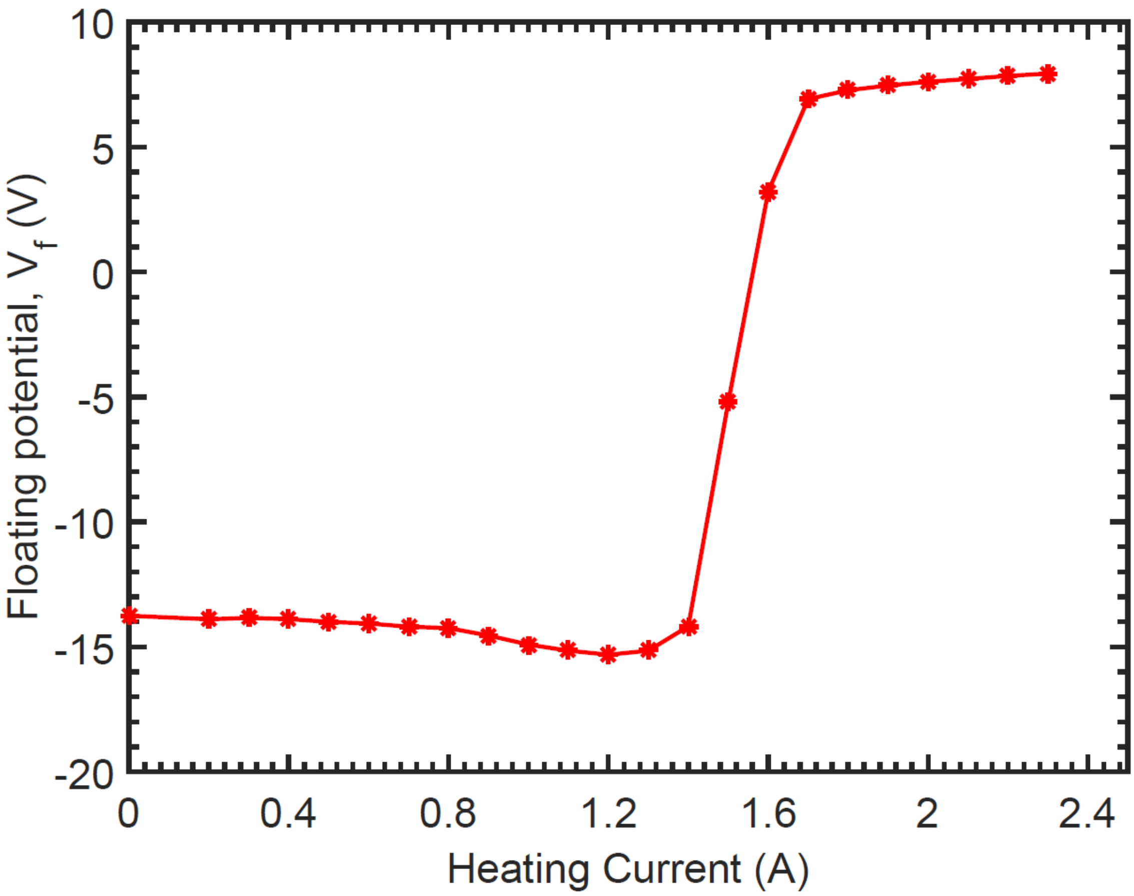

Figure 2.18: Variation of floating potential, (V_f) with filament heating current to estimate plasma potential, (V_p)

The floating potential of the plasma is the voltage where electron current and ion current balances each other and make the net current zero at the probe. When the heating of filament is started, after a certain value of current the electron emission from the filament started. As the emission of the probe is increased lesser amount of ion current is required to balance the electron current due to compensation by emitted current. Thus, as the electron emission increases, the floating potential of the probe is shifted toward the plasma potential until a saturation is reached. This value is assumed to be a sufficiently good approximation of plasma potential (V_p). figure 2.18 shows the variation of floating potential with increasing filament heating current. In the absence of electron emission from filament, the probe remains at the floating potential.

2.4.5 Mach Probe

Mach probe provides a direct measurement of the plasma flow velocity, which is based on the principle of the asymmetry in the particle flux in upstream and downstream direction, when a flow exists. Several theoretical models exist to estimate the flow velocity using fluid [135–137] and kinetic [138] approaches. The Mach probe used in this Thesis for estimating net axial flow in MPD consists of two circular metallic collection surfaces.

The model used for net flow measurements in MPD is based on the magnetic field symmetry arguments to eliminate the magnetic field dependence [139]. The cylindrical axis of Mach probe is usually aligned perpendicular to the cusp magnetic field lines and difference of ion saturation currents of two collecting surfaces provides net poloidal flow, at Z = 75 plane. The net axial flow is estimated from the following equation, $v_{net} = u_m c_s$, $u_m = \frac{1}{k} \ln\left(\frac{J_U}{J_D}\right)$, where c_s is the local ion acoustic velocity, u_m is Mach number, J_U and J_D is upstream and downstream current density and, k is a calibration factor. The value of k can be accurately estimated by using a "known flow". The calibration factor k is estimation and description of possible uncertainties in flow measurement is described in Chapter3.

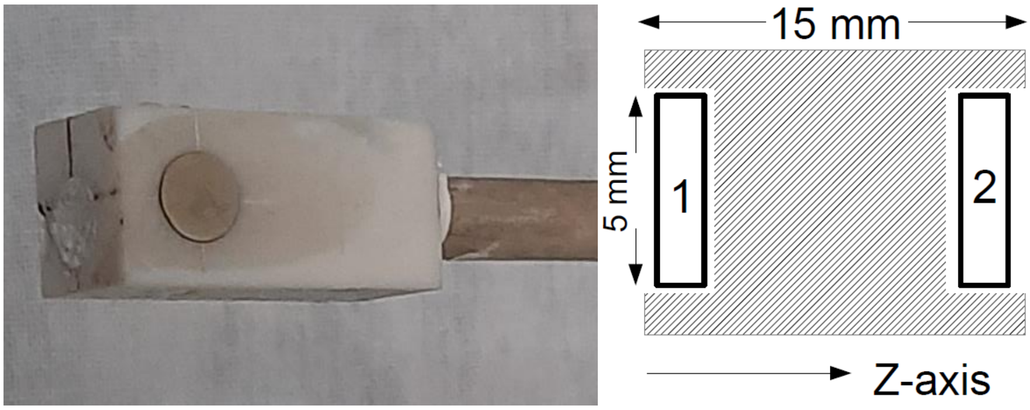

Figure 2.19: Picture of Mach probe and it's schematic showing both probes with ceramic insulator Schematic view of Mach probe used for net axial flow measurements at Z = 75 plane. Upper and lower collectors diameters are shown to be 5mm, such that probe radius $r_P < r_{L_i}$, where r_{L_i} is the ion Larmor radius.

Though the derivation of net flow is based on elimination of magnetic field effects, the method is applicable for the condition $r_{L_i}/r_P > 1$, where r_{L_i} is ion Larmor radius and r_P is probe radius [139]. The open aperture of Mach probe used is chosen such that the ions should be unmagnetized with respect to the probe. The Mach probe used here is a pair of two disk probes of ϕ5 mm diameter each, separated by a ceramic insulator and is mounted so as to measure the plasma flow in the axial direction (Z-axis) as shown in figure 2.19. The entire probe assembly has been mounted on an SS shaft, which can move radially at Z = 75 plane and mounted on the vacuum vessel perpendicular to the magnetic field. The schematic view of the Mach probe is shown in figure 2.19. Both disks are biased to negative potential to measure ion saturation current which will be further used to calculate the Mach number (u_m). Mach number is calculated using upstream and downstream current density collected by probe 1 and probe 2. The net axial plasma flow (v_{net}) can be calculated using Mach number (u_m) and ion-acoustic velocity ($c_s = \sqrt{k_B T_e/m_i}$) measured by Langmuir probe, $v_{net} = u_m\, c_s$. To check the area asymmetry in two collecting surfaces, the ion saturation current is collected on both the surfaces. Let us say probe-1 is collecting upstream and probe-2 is collecting downstream current then the probe is rotated by 180^0, such that probe-1 now collects downstream current and probe-2 upstream. Ideally speaking, if the area of both the probes is same, then the upstream or downstream current collected by either probe should be same, therefore, a difference of the upstream or downstream current collected by probe-1 and probe-2 provides area asymmetry in the Mach probe. The ratio of ion saturation current for both cases, the previous arrangement and after the 180° rotation is compared and found to be the same which implies the equal probe area. The other uncertainties in the measurement include an error in estimating k, uncertainty in ion saturation current measurement and statistical variation over various shots.

2.4.6 Fluctuation measurement

The plasma quiescence can be understood from the fluctuation levels in the various plasma parameters. The fluctuations in plasma density and floating potential are measured using the single Langmuir probe. The fluctuations in density and potential are obtained by measuring the fluctuating components of ion saturation current (I_{is}) and floating potential (V_f). For plasma density fluctuation measurement, the ac voltage signal across the 10 kΩ resistance is measured when probe tip is biased to -80 V with respect to the grounded chamber. The floating potential fluctuation is measured by recording the ac voltage using a voltage divider of 10 $M\Omega$ and 100 Ω when the probe is grounded. The fluctuation in plasma potential (V_p) is measured using emissive probe. The emissive probe is heated with a constant current, at which it measures the dc plasma potential. For this condition when the ac component is measured, it provides the fluctuation in plasma potential. In order to identify any intrinsic instabilities, the important characteristic features such as fluctuations in plasma parameters, power spectra of fluctuations, cross correlation functions, wave number-frequency spectra are necessary [140,141]. The data (times series) are acquired at different sampling rates and the record length in oscilloscope. The MATLAB codes are developed for analysis of fluctuation spectra, cross correlation, wave number-frequency spectra etc.

In summary, this Chapter describes the details of the experimental apparatus including the vacuum vessel, vacuum pumps and other subsystems in detail. It also covered, the details of plasma production using filamentary cathode source, various diagnostics and their applicability. In the next chapter, we will use these tools to determine the plasma characteristics in cusp magnetic field and also for the experimental studies of rest of thesis work.

Chapter 3

Plasma Characterization in Different Cusp Configurations

The **M**ulti-pole line-cusp **P**lasma **D**evice (MPD) [67] has adopted this multi-line pole cusp magnetic field geometry for plasma confinement. The usage of electromagnets in MPD facilitates the confinement of plasma with various cusp geometries and a wide range of magnetic field strengths. The characteristics of the filamentary produced argon plasma in MPD have been studied and reported before [58,67]. Drift waves [142] have been observed in the edge region of the Six Pole Six Magnet (SPSM) configurations in which the wave vector changing its direction has also been seen for the first time. Since these drift wave fluctuations cannot reach the central regions because of the good curvature physics, the plasma in the central region of the MPD is found to be very quiescent. This quiescent and uniform plasma volume can be used to study fundamental plasma phenomena. Since the cusp fields are produced by electromagnets, the number of pole cusps can be changed by changing the direction of the current in the coils.

In a quest for more quiescent plasma, experiments are done in the MPD with various configurations of line-cusp fields by changing the current direction in the electromagnets appropriately. Thus, by passing the current in the same direction in all the six magnets, a Twelve Pole Six Magnet (TPSM) line cusp configuration can be created in the same volume. Due to the increase in number of poles, the volume with small magnetic field increases and one can thus get a larger volume of uniform and quiescent plasma. The plasma confined in Twelve Pole with Six Magnet (TPSM) is rigorously compared with that of produced by the Six Poles with Six Magnet (SPSM) with same current in both the configurations. Various plasma parameters such as plasma density, electron temperature, plasma potential, floating potential, plasma quiescence level, and axial plasma flow are compared for these two cusp configurations. In this chapter, we discuss the investigations of plasma characterization in these two magnetic configurations. It has been explored to obtain high quiescence level, large uniform plasma region with nearly flat mean density and temperature profiles. A detail experimental study of plasma characteristics in both the magnetic field configurations includes the radial variation of plasma parameters and variation of plasma parameters with increasing magnetic field strength. The experimental investigation of plasma parameters in SPSM and TPSM provides very strong evidence that the magnetic field profile plays a crucial role in transforming the characteristics of plasma. This larger uniform and quiescent plasma volume allows to observe the plasma interaction and response to any external perturbation to excite the various waves. The detailed plasma characteristics in the Twelve Pole Six Magnet (TPSM) configuration is compared to the Six Pole Six Magnet (SPSM) configurations while bringing out the advantageous property of the former.

3.1 Experimental Setup and Diagnostics

The experiments reported here are performed in a linear cylindrical device MPD [58,67], which has been described before in previous Chapter 2.

The schematic of the MPD, its diagnostics, and coordinate system are shown in figure 3.1. The system is pumped down to 2×10^{-6} mbar base pressure and the operating pressure of filled Argon gas varies from 5×10^{-5} mbar to 3×10^{-3} mbar. The filaments are heated for thermionic emission of electrons using a 15 V, 500 A floating power supply biased at -50 V with respect to an anode (wall of the cylindrical chamber) using 128 V, 25 A power supply.

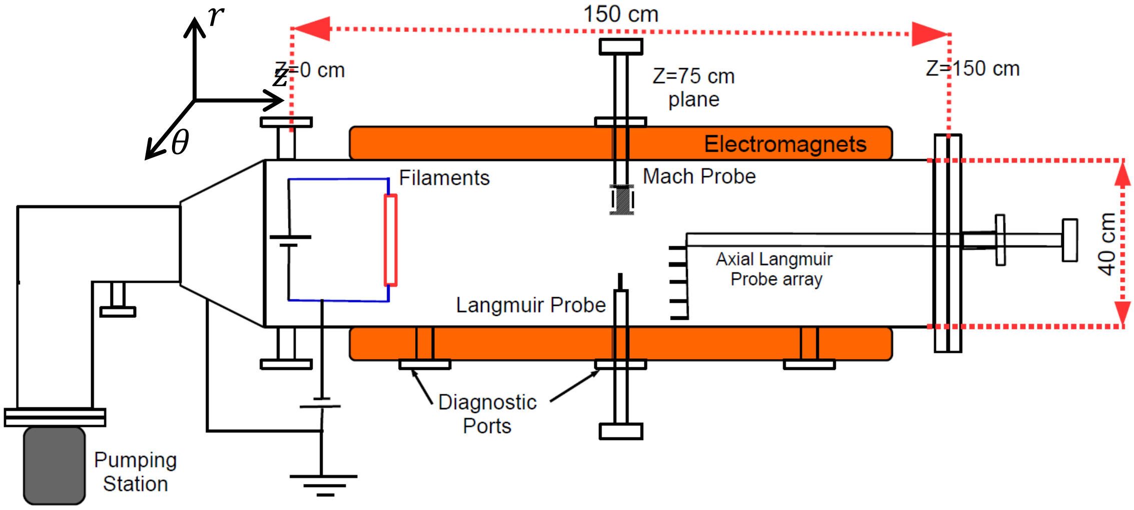

Figure 3.1: Schematic of the side view of the MPD device, electromagnet, and its diagnostics, inset of the figure shows the opted coordinate system of the device. All the measurements have been performed on $z = 75$ *cm.*

3.1.1 Magnetic field configuration

Six electromagnets with 120 cm long rectangular bars of vacoflux-50 embedded in copper coils are installed on the periphery of the cylindrical chamber with 60° azimuthal spacing as shown in cross-sectional view of device [figure 3.2 (a)] [58,115].

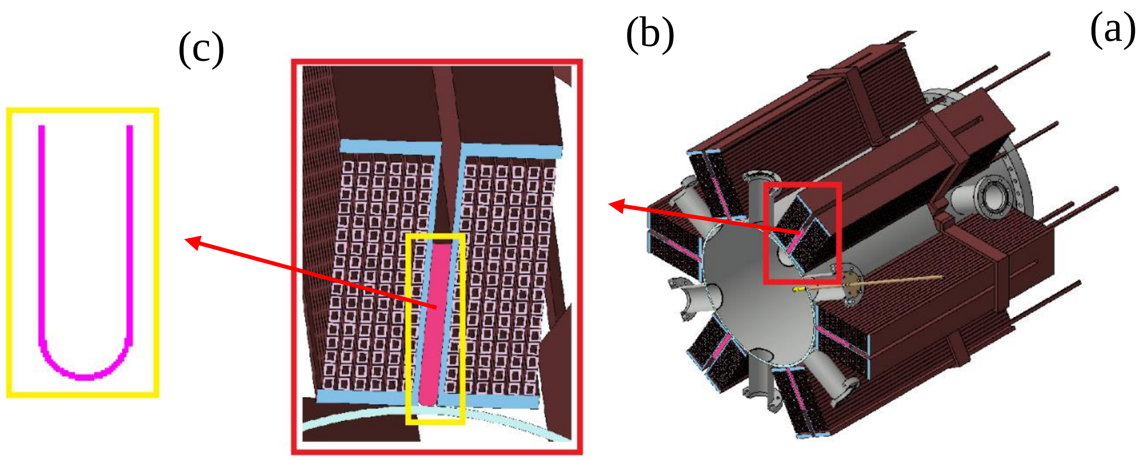

Figure 3.2: (a) cross-sectional view of MPD, it shows six electromagnets with embedded vacoflux-50 core, placed over a periphery of the chamber, (b) cross-section of one electromagnet and, (c) zoomed view of Vaccoflux-50 core material.

In electromagnets, by changing the value of current in copper coils, the cusp field strength can be varied. The current passing through copper coils produces heat, which limits the maximum achievable surface magnetic field value. Hence, cooling of the electromagnets is required. There are different techniques in winding for making electromagnets with active cooling. The double-pancake windings give very effective cooling. In this technique the number of turns of magnets can be broken to different segments such that the forced chilled water goes in parallel scheme and the current goes in series. To avoid the effect of non-uniformity in the windings along the length, the use of an appropriate core material was chosen. The vacoflux-50 is chosen as the core material for its high Curie temperature and high saturation flux density. The vacoflux-50 is an alloy of iron and cobalt in 50:50 ratio. The edge of vacoflux-50 core material is profiled as smooth curvature shape to avoid edge effect on magnetic field lines (shown in figure 3.2 (c)). The unique feature of cusp magnetic field in MPD is the use of profiled core material embedded in copper coils of electromagnets. This allows changing of field values with the effect of using permanent magnets of various surface field strength.

Table 3-1: Magnet System details.

Core material	Vacoflux-50
Relative permeability	>4000
Saturation flux density	2 kG
Curie temperature	>700^0 C
Length of core	120 cm
Width of core	12 cm
Thickness of core	2 cm
Rectangular electromagnet	
Length	130 cm
Width	19 cm
height	14 cm
Power supply features	
Current	160 A
Voltage	60 V

Maximum operating current	200 A (with cooling)

The use of electromagnets in MPD, gives the flexibility to work with different multi-cusp geometries by changing the current directions in the said coils, while the field strength can be varied by changing the current values. It gives us the opportunity to study the effect on plasma parameters for various field values and cusp configurations. The direction of the current in these electromagnets determines the North (N) and South (S) poles of each. In this chapter, the results from two different configurations are presented. The first one is called Six Poles with Six Magnets (SPSM), in which the current in the alternate coils will have opposite directions. Thus, surface of each magnet acts as a pole, hence it will provide six poles as we have six electromagnets. Thus, it is named as six pole six magnet (SPSM) configuration. Alternate opposite directions of current in all six electromagnets give alternate north and south poles.

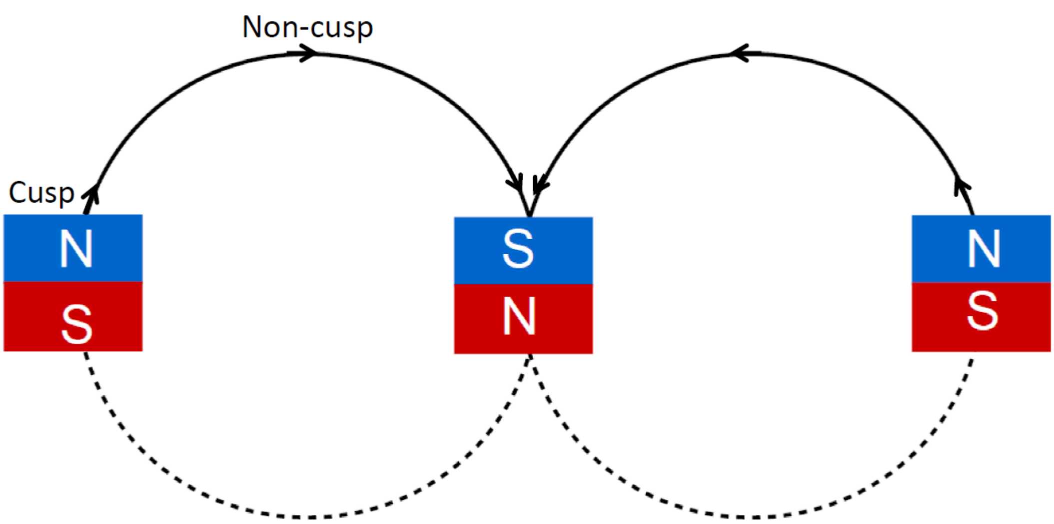

Figure 3.3: Schematic of magnetic field lines when the current direction is alternate opposite in all six electromagnets. This cusp configuration is named as Six pole six magnet (SPSM) configuration.

The schematic of magnetic field lines of alternate north and south poles is represented in figure 3.3. The field lines emerging from north pole converges at the south pole. The surfaces of electromagnets are north or south pole and the regime parallel and near to poles is known as cusp regime. On the other hand, the regime in between two conjugative poles or cusps is noted as non-cusp regime. Both cusp and non-cusp regions are shown in figure 3.3.

A simulation to get a 2D profile of cusp configuration is performed using Finite Element Method Magnetics (FEMM) tool [143]. While performing the simulation, actual dimensions and properties of core material are used as input information along with the copper coils as magnet in FEMM. In FEMM the value and direction of current in coils can be assigned and changed as per the requirement.

The simulated 2D profile of cusp magnetic field for SPSM configuration is shown in figure 3.4.

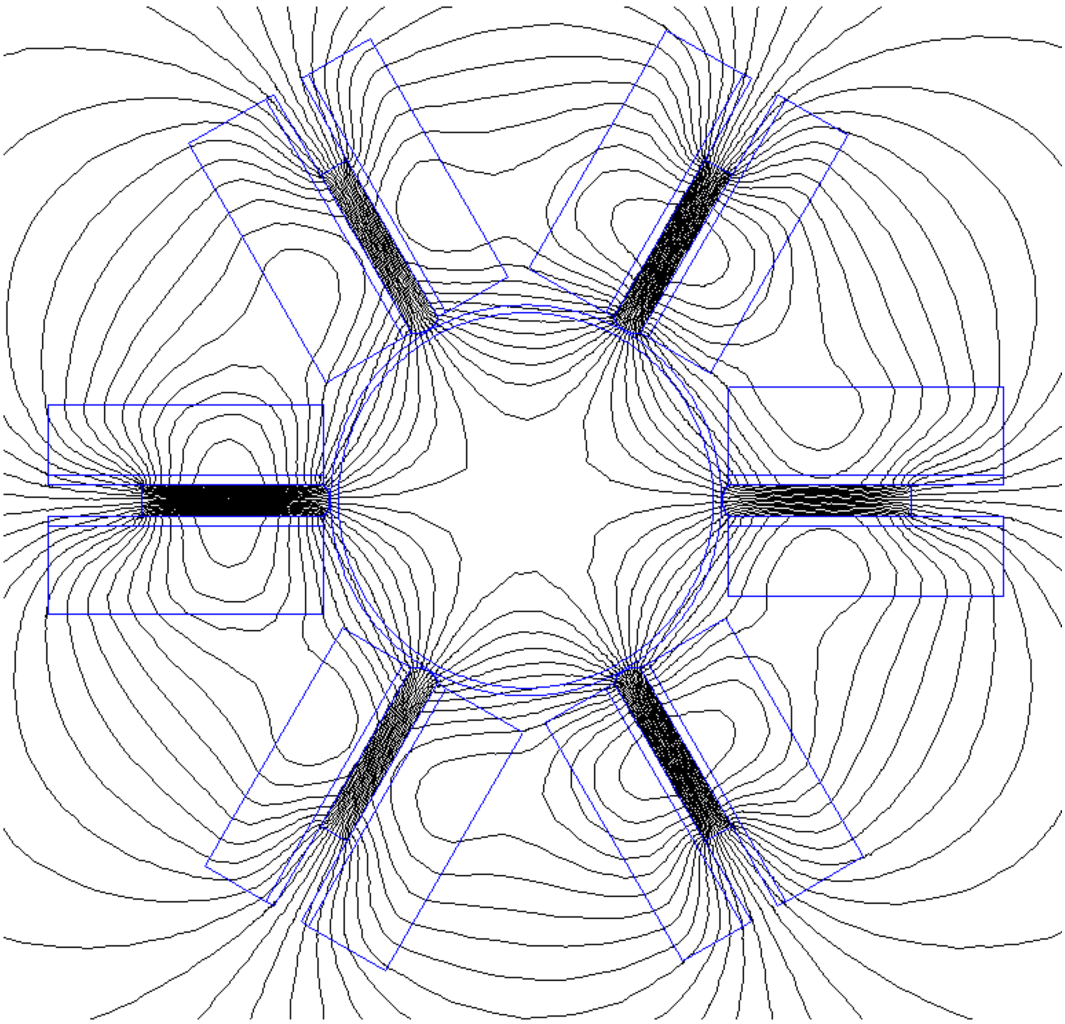

Figure 3.4: Cusp magnetic field profile simulated using FEMM for SPSM configuration.

One configuration SPSM is discussed above and the other configuration is called Twelve Poles with Six Magnets (TPSM) in which the current in all six magnets are in the same direction. The surface of each magnet acts as a pole; hence it will provide six poles as we have six electromagnets. The same direction of current in all six electromagnets creates all six north or south poles at the inner wall of the device. In this configuration, while all the magnets will produce one type of poles, say north-pole, the schematic of magnetic field lines of adjacent north poles is represented in figure 3.5.

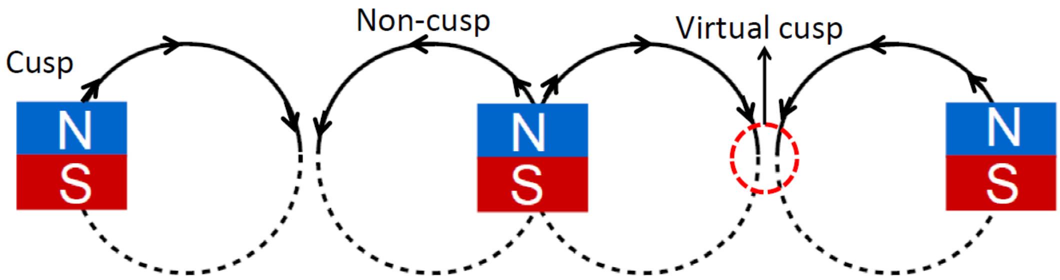

Figure 3.5: Schematic of magnetic field lines when the current direction is alternate opposite in all six electromagnets. This cusp configuration is named as Twelve pole six magnet (TPSM) configuration.

The field lines emerging from north pole tries to converges at the south pole. In this configuration nearest pole is same north. Therefore, while traveling towards south pole, the field lines will be parallel to each other in between two alike poles. This region (in between two alike poles), virtually acts as south pole. The surfaces of electromagnets are north poles. The regime parallel and near to poles is known as cusp regime. On the other hand, the regime parallel to virtual south poles can be named as virtual cusp region. The regime in between two conjugative poles or cusps (and virtual cusps) is noted as non-cusp regime. Cusp, virtual cusp and non-cusp region are shown in figure 3.5. Six virtual complementary poles (south) are created in between the magnets. In this configuration, there are six cusps (north poles) and six virtual cusps, thus having totally 12 poles. Thus, it is named as twelve pole six magnet (TPSM) configuration, produced using same six electromagnets as used in SPSM configuration.

The 2D profile of TPSM configuration, simulated using FEMM is shown in figure 3.6. The simulated cusp magnetic field profile for both SPSM and TPSM (shown in figure 3.4 and 3.6) are produced using same value of current in electromagnets. On comparing the visual look of 2D simulated profile of SPSM and TPSM configuration represented in figures 3.4 and 3.6, it can be noticed that, the field free cusp region is larger in TPSM compared to SPSM. As earlier mentioned, the current value is kept same, while performing the simulation for both the configurations.

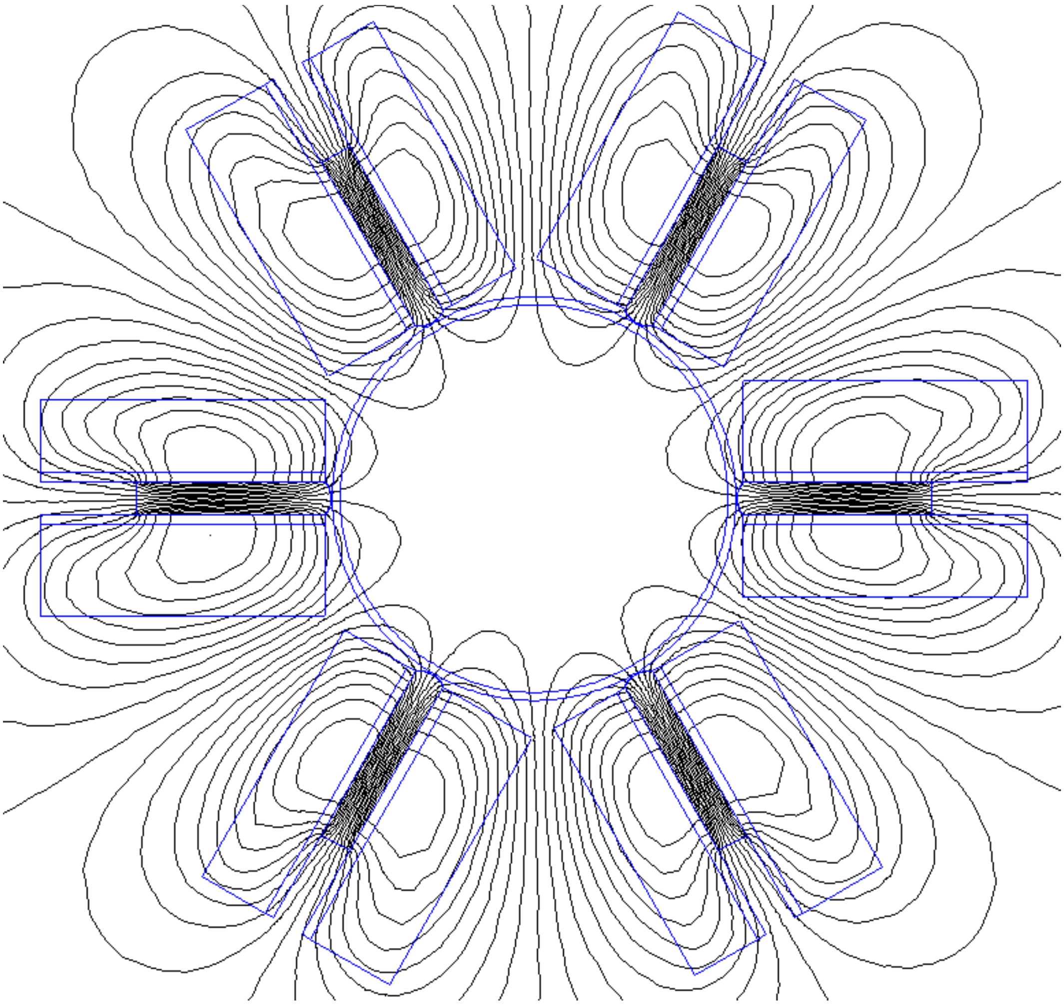

Figure 3.6: Cusp magnetic field profile simulated using FEMM for TPSM configuration.

The simulated profile of cusp magnetic field shows that the field free area is larger in TPSM configuration. Next the magnetic field is measured experimentally, compared and ensured the above observation made based on the simulated cusp field profiles.

The magnetic field is measured over the different (r, θ) planes of the device using triple axis Gauss probe (F. W. Bell, model Z0A99-3202) and suitable Gauss meter (F. W. Bell series 9900). The radial variation of net field values measured using Hall probes for both SPSM and TPSM are shown in figure 3.7. It shows the radial variation of the magnetic field along the cusp region (parallel to the pole) and a non-cusp (in between two poles) regions for both configurations. Radial variation of magnetic field is performed for same value of current passed through the coils in both SPSM and TPSM configurations. The surface value (value at the pole itself) of magnetic field depends on the current flows in coils. Therefore, it is equal for both cusp configurations. The radial profile of cusp magnetic field depends on various factors; in this case it differs with change in number of poles.

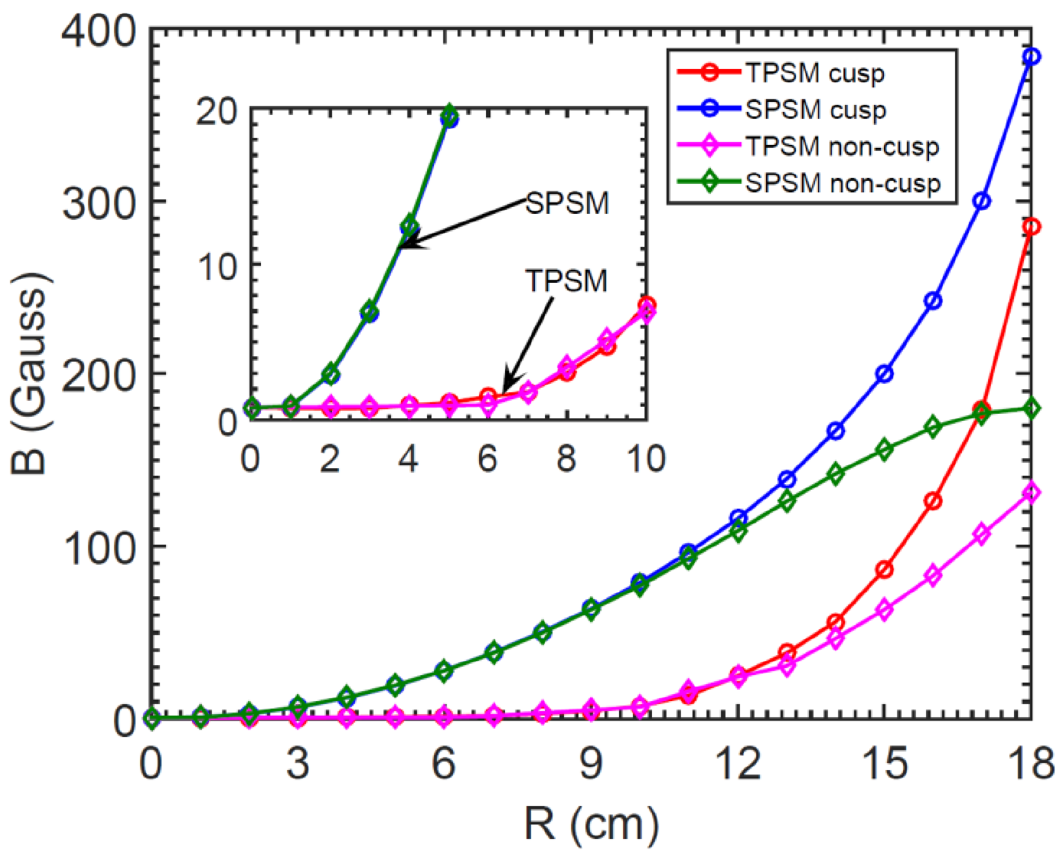

Figure 3.7: Radial variation of magnetic field strength for six pole six magnet (SPSM) and twelve pole six magnet (TPSM) cusp configuration. The non-cusp (the regime from the centre of the device to exactly middle of the two pole surface), and cusp (the region from center of the device to pole of the magnets in TPSM the regime from centre of the device to virtual pole is also cusp regime).

The field strength falls rapidly for TPSM configuration, shown in figure 3.7, as the value of field at R=18 cm is less for TPSM than SPSM for cusp and non-cusp both regions. The subfigure of figure 3.7 represents the variation of magnetic field up to R=10 cm. In TPSM up to R=10 cm, the field value is less than $\sim$ 10 G. In case of SPSM field value is less than $\sim$10 G for R$\sim$4 cm. It can be seen that the net field values for TPSM are less for larger radial extent compared to the SPSM which means the radial extent of nearly field-free region is more in TPSM as expected and also shown by FEMM simulation. In TPSM the magnetic field value is even < 2 G for 8 cm of radial extent.

The net magnetic field B is average of radial and poloidal component of cusp magnetic field B_r and B_θ, respectively, $B = \sqrt{B_r^2 + B_\theta^2}$. In cusp magnetic field the axial z component is non-zero only near both edges of the electromagnets and for rest of the $\sim$ 100 cm device length, B_z is negligible. When we measure the magnetic field strength using Hall probe along the cusp region, B_r gives maximum contribution and B_θ is negligible. In cusp region B_θ comes in picture near to the pole only. Similarly, along the non-cusp region, B_θ gives maximum contribution and B_r stands negligible and comes in picture near to wall of the device only. Therefore, in radial variation of magnetic field profile, the magnetic value in cusp region is measured along the field lines (field varies along B_r) and the magnetic value in non-cusp region is measured perpendicular to the field lines (field varies along B_θ). This is important point to keep in mind, when we discuss the plasma parameters in coming sections.

The photos of the argon plasma in those two configurations (viz. SPSM and TPSM) are shown in figure 3.8, which are taken from the machine end opposite to the source. In figure 3.8(b) and 3.8(d), the bright glow of filaments has been shadowed to capture the feeble light from wings or the cusp regions. Six wings structure representing six cusps in the SPSM (figure 3.8(b)) and twelve of the same (figure 3.8(d)) for TPSM can be seen in the respective figures. It is because the electrons travel along the magnetic field lines thus ionizing and exciting line radiations on the way, till the field lines touch the walls of the vacuum chamber.

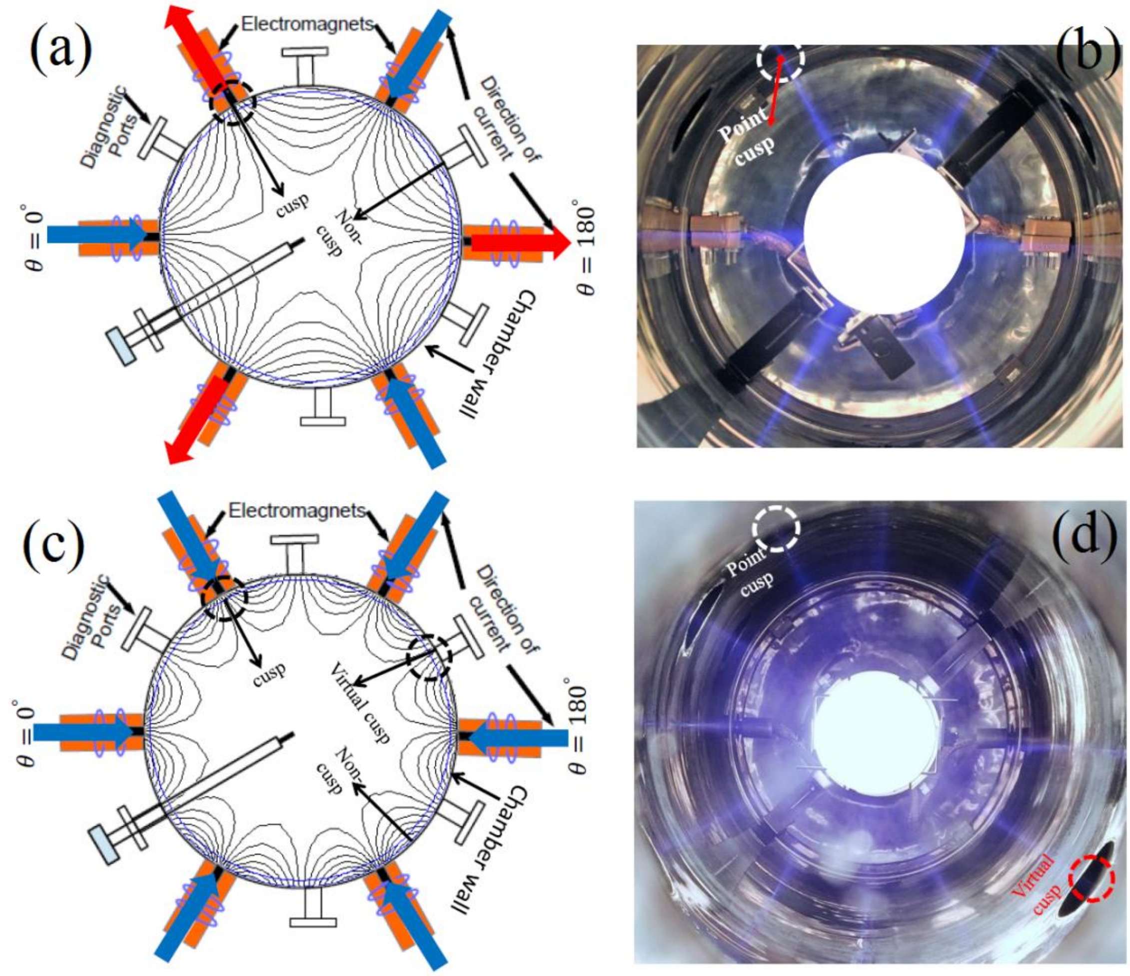

Figure 3.8: (a) and (c) shows the arrangement of electromagnets over the chamber, diagnostic ports, Langmuir probe for diagnostic and magnetic field lines simulated using FEMM in SPSM and TPSM configuration respectively. Arrow in figures shows the current direction in electromagnets. Figure (b) and (d) shows the pictures of plasma confined in SPSM and TPSM observed through the viewport from one end of the device, the center region of bright glow of filaments has been shadowed to capture the feeble light from wings or the cusp regions.

It can also be seen from the photographs that the radial extent of visible light, hence plasma, is more in the TPSM compared to the SPSM. This is because of the more field free region in the TPSM. The figure 3.8 also shows that, plasma confined in cusp configuration, reflects the similar picture as FEMM simulation of magnetic field shows for both the configurations (figure 3.7 (a) and (b) for SPSM and figure 3.7 (c) and (d) for TPSM).

3.1.2 Implemented Diagnostic

The characterization of the plasma in both configurations is done using Langmuir probes and Mach probes. The Langmuir probes are of 1 mm diameter and 5 mm length and are used to deduce the plasma parameters like electron temperature (T_e), plasma density (n), plasma potential (V_p), floating potential (V_f) and fluctuations. The details about the probe measurements and the corrections applied to deduce the respective values are given in the references [16, 20, 21].

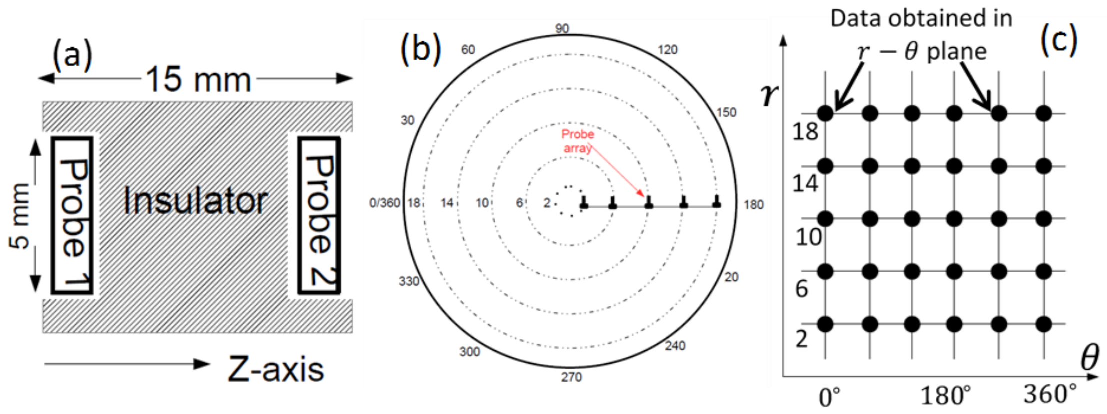

Figure 3.9: Schematic of (a) Mach probe, (b) five radial probe array integrated with a rotatable axial shaft, (c) 2-d measurement in $\boldsymbol{r-\theta}$ plane.

The Mach probe used here is a pair of two disk probes of ϕ5 mm diameter each, separated by a ceramic insulator and is mounted so as to measure the plasma flow in the axial direction (Z-axis) as shown in figure 3.9(a). This probe is constructed and operated according to the details given in the references [144,145]. Probe 1 is upstream collector facing the filaments and probe 2 is a downstream collector in the direction of the Z-axis respectively. The Mach probe is used to determine the radial profile of the axial plasma flow. Both disks are biased to negative potential to measure ion saturation current which will be further used to calculate the Mach number (u_n). The plasma flow (V_d) can be calculated using Mach number (u_n) and ion-acoustic velocity ($C_s = \sqrt{KT_e/m_i}$) measured by Langmuir probe, $V_d = u_n\, C_s$. In Mach probe, area of the collectors should be same. For reliability and authenticity of the results, the probe is rotated by 180° and ion saturation current is measured. The ratio of ion saturation current for both cases, the previous arrangement and after the 180° rotation is compared and found to be the same which implies the equal probe area.

Measurement of the radial variation of plasma parameters along the cusp region of SPSM and the non-cusp region of TPSM is not possible. Electromagnets are aligned on these regions and it is not possible to probe these regions. Therefore, a linear Langmuir probe array is constructed to measure the azimuthal variation of ion saturation current which covers the cusp as well as non-cusp regions of both TPSM and SPSM. This array consists of 5 probes placed at five radial locations with an interval of 4 cm i.e., at R=2, 6, 10, 14, and 18 cm, as shown in figure 3.9(b). This array is mounted on a rotatable axial shaft and the shaft itself is fitted to the endplate of the vacuum chamber such that the shaft is at the center of the device at R=0. This arrangement gives a 2-d measurement on the r-θ plane as shown in figure 3.9(c). The details of the experimental results obtained using the above mentioned diagnostics are presented and discussed in the following section 3.2.

3.2 Characterization of Mean Plasma Parameters

The experiments are carried out for the comparison of SPSM and TPSM configurations, for 2×10^{-4} mbar Argon pressure and -50 V discharge voltage. The radial variation of mean plasma parameters is measured at Z = 75 cm, on the vertical midplane of the device.

3.1.1 Variation of Plasma Parameters with Cusp Magnetic Field Strength at the centre

It is well documented that the cusp magnetic field traps the primary electrons by the mirror effect [52,54,56,146,147]. The number of electrons trapped and their maximum energy for a given discharge conditions depend upon the field strength at the pole cusp which depends on the magnitude of current. If the current passed in both SPSM and TPSM configurations are same in magnitude, the pole strength in each cusp will be same in both configurations. The observed variation of plasma parameters with increasing cusp magnetic field strength measured at R=0 cm for both cusp configurations are shown in figure 3.10. The red line with circle and blue line with diamond shape marker show plasma parameters for TPSM and SPSM, respectively. Figure 3.10(a) shows the variation of floating potential (V_f). The value of floating potential is relatively more negative in SPSM as compared to TPSM for all magnetic field values. It indicates higher confinement of hot electrons in SPSM relative to TPSM. This can also be confirmed in figure 3.10(b), which shows the relative hot electron population for both cusp configurations. The hot electrons density relative to plasma density, $(n_{eh}/n_e) \times 100$), varies from 7%-15% in SPSM and 4%-8% in TPSM. It indicates that SPSM can confine the same amount of hot electrons with a smaller magnetic field. As reported earlier [58] when the cusp field strength increases, the leak width [148,149] of plasma (plasma loss to the chamber wall while following the field lines) decreases. As a consequence, the population of the hot electron increases, which further leads to an increase in the magnitude of plasma density. Plasma density in both cusps increases with an increase in the cusp magnetic field strength as shown in figure 3.10(c). It is clearly observed from the figure, that the values of plasma density are nearly comparable in both cusp configurations for equal cusp magnetic field strength. The variation of plasma bulk electron temperature (T_{ec}) with increasing cusp magnetic field strength is shown in figure 3.10(d).

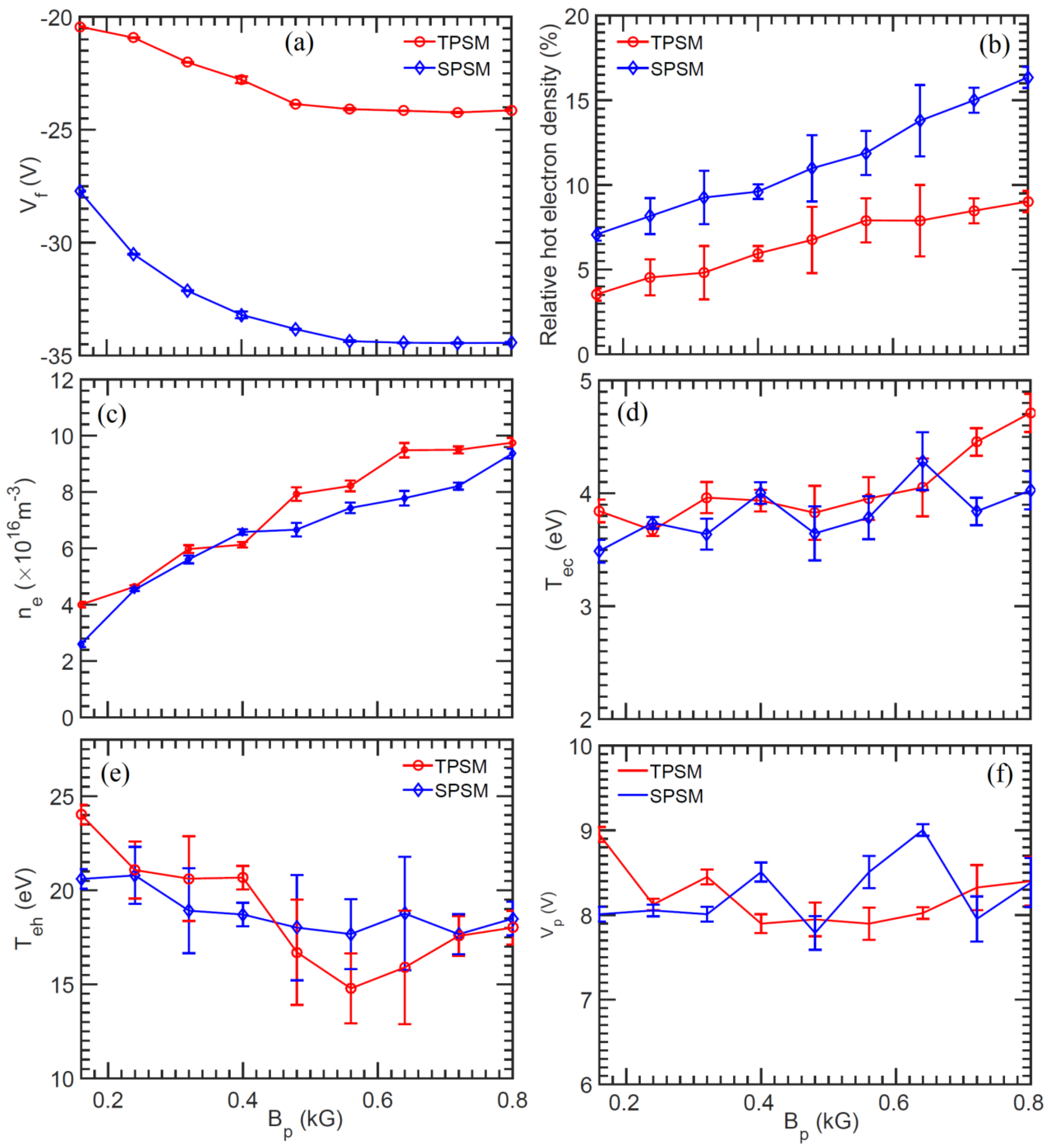

*Figure 3.10: Variation of plasma parameters with various cusp magnetic field strength (a) floating potential ($\boldsymbol{V_f}$), (b) hot electron density ($\boldsymbol{n_{eh}}$), (c) plasma density ($\boldsymbol{n_e}$)***,** *(d) temperature of bulk electron ($\boldsymbol{T_{ec}}$), (e) temperature of hot electron ($\boldsymbol{T_{eh}}$), and (f) plasma potential ($\boldsymbol{V_p}$) measured at* ***R=0 cm****, for SPSM and TPSM cusp configuration at* $\boldsymbol{2 \times 10^{-4}}$ ***mbar*** *pressure and* ***-50 V*** *discharge voltage.*

The bulk electron temperature does not vary much with respect to cusp magnetic field strength and it is nearly same for both TPSM and SPSM. It suggests that the physical mechanism that governs the electron temperature in plasma is likely to be independent of the magnetic field. The variation of hot electron temperature (T_{eh}) with increasing cusp magnetic field strength is shown in figure 3.10(e). It does not vary much with respect to cusp magnetic field strength and is comparable for both TPSM and SPSM. The energy of hot electrons depends upon the discharge voltage and neutral density. Both parameters are kept constant at -50 V and 2×10^{-4} mbar for both types of configurations. Therefore, the temperature of hot electrons does not vary with the cusp magnetic field. The plasma potential (V_p) is also nearly constant with the variation of cusp magnetic field strength in both configurations and it is observed to have similar values, as shown in figure 3.10(f).

From figure 3.10, it can be observed that confinement of hot electrons is higher in SPSM compared to TPSM. It suggests more ionization of neutral Argon particles in SPSM leads to enhancement in plasma density but figure 3.10(c) shows the comparable values of density in both cusps. This is discussed in details later. The various other plasma parameters such as electron temperature and plasma potential show comparable values for both cusp configurations and follow the similar trend with increasing cusp magnetic field strength.

3.1.2 Azimuthal Variation of Ion Saturation Current

In SPSM, there are six cusp regions and six non-cusp regions, and the data is obtained at 12 azimuthal locations. In TPSM, there are six cusp, six virtual cusp and twelve non-cusp regions and the data are obtained at 24 azimuthal points. The probe array is used to measure the azimuthal variation of ion saturation current at all cusp and non-cusp regions for five radial locations at Z=75cm. The measured profile of azimuthal variation of ion saturation current is shown in figure 3.11(a) and 3.11(b) for SPSM and TPSM respectively. The X-axis of both figures represents azimuthal locations in θ coordinates.

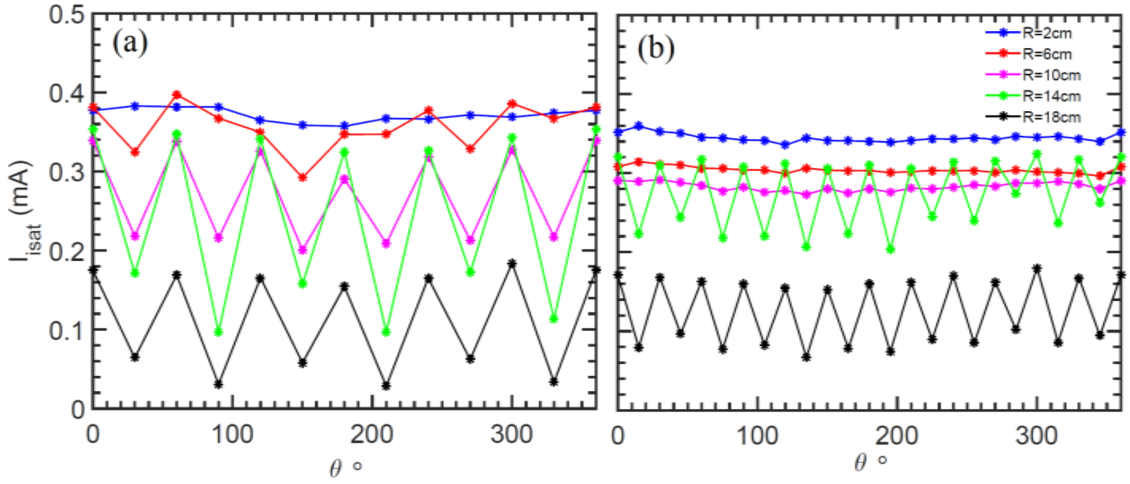

Figure 3.11: Azimuthal variation of ion saturation current (a) in SPSM, and (b) TPSM for five radial location R=2, 6, 10, 14, and 18 cm, measure at Z=75 cm, midplane of the device for $\mathbf{2\times 10^{-4}}$ *mbar, -50 V discharge voltage and* $\boldsymbol{B_p} = \mathbf{400}$ *Gauss.*

Figure 3.11(a) shows the values of ion saturation current do not vary much azimuthally, traversing from cusp to non-cusp regions for R=2 cm. Beyond R=2 cm, at all other radial locations, the values changes noticeable at the cusp and non-cusp regions. It can be observed from figure 3.11(b) that in TPSM at R=2, 6, and 10 cm, values of ion saturation current do not vary much azimuthally, traversing from cusp to non-cusp regions. At R=18 cm, it can be observed that the value of ion saturation current is higher in the cusp region (0.18 mA) but it falls down in non-cusp region (0.08 mA) while the values are changing for cusp and virtual cusp regions. From figure 3.11, it can also be observed that the decrease in ion saturation current from cusp to non-cusp is observed to be larger in SPSM (~0.18 to ~0.02 mA) compared to TPSM (~0.18 to ~0.08 mA).

The figure 3.11 is linear representation of azimuthal variation of I_{is}. For better understating and picturization of azimuthal profile of I_{is}, the I_{is} is plotted in polar coordinates. While plotting in polar coordinates the actual values of I_{is} are not considered and the figure is a mere pictorial representation as shown in figure 3.12. The pictorial representation is only to compare the uniform area of I_{is} in both SPSM and TPSM configurations.

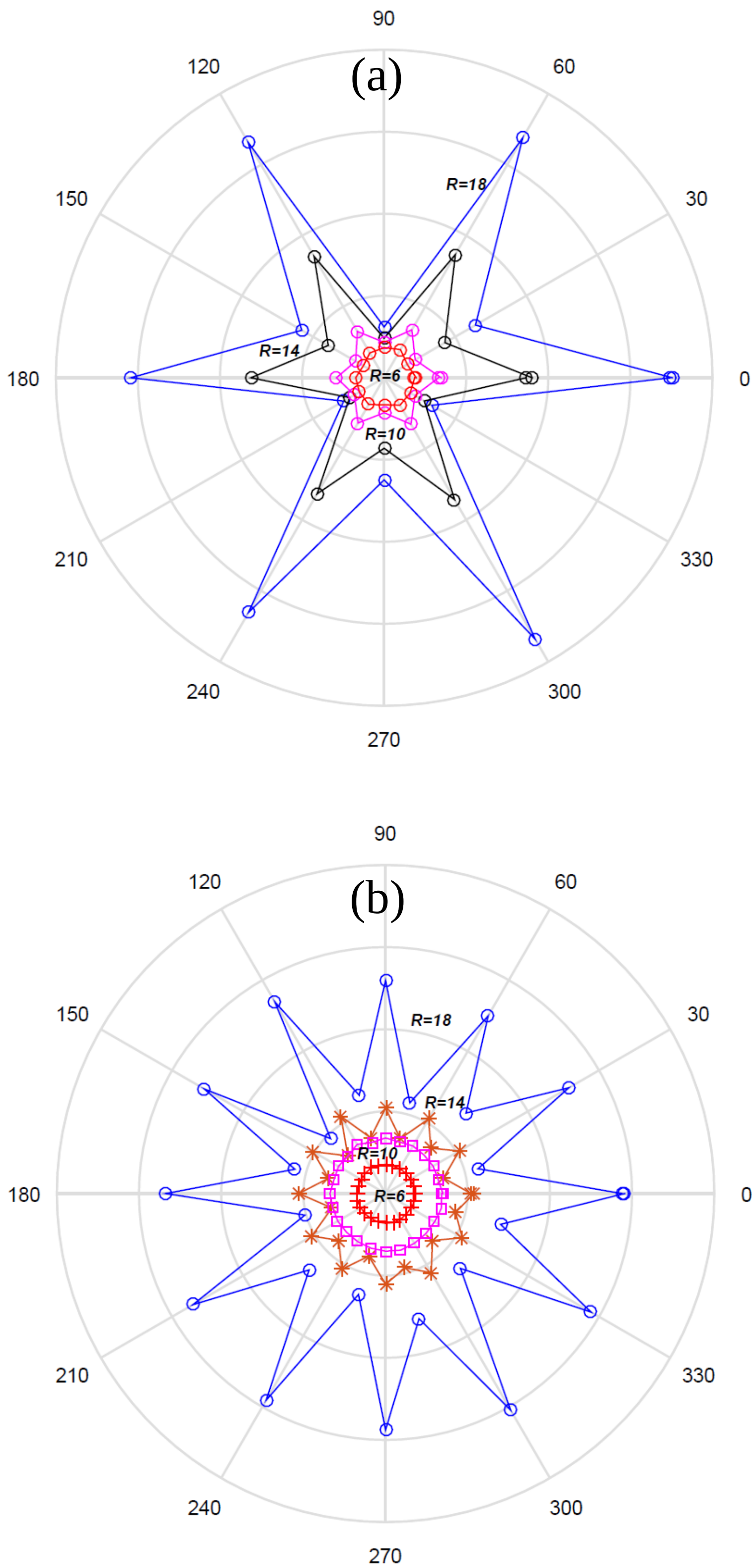

Figure 3.12: Azimuthal variation of ion saturation current for (a) SPSM (b) TPSM cusp configuration, showing in form of polar coordinates.

Figure 3.12 (a) shows the azimuthal variation of I_{is} for SPSM configuration and figure 3.12 (b) represents the profile for TPSM. The color code is kept same in both figures for easy comparison.

The azimuthal values of I_{is} measured at R=2 cm is both incorporated in figure 3.12. Since, it is already shown in figure 3.11 that at R=2 cm, the variation of I_{is} is uniform for both configurations. This shows the volume of uniform plasma in the TPSM is larger than the volume in SPSM which matches with the field free region volume.

3.1.3 Radial Variation of Plasma Parameters

The radial measurement is only possible in between two consecutive magnets, due to the limitation of the device. The location of the radial measurements is shown in figure 3.8(a) and 3.8(c), this location is a virtual cusp region in TPSM and non-cusp region in SPSM. The non-cusp region of TPSM and cusp region of SPSM are not accessible radially; therefore, the axial probe array is used to measure plasma parameters in these regions but only at five radial locations. The radial profiles of cusp magnetic field and plasma density for both types of cusp configurations are shown in figure 3.13. The radial profile of cusp field is shown in figure 3.13 (a), 3.13(b) for SPSM and TPSM, respectively. The radial profiles of plasma density are shown in figure 3.13(c) and 3.13(d). In SPSM, $< 5\%$ variation in density is observed upto R$\sim$4 cm, as shown in figure 3.13(c). The plasma density is nearly constant and varies $< 5\%$ upto R$\sim$10 cm for TPSM which corresponds to the respective field free region for the same configuration (shown in figure 3.13 (b)). Beyond this spatial location, the plasma density gradually decreases towards the chamber wall as shown in figure 3.13(d). The density has a sharper gradient for non-cusp region of SPSM compared to TPSM. A dotted line is drawn in figure 3.13 (a) and (c) at R=4 cm, the radial extent upto which the density is uniform and plasma is nearly field free in SPSM.

Similarly, a line is drawn in figure 3.13 (b) to 3.13 (d), at R=10 cm upto which the density is uniform and plasma is nearly field free in TPSM.

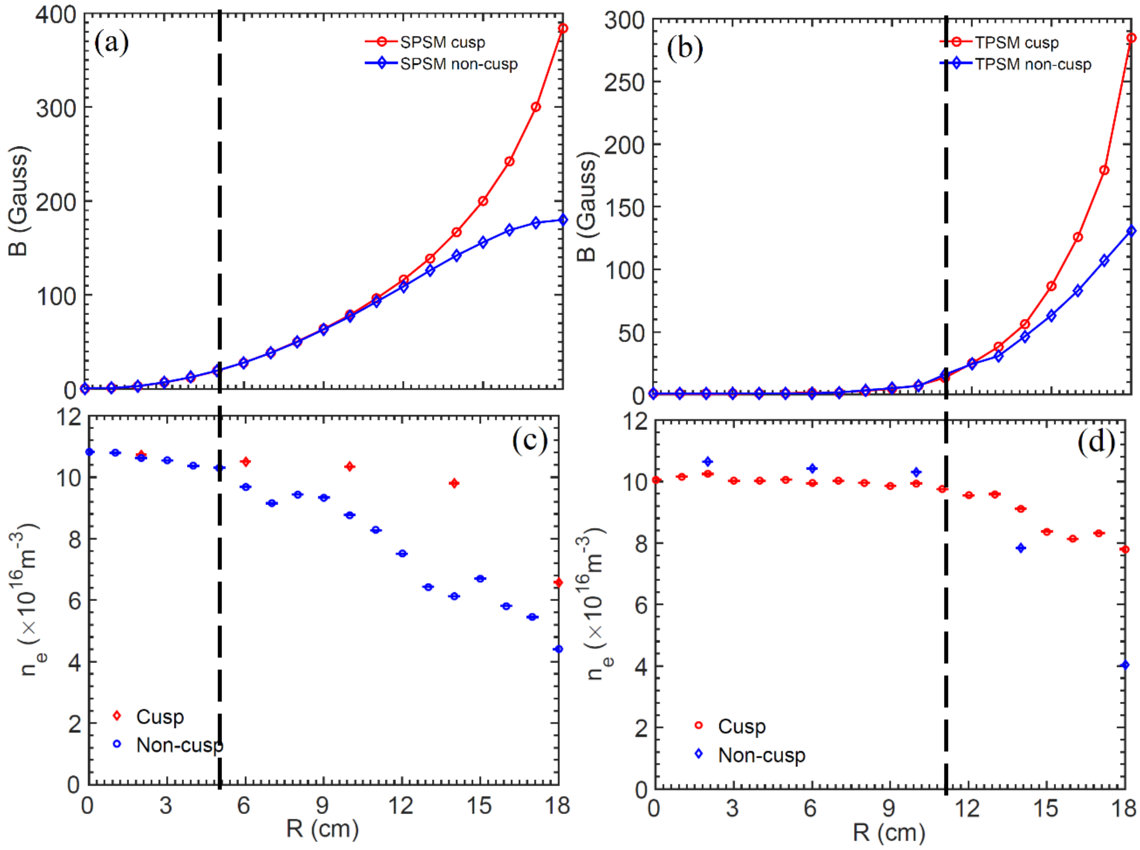

Figure 3.13: Radial variation of (a), (b) plasma density, n, (c), (d) bulk plasma electron temperature, $\boldsymbol{T_e}$, and (e), (f) plasma potential, $\boldsymbol{V_p}$, for SPSM and TPSM respectively. $\boldsymbol{B_p} = \mathbf{800}$ Gauss, $\mathbf{2 \times 10^{-4}}$ mbar pressure, and $\mathbf{-50}$ V discharge voltage.

Figure 3.14(a) shows the radial variation of electron temperature in SPSM configuration. In cusp region, the temperature is nearly constant and shows a shallower gradient after R~10 cm. On the other hand, in non-cusp region of SPSM the temperature has a sharp gradient around R~4 cm to 10 cm and becomes flat near to R~14-18 cm. Figure 3.14(b) shows the radial variation of electron temperature for TPSM, which suggests that the bulk electron temperature is nearly constant upto R~10 cm in both cusp and non-cusp regime and then it has a shallower gradient around R~12 cm in cusp region and fast fall is observed in non-cusp region. In non-cusp regime of SPSM, the R~4 cm and R~10 cm for TPSM non-cusp regime is where the magnetic field start filtering out the primary high energetic electrons and the bulk plasma electrons diffuses through these field lines working as magnetic filter layers for energetic electrons. As the magnetic field strength increases the energetic electrons can travel less distance across the magnetic field lines and the temperature or energy of electrons keep on reducing [150]. In other words, energy of electrons allowed to diffuse across the magnetic field lines is inversely proportional to magnetic field strength, depending upon the Larmor radius. So as the cusp magnetic field strength increases radially outward, the probability of electrons with high temperature reduces. On further going radially outward it shows saturation in electron temperature and the only species found here is low temperature diffused electrons.

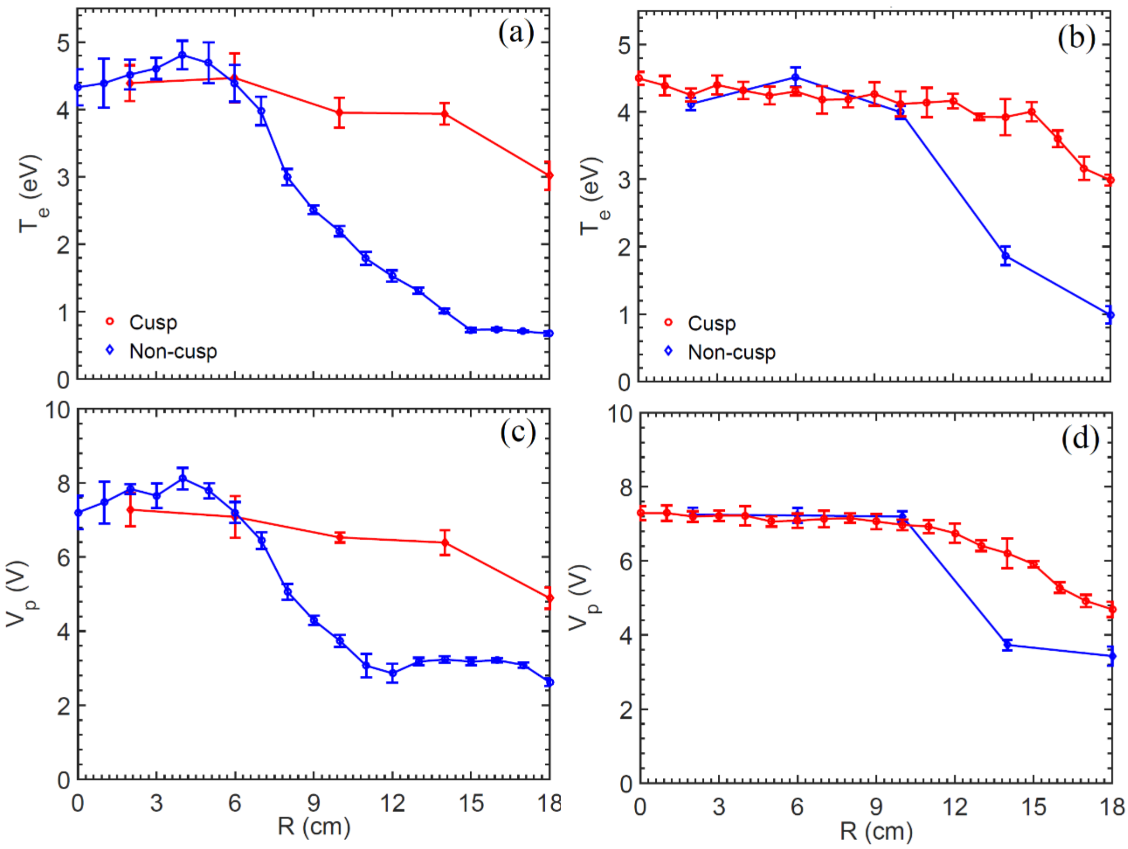

Figure 3.14: Radial variation of (a), (b) bulk plasma electron temperature, $\boldsymbol{T_e}$, and (c), (d) plasma potential, $\boldsymbol{V_p}$, for SPSM and TPSM respectively. $\boldsymbol{B_p = 800}$ Gauss, $\boldsymbol{2 \times 10^{-4}}$ mbar pressure, and -50 V discharge voltage.

It is reported in earlier work that the electron temperature across the cusp magnetic field [37,151–154], produced by permanent magnets or the electromagnets [155,156], reduces remarkably. Reduction in electron temperature across the cusp is a result of transport of electrons across the perpendicular magnetic field, which is dependent on the energy of the electrons. The plasma potential shown in figure 3.14(c) and 3.14(d) shows a similar trend as the electron temperature in both cusp configurations. It is uniform up to R∼10 cm in cusp and non-cusp region of TPSM and decreases gradually in cusp region compared to non-cusp. Plasma potential is used to estimate the electric field in plasma. The radial profile of plasma potential suggests, that radial electric field is either not present or it is very feeble up to R∼10 cm in TPSM followed by a very weak gradient outboard for other radial locations. The non-cusp region of SPSM has a sharp gradient in electric field from R∼4-10 cm and it is negligible afterwards. From figure 3.13 and 3.14, larger radial extent of uniformity in all plasma parameters is observed in TPSM (R∼10 cm) in comparison to SPSM (R∼4 cm). The plasma production with permanent magnets has not been attempted in this device and only electromagnets have been used. A large volume, quiescent plasma confinement device by using multi-dipole magnetic field geometry was first reported by (Limpaecher and Mackenzie 1973) [157]. Multi-dipole devices with permanent magnets show that the main contribution to enhancement in density comes from the confinement of primary electrons and increase in their path length before they are lost to the wall. The increase in density is also due to the increased electrostatic confinement for ions in the steady state, and an increase in the plasma production by a factor of 2-3 [77,146,157,158]. Two subtle differences between our device and other multi-dipole devices are (1) use of line cusps in our device as opposed to large number of cusps in other devices and (2) the location of filaments for producing plasma. The filaments in our device are located at one end of the vacuum chamber, whereas, in other devices the filaments are placed near the surface. A large field free region and a large volume of quiescent plasma in the field free region are characteristics of both type of devices, although in our device, the use of electromagnets facilitates change of number of poles [159] and the strength of magnetic fields in cusp regions. In summary, the plasma parameters shows nearly uniform nature up to the field free region of the device [148,157,160].

3.2 Characterization of Plasma Fluctuations

3.2.1 Quiescence Level

The level of fluctuation in plasma density is measured for both configurations and its radial variation is shown in figure 3.15.

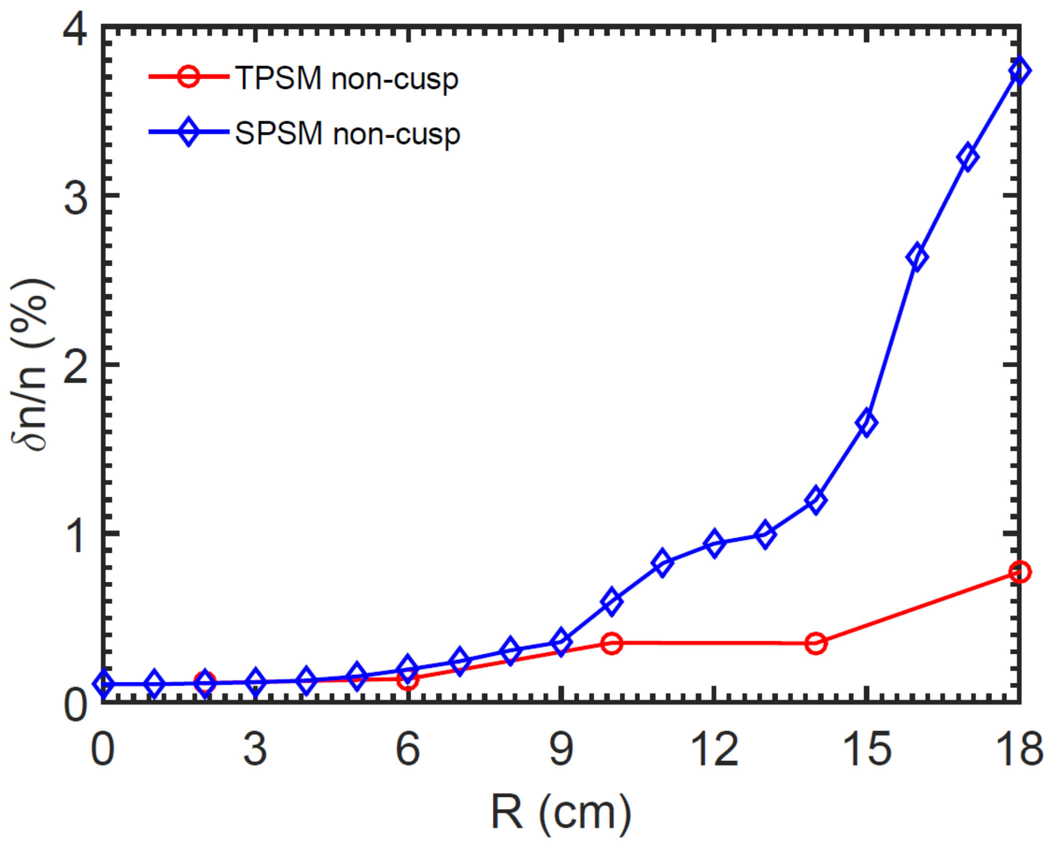

Figure 3.15: Radial variation of level of fluctuation in plasma density measured for pole cusp magnetic field $\boldsymbol{B_p = 800}$ *Gauss,* $\mathbf{2 \times 10^{-4}}$ *mbar pressure and* $\mathbf{-50}$ *V discharge voltage. The line with circle is for TPSM and line with diamond shape marker is for SPSM.*

The figure 3.15 shows the relatively lower (< 0.1%) values of level of fluctuation in density for both configuration up to the radial extent of ~4-5 cm. The level of fluctuations in SPSM increases radially outward from R~4-5 cm, rising sharply near to wall of the device. The level of fluctuation in TPSM has a constant low (<0.1%) values up to R~14 cm rising to

~0.8% towards wall of the device. The radial extent where the plasma density variation is uniform and <5%, the density fluctuation is $< 0.1\%$ and uniform. The value of level of fluctuation near to chamber wall at R=18 cm is less in TPSM ($\sim$ 0.8%) compared to SPSM ($\sim$ 4%). A detailed study of density fluctuation in SPSM near to wall is reported earlier [142], in which the presence of drift wave due to the gradient in plasma density is observed in non-cusp regime. In non-cusp regime of SPSM, the plasma density has a gradient from R=12 to 18 cm and in that similar radial extent the electron temperature is nearly flat in comparison to the density gradient. This supports the excitation of drift wave instability. On the other hand, in TPSM the density gradient and temperature are nearly similar and it cannot support the drift wave excitation. To ensure this, the same experiment is carried out in non-cusp regime of TPSM to determine the nature of fluctuations and to explore the presence of the drift wave mode. The density fluctuation is measured from the ion saturation current fluctuation, using a Langmuir probe. The auto power spectra of density fluctuation, measured at R=14 cm in non-cusp regime of both configurations, is presented in figure 3.16, for pole magnetic field B_p=800 Gauss. The density power spectrum shows a peak at 10 kHz for SPSM confirming the presence of drift wave while no signature of drift wave is observed in TPSM. The same measurement is performed in the cusp regime of both configurations as well as for the virtual cusp of TPSM. The signature of the drift wave is not observed in the cusp regimes.

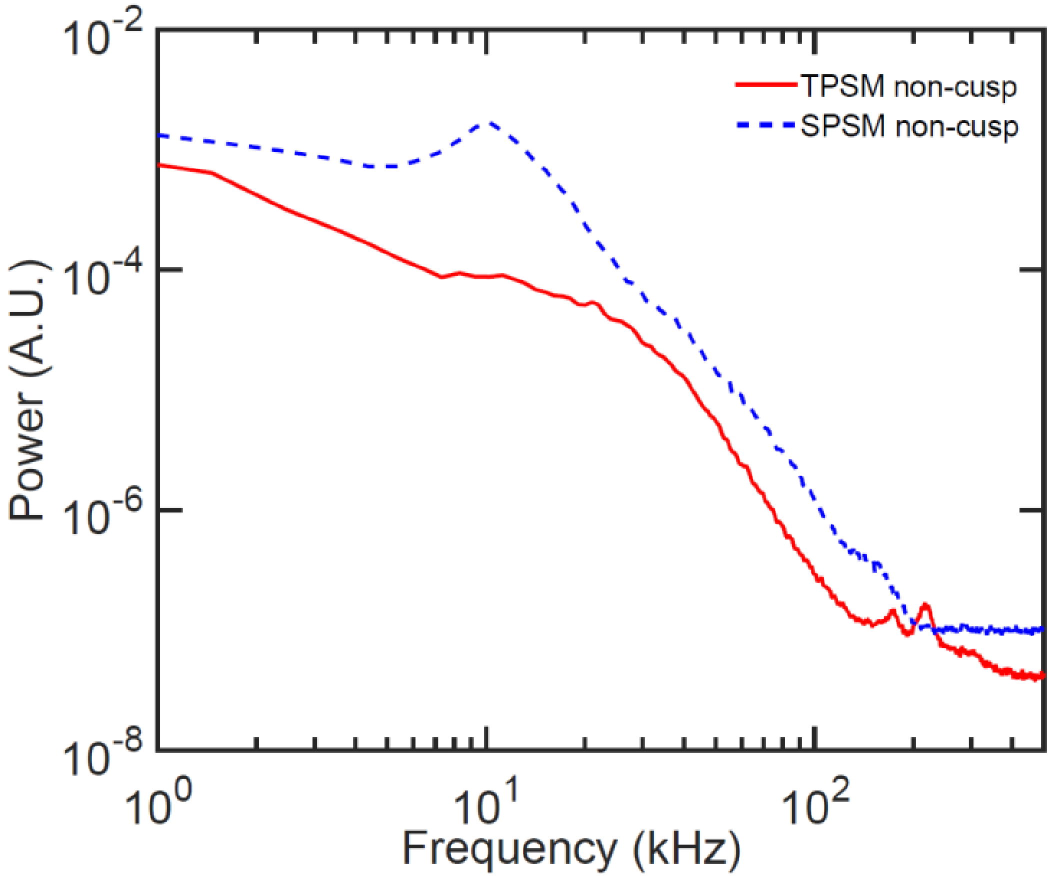

Figure 3.16: Auto-power spectrum of density fluctuation at $\boldsymbol{R} = \mathbf{14}$ *cm, for pole cusp magnetic field* $\boldsymbol{B_p} = \mathbf{800}$ *Gauss.*

It can be explained by observing the radial profiles of plasma density and azimuthal profile of ion saturation current that the gradient in the profiles of TPSM is relatively weak to excite any gradient driven fluctuation like the drift wave observed in SPSM.

3.2.2 Axial Plasma Flow

The net axial plasma flow (V_d/C_s) is measured using Mach probe and the results are shown in figure 3.17. It is observed that the net axial flow in the centre of the device is negligible i.e. $< 0.1C_s$ for both cusp configurations. As we move radially outboard the axial flow increases in SPSM, while it remains constant in TPSM.

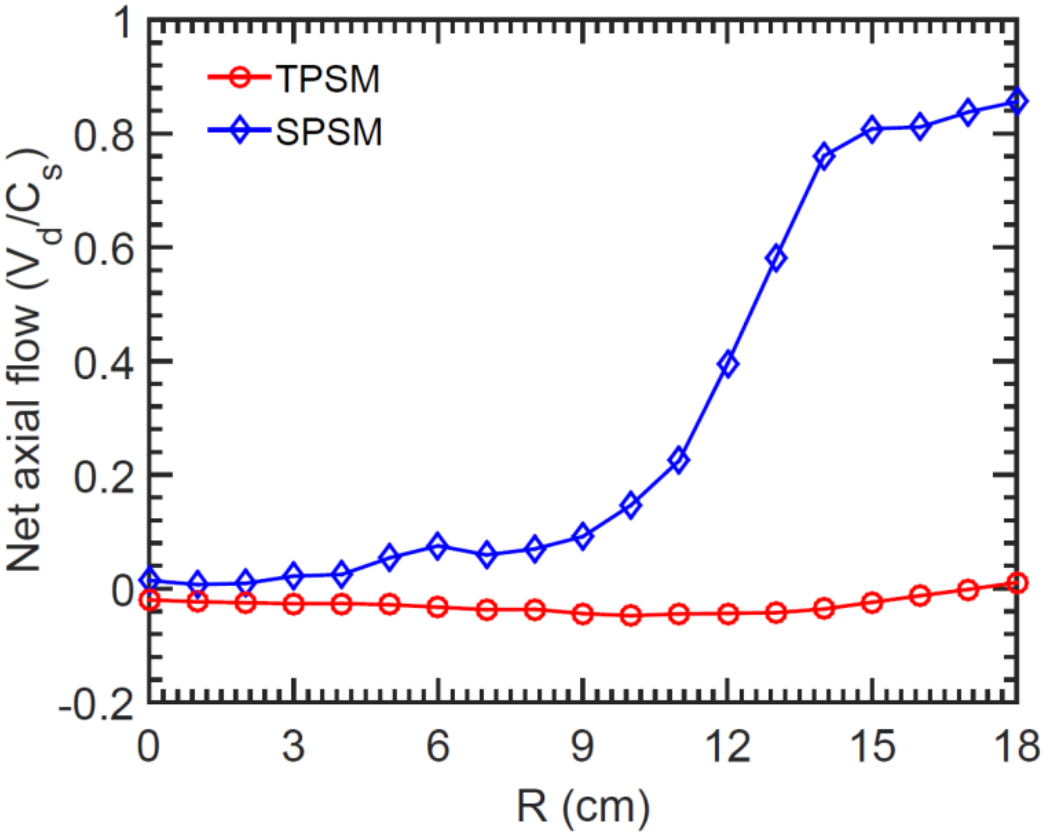

Figure 3.17: Radial profile of net axial plasma flow measured using the Mach probe, for pole magnetic field $\boldsymbol{B_p} = \mathbf{800}$ *Gauss.*

The net axial flow in TPSM is <$0.02C_s$ throughout the radial extent while for SPSM net axial flow increases sharply from $\sim R = 8\ cm - 18\ cm$. The flow driven by drift wave is found along the Z-axis as reported in earlier work [142]. The driver of the mechanism behind this observation is found to be a radial density gradient. In earlier reported work it has been discussed in detail [142]. In TPSM the absence of the driver leads to negligible axial flow. It also shows that, when plasma is confined in TPSM, there is no background axial flow. The value of net axial flow for TPSM is < 0.02 and it falls within the limit of error.

3.3 Discussion

The advantage of cusp magnetic field over conventional magnetic field configurations is the confinement of primary electrons. Primary electrons trapped along the cusp field lines are forced to spend a longer time inside plasma. The primary electrons follow the cusp field and get reflected from the magnetic mirror field at the poles of magnets. In this way, they bounce back and forth before escaping to wall. The increase in cusp field increases their path length and flight time. Following this procedure as the cusp magnetic field strength increases, the path length of primary electrons increases, hence the confinement of primary electrons enhances. A simple indicator for the confinement of primary electrons is the enhanced negative value of floating potential in plasma.

As it is observed in experimental results, when the plasma parameters are compared for SPSM and TPSM, the floating potential profile shows more confinement of primary electrons in SPSM than in TPSM (figure 3.10(a,b)). The increased confinement of primary electrons leads increase in ionization in SPSM as compared to TPSM. Therefore, the plasma density in SPSM is expected to be higher than the value of plasma density in case of TPSM. Our experimental observation shows comparable plasma density in both configurations (figure 3.10(c)). M. Q. Tran in 1974 [35] has observed the same plasma density, he argued that, the ionization length in TPSM is nearly twice to SPSM and it makes the plasma density comparable in both cusps. Leung et al., in 1975 [36] has performed the study on three cusp geometries. Leung et al., argued that Tran used the magnets over the periphery of the device instead of covering the complete enclosure of the device and observed the comparable plasma density. In the main cylindrical device of MPD the electromagnets are embedded only on the outer periphery of the cylinder as shown in figure 3.1, no magnetic trap is used for the end blank flange and behind the filaments for confinement of electrons emitting from hot cathode filaments. Hence the MPD has no confinement mechanism for plasma loss at the two ends of the device. We also support the argument of Tran for enhancement of primary electrons path length in TPSM as it has twelve cusp regimes to trap the primary electrons and it is six in SPSM. The enhanced fluctuation in plasma density in SPSM indicates more loss of plasma and the increased path length of primary electrons suggests the increase in ionization in TPSM. These device and plasma characteristics make the plasma density comparable in SPSM and TPSM, despite of the number of loss cones. The level of fluctuation in density shows significant enhancement of fluctuations in SPSM. It leads to more plasma loss in SPSM due to plasma density fluctuations. The observation of level of fluctuation in density supports the observation of same density in both configurations, since plasma loss is more in SPSM and it makes the density in SPSM comparable to density in TPSM. The more detail study on fluctuations is discussed in earlier work reported by [Patel et al., POP, 2019]. The experimental observation of significant enhancement of level of fluctuation in SPSM, increase in path length of primary electrons in TPSM and the two end plates without any confinement mechanism are the possible cause for the observation of comparable plasma density in SPSM and TPSM. A more detail study on the loss mechanism of plasma in both the configuration is required to accurately describe this phenomenon.

3.4 Summary

The detailed observation of variation of plasma parameters in SPSM and TPSM configurations is carried out. It provides very strong evidence that the magnetic field profile plays a crucial role in the formation of mean plasma profile, plasma fluctuations, and transforming the plasma characteristics. TPSM has larger field free volume and shows more radial uniformity in plasma density with $< 5\%$ variation for the circular area with $R \sim 10$ cm and $\delta I_{isat}/I_{isat} < 1\%$ throughout the plasma. The azimuthal uniformity for a circular area of $\sim$10 cm radius, absence of drift wave mode, absence of any background plasma flow and fluctuations makes the ideal plasma background to excite any wave mode or perturbation. The examination of plasma parameters suggests that the plasma confined in TPSM is more uniform and quiescent. It is one of the best configurations for the fundamental plasma study such as excitation of plasma waves, the study of wave-particle interaction, Landau damping etc.

Chapter 4

Basic Ion Acoustic Wave Perturbation

4.1 Introduction

Perturbation of the plasma using a known perturbation method and study how the plasma responds to this perturbation is one of the objectives of this thesis. There are many ways to perturb the plasma as reported in literature. Low frequency ion-acoustic (IA) wave is one of the well documented methods to perturb the plasma. Ion Acoustic (IA) waves are low-frequency electrostatic, longitudinal waves in plasma.

In this chapter, after a brief about the requirements for a reasonable potential perturbation for the IA wave, like the frequency, the voltage magnitude, the voltage required for overcoming the sheath etc. has been given. Then the IA wave exciter used in MPD and its basic characteristics like the size and opacity of the exciter grid, etc. are given in detail. The details about the IA wave exciter circuit and signal receiver directional probe are also added in this chapter. The basic launching and detection and the method to infer the required information like wave velocity, propagation length etc. are given here.

The ion-acoustic wave propagation study is performed in a cylindrical **M**ulti-pole line cusp **P**lasma **D**evice (MPD) [67,68]. This device has facility to operate with or without magnetic field, and for present experiments the MPD is used as an unmagnetized linear plasma device. The schematic of the experimental setup shown in figure 4.1. The schematic (presented in figure 4.1) shows the side view of the device with the arrangement of wave exciter set up integrated with the device.

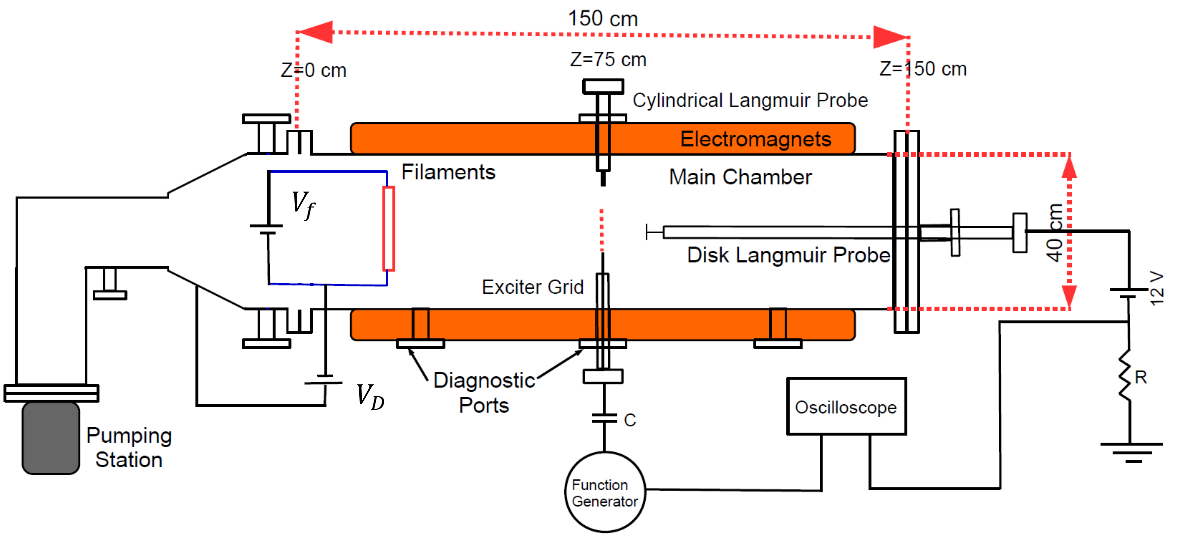

Figure 4.1: Schematic of the Experimental Device and exciter circuit.

The plasma parameters such as plasma density (n_e), electron temperature (T_e), plasma potential (ϕ_p), and floating potential (ϕ_f) are measured by using Langmuir probe (LP) [122].

Next, we will discuss the new integrated part to the MPD device to excite the IA wave in detail.

4.2 Wave Excitation

Several techniques have been reported to excite the IA wave, excitation by modulation of magnetic field [35], electrostatic excitation outside the plasma [36,37], excitation through a grid placed inside the plasma column [38]. After Hata first introduced the grid technique, it has been used extensively for externally controlled IA experiments [39] and we are using the same technique.

A circular grid is installed at $R = 0$, $Z = 75$ cm, at the center of the device, shown in Figure 4.2 (a). This exciter grid is made of a stainless steel (SS304) mesh of 50 mm diameter and made out of a wire of diameter 0.08 mm and 0.3 mm aperture (space between the two wires), with 85% transparency. Actual picture of the exciter grid is shown in figure 4.2 (b).

This exciter grid is inserted in the device through a radial port using a feedthrough, it is placed at Z=75 cm, middle plane of the device centred at R=0 cm as shown in figure 4.2 (a). An enameled copper wire and coaxial Teflon cable (of < 70 cm length) is used to carry the signal to the exciter grid covered by insulated ceramic tube, as shown in figure 4.2 (b).

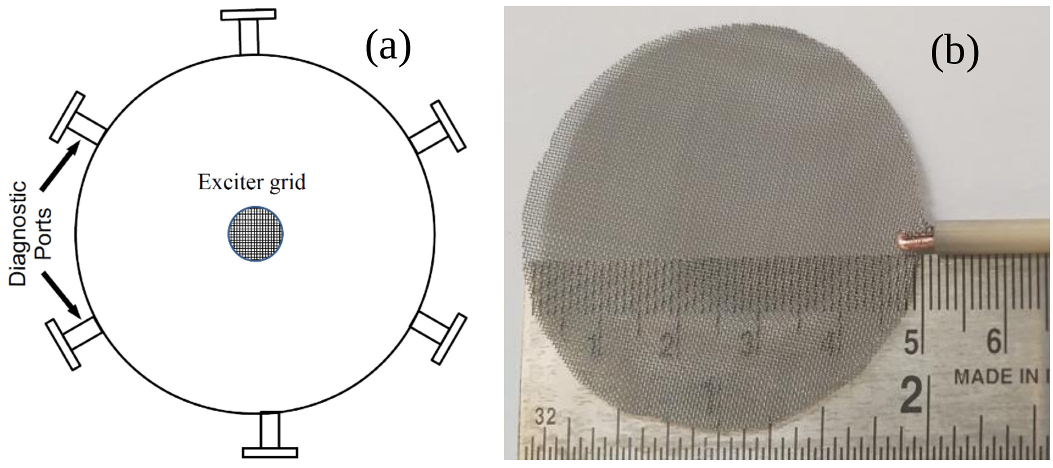

Figure 4.2: (a) cross-sectional view of MPD showing the location and dimension of exciter grid, (b) actual picture of exciter grid made of SS-304 with 50 mm diameter, 0.3 mm aperture width.

To excite the IA wave in plasma through the grid, we need to apply some potential on the gird. A schematic is shown in figure 4.3 after applying a potential on the exciter grid.

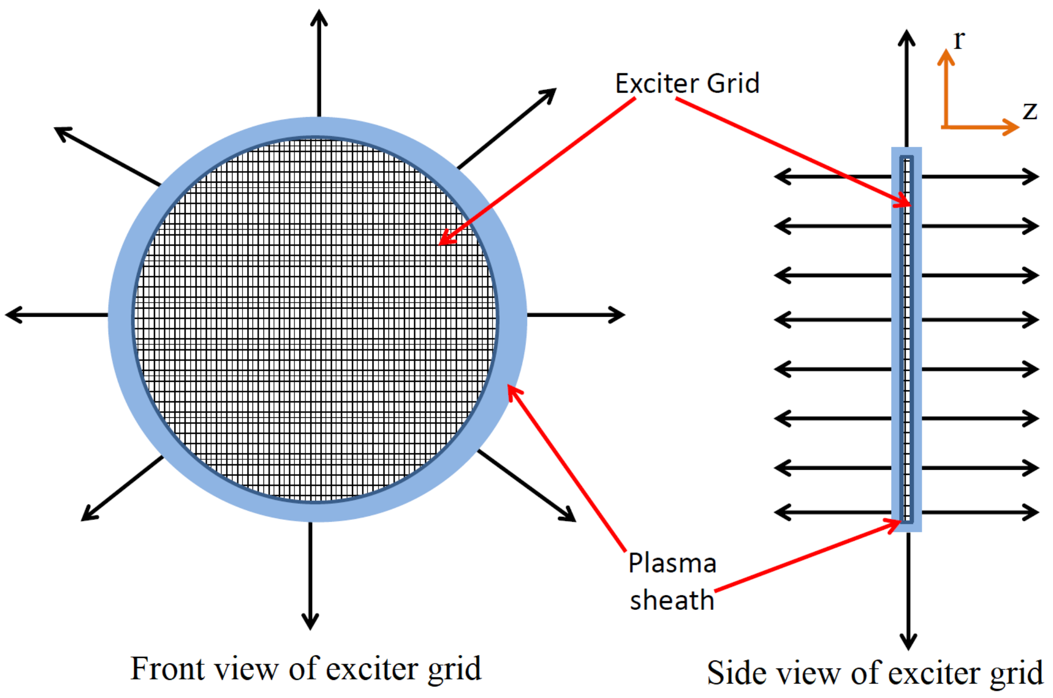

Figure 4.3: Schematic of exciter grid and distribution of electric field.

Front and side view of the grid with applied potential is shown in figure 4.3. The grid is circular with 5 cm diameter and 0.3 mm thickness, facing in the z-direction as shown in the Figure 4.1. Therefore, with the given thickness of grid, the spread of the signal in radial and azimuthal direction will be negligible. However, the applied signal will form a planner wave front in $+z$ and $-z$ direction. The applied potential will disperse in all directions, but the shape and dimension of grid make maximum transfer along z-direction. Hence, the wave will be excited along z-axis of cylindrical device. When, we apply a potential in plasma using any form of metallic instrument a sheath forms around that. The sheath restrains the applied voltage to penetrate and perturb the plasma, therefore the strength of the applied potential reduces when it appears in the plasma.

To excite the IA wave in plasma, we are going to use a time varying signal. The frequency of this applied signal should be less than the ion plasma frequency ($\omega_{pi} = \sqrt{ne^2/m_i \in_0}$). To estimate the ion plasma frequency, plasma density is measured at R=0 cm, and Z=75 cm, center of the cylindrical device, for -50 V discharge voltage. As the neutral pressure (density) is increased from 2×10^{-4} mbar to 30×10^{-4} mbar the plasma density is found to increase from $1.5 \times 10^{15} - 3 \times 10^{16}$ m^{-3} and electron temperature is found to decrease from ~6 eV to ~2 eV for -50 V discharge voltage. For these background plasma conditions, the ion plasma frequency $\omega_{pi}/2\pi$ varies from $1.3 \times 10^6 - 5.8 \times 10^6$ Hz. Therefore, to excite the IA wave, the perturbation frequency should be $< 10^6$ Hz. Another factor playing a role choosing the frequency to excite the IA wave is the dimension of the exciter grid. Exciting the IA wave, having a wavelength greater than the dimension of exciter grid is very difficult. As the dispersion relation of IA wave says:

$$\frac{\omega}{k} = C_s, \qquad \frac{2\pi f}{2\pi/\lambda} = C_s, \qquad \lambda = \frac{C_s}{f}, \qquad C_s = \sqrt{kT_e/m_i}$$

The wavelength of the excited IA wave depends on frequency and ion acoustic velocity, which can be estimated by electron temperature measured by Langmuir probe. A table 4.1 is presented below to describe a range of expected IA wave wavelength depending on various possible electron temperature and frequency.

Table 4-1: Information to estimate the wavelength using electron temperature and perturbation frequency.

Electron Temperature	1 eV	2 eV	4 eV	6 eV	8 eV
Ion-acoustic velocity (C_s)	1547.64	2188.70	3095.29	3790.94	4377.40
Frequency (f) kHz	Wave length $\lambda = C_s/f$ (cm)				
10	15.47	21.88	30.95	37.90	43.77
20	7.73	10.94	15.47	18.95	21.88
30	5.15	7.29	10.31	12.63	14.59
40	3.86	5.47	7.73	9.47	10.94
50	3.09	4.37	6.19	7.58	8.75
60	2.57	3.64	5.15	6.31	7.29
70	2.21	3.12	4.42	5.41	6.25
80	1.3	2.73	3.86	4.73	5.47
90	1.72	2.43	3.43	4.21	4.86
100	1.54	2.18	3.09	3.79	4.37
200	0.77	1.09	1.54	1.89	2.18
300	0.51	0.72	1.03	1.26	1.45
400	0.38	0.54	0.77	0.94	1.09
500	0.31	0.43	0.62	0.75	0.87
600	0.25	0.36	0.51	0.63	0.73
700	0.22	0.31	0.44	0.54	0.62
800	0.19	0.27	0.38	0.47	0.54
900	0.17	0.24	0.34	0.42	0.48
1000	0.15	0.22	0.31	0.37	0.43

The electron temperature for our operating regime varies from ~2 eV to ~6 eV. As we can observe from the table, at frequencies less than 50 kHz, the wavelength is greater than 5 cm for electron temperatures 2 eV to 6 eV. The table 4-1 suggests that the wavelength is less than 5 cm for all freqencies greater than 50 kHz (50×10^3 Hz) and electron temperature greater than 2 eV. Hence, the lower limit of perturbation frequency to excite IA wave is 50×10^3 Hz based on exciter grid dimension and upper limit is 10^6 Hz. Therefore, in this work the perturbation frequency to study the IA wave propagation is chosen to be 10^5 Hz.

After choosing the perturbation frequency to excite IA wave, the next step is to choose the potential or voltage to apply on exciter grid. The excitation or perturbation potential should not be greater than plasma potential, which varies form ∼9 V to ∼7 V for our operating regime. It should not be of such low value that, either it cannot excite the wave or the excited wave is not in the detectable range. The perturbation potential is choosen to be 2 V_{p-p}.

A time varying sinusoidal potential of 2 V_{p-p} (peak to peak voltage) and 100 kHz frequency is applied to the exciter grid to perturb the plasma density using a function generator. The plasma response to applied perturbation is detected by an axially movable disk Langmuir probe (receiver probe) of 8 mm diameter at R = 0 cm.

After choosing the frequency and potential to excite the IA wave, the next step is a set up or circuit to carry the excitation signal to the exciter grid and carry back the recieved signal from the receiver disk probe to the oscilloscope to record the plasma response. The circuit used for excitation and detection of IA wave is shown in the figure 4.4 and 4.5. A function generator is used to launch the sinusoidal signal in plasma. This sinusoidal signal is being carried by a coaxial teflon coated cable from function generator to a capacitor of $0.01\mu F$. The capacitor is used to protect the function generator from the effect of floating potential apearing on the grid, when it is immersed in the plasma. It is a characteristic of capacitor that it blocks the DC signal and allows AC signal to pass through (high-pass filter). Hence, it blocks the floating potential and allows to pass the time varying signal of 100 kHz towards the exciter grid. The signal from capacitor to the grid is carried by another coaxial cable and the sinusoidal signal is launched in plasma through the exciter grid. A receiver disk probe is placed opposite to the grid to measure the plasma response.

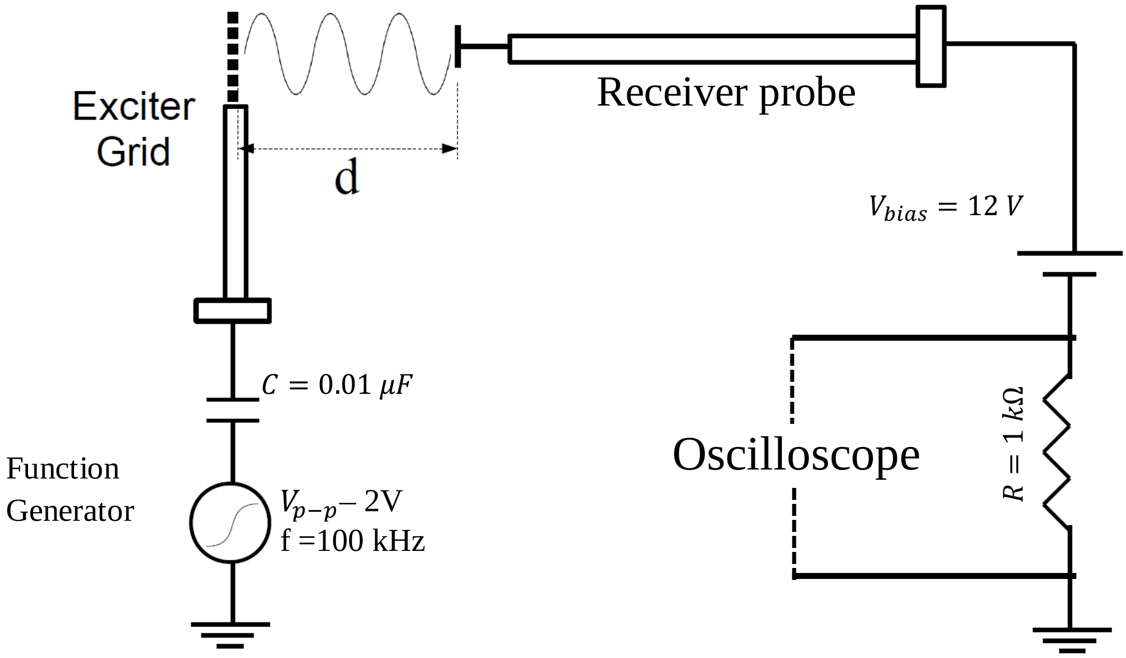

Figure 4.4: Schematic of IA wave exciter circuit using function generator.

A perturbation in plasma density in created, to excite the IA wave in plasma and both ion and electron densities get equally disturbed. Therefore, measurement of any of both plasma species can provide the excited IA wave signal. For better resolution of IA wave signal, the receiver probe is biased near the local plasma potential ($\sim 12\,V$) to measure electron saturation current through a 1 kΩ resistance. The measurement of electron saturation current (IA wave signal) is performed using a 12 V battery based circuit. The data is acquired using 8-bit digital oscilloscope at a sampling rate of 250 MSa/sec, and stored for further analysis. This complete wave excitation circuit is shown in above figure 4.4.

In this kind of circuit the exciter is always at floating potential of plasma, as we trigger the function generator, a sinusoidal signal appear on the grid. This applied signal of potential 2 V_{p-p} varies around the reference floating potential, say that for a certain plasma condition the floating potential is -15 V, then the applied sinusoidal signal varies from – 17 V to – 13

V. The floating potential in plasma depends on plasma conditions, like neutral density, magnetic field, changing with plasma conditions.

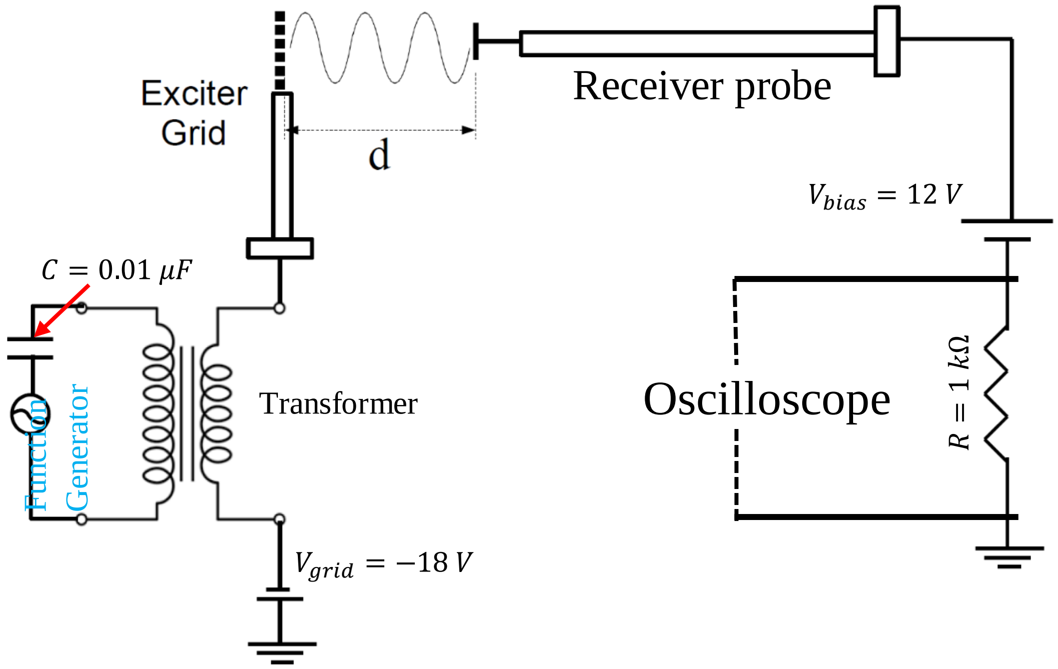

Figure 4.5: Schematic of IA wave exciter circuit with -18 V applied bias to the exciter grid using a transformer and batteries.

Therefore, this circuit is improved to remove the uncertainty in the reference potential on exciter grid. For this, the grid is biased at -18 V using a transformer circuit and batteries of 18 V. A transformer circuit with batteries is added after capacitor to bias the grid at -18 V. The schematic of circuit after adding the transformer circuit is shown in figure 4.5.

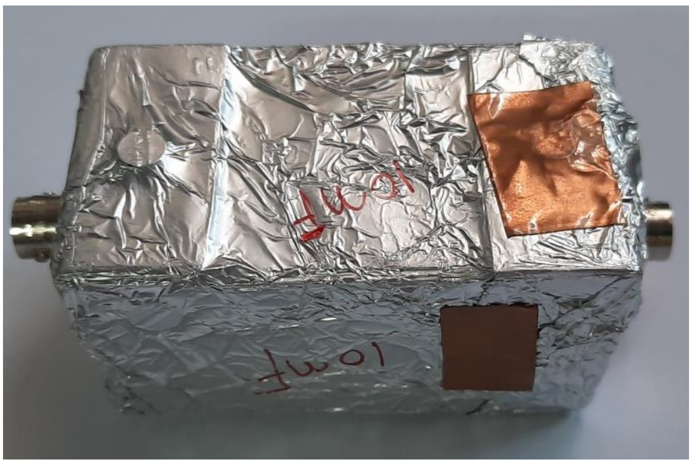

Figure 4.6: Capacitor in aluminum box and wrapped in aluminum foil

The picture of capacitor used in the circuit is shown in figure 4.6. It is placed in aluminum box wrapped in an aluminum foil to prevent the signal loss and penetration of outer atmosphere noises. We are dealing with high frequency signal (100 kHz), so taking proper measures are customary. A picture of capacitor is shown in figure 4.7.

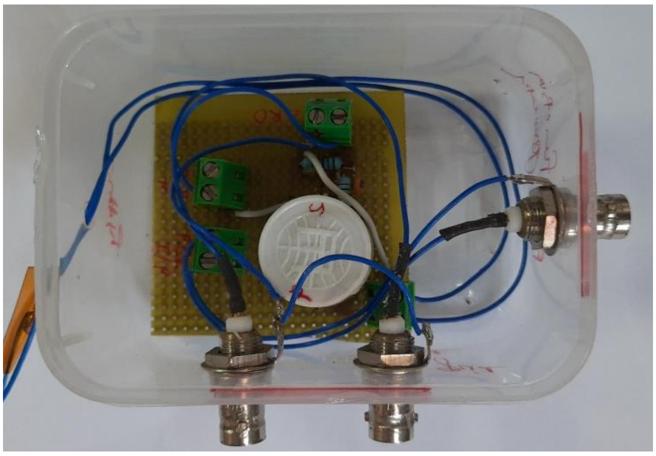

Figure 4.7: Circuit of transformer to bias the exciter gird at certain voltage.

The perturbation frequency to excite IA wave is choosen to be 100 kHz and perturbation voltage is choosen to be 2 V_{p-p}, with considering all required parameters to launch IA wave in plasma. A sinusoidal signal is launched in plasma to excite the IA wave. In next section 4.3, we will discuss the typical features of IA wave and varify that the siganl launched in plasma is satisfying the criteria of IA wave.

4.3 Typical features of ion-acoustic wave

A potential perturbation of $2V_{p-p}$ is launched in the plasma for 30×10^{-4} mbar neutral pressure. The nature of perturbation is sinusoidal with a frequency of 100 kHz, which is well below the ion plasma frequency ($\omega_{pi}/2\pi \sim 10^{6}\ Hz$). The propagation of this potential perturbation is recorded at different axial locations using a movable receiver probe away from the exciter grid. The separation between exciter grid and receiver probe is denoted as d, see Fig. 4.5.

4.3.1 Excitation of Ion Acoustic Wave

The typical experimental observation of wave propagation is shown in figure 4.8. It shows the temporal evolution of normalized plasma density fluctuation ($\delta n/n$) measured at different axial separation, *d* from exciter grid.

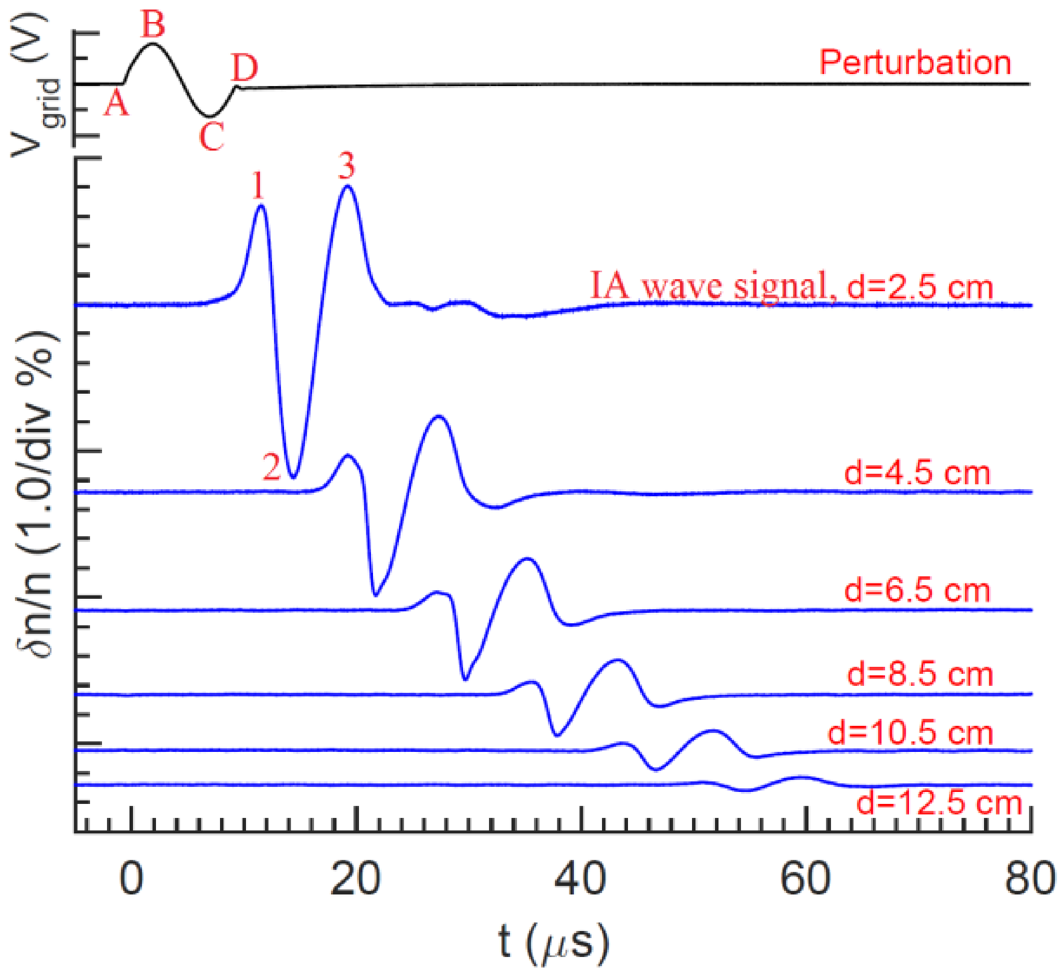

Figure 4.8: Shows a temporal evolution of density perturbation ($\boldsymbol{\delta n/n}$) at different axial locations as the receiver probe moves away from the exciter grid along the z-axis for -50 V discharge voltage, $\mathbf{30 \times 10^{-4}}$ mbar neutral pressure, and 100 kHz perturbation frequency, here d is the distance between exciter grid and receiver probe.

We assumed that while density perturbation for IA wave excitation by a 2 V_{p-p} sinusoidal pulse, the electron temperature fluctuation is negligible [161], $\delta T_e/T_e \ll \delta n/n$ and hence for relative density fluctuation measurement we assumed that $\delta n/n = \delta I_{esat}/I_{esat}$. The received signal of I_{esat} is stored in both ac and dc format. The ac signal of I_{esat} gives δI_{esat} and the dc signal gives mean value of I_{esat}. Experimental observation shows that received wave amplitude ($\delta n/n$) decreases as the wave propagates spatially in the plasma column. The received wave signal has three peaks, and the perturbation signal has only two peaks, so the phenomena can be described as plasma response to the perturbation as follows. During the rise phase of perturbation signal (from A to B) a change in local potential is excited in plasma, and as plasma response peak 1 is observed, similarly during the long fall phase of perturbation signal (from B to C), plasma response to the change in local potential excites the second peak, and on the same way the third peak is also observed.

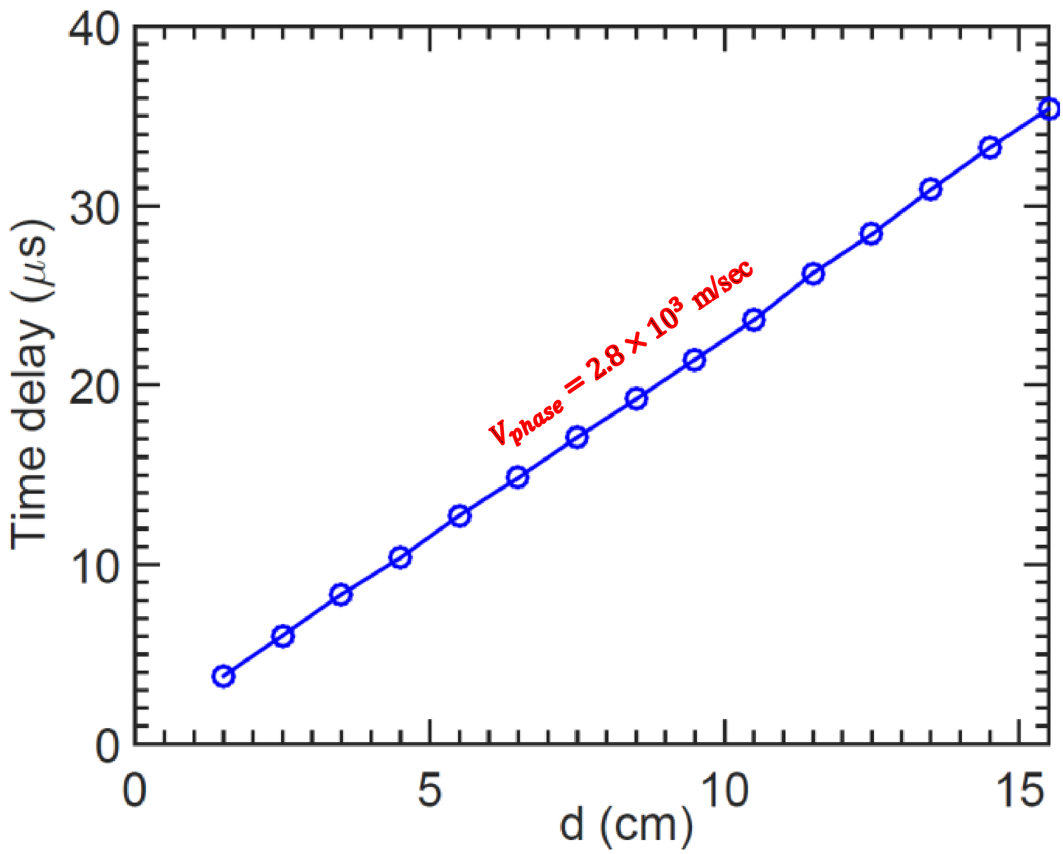

Figure 4.9: Time delay of the first peak of wave as the receiver probe moves away from the exciter grid along the z-axis for -50 V discharge voltage, $\mathbf{30 \times 10^{-4}}$ *mbar neutral pressure, and 100 kHz perturbation frequency, here d is the distance between exciter grid and receiver probe.*

The probe signal shows the local measurement of plasma response to the given perturbation, hence 3 peaks are observed in IA wave signal. When the IA wave is propagating in space, it demonstrates time delay at every 2 cm separation. The velocity of IA wave can be calculated using the information of time delay of wave and distance it has traveled during this time.

Figure 4.9 shows the time delay of the first peak of wave versus the position of receiver probe which shows a linear variation. The phase velocity of IA wave propagation is 2.8×10^3 m/sec measured by the time of flight method of first peak, as shown in figure 4.9. It is compared with theoretically calculated ion-acoustic velocity for Argon plasma, $C_s = 2 \pm 0.3 \times 10^3$ m/sec and matches well ($C_s = \sqrt{K_B T_e / m_i}$).

Figure 4.10 shows the actual CRO image with perturbation sinusoidal signal, recorded plasma response through receiver probe and all other details of data recording.

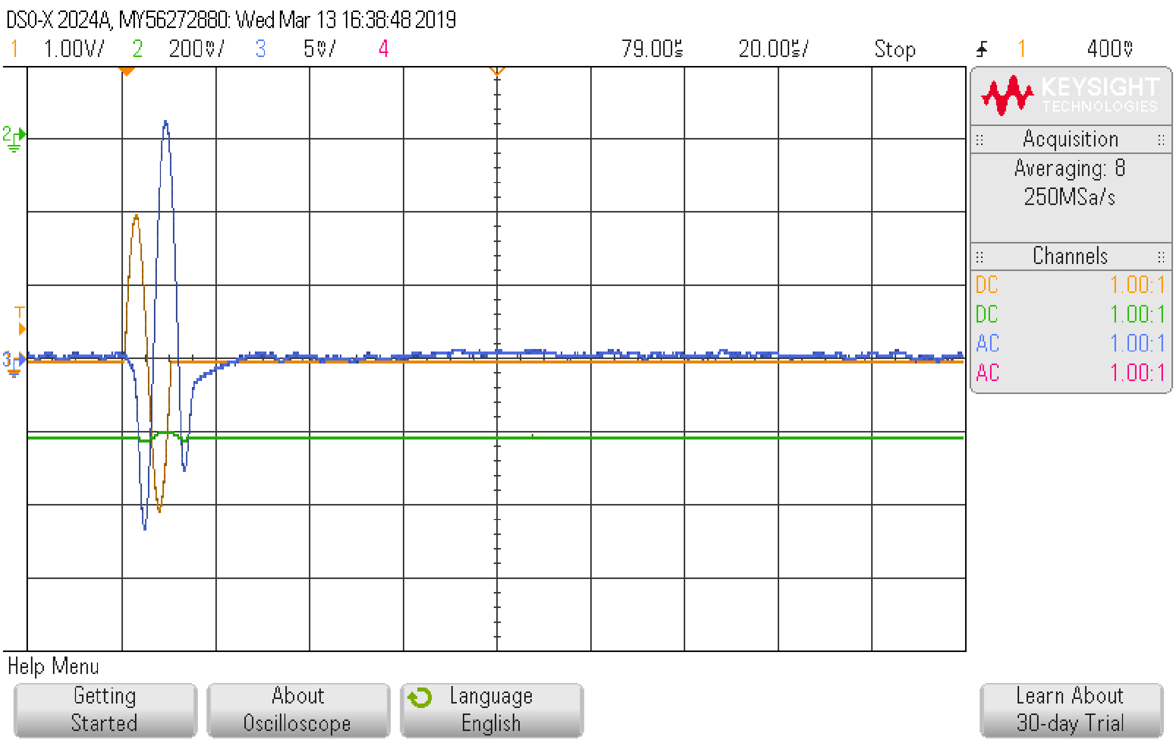

Figure 4.10: CRO image of IAW launching.

Further experiments are performed to obtain the wave features such as $\omega - k$ relation, plasma density and potential phase relation, and power spectrum.

4.3.2 Dispersion curve of IA wave

Figure 4.11 shows the dispersion relation for the mentioned experimental observations. In this figure, the propagation frequency of wave is same as the perturbation frequency. The wavenumber k, is governed by plasma conditions. In this experiment, the wave frequency, ω (perturbation frequency) is varied externally. The wavenumber k is calculated using ω and measured phase velocity, v_{phase}, $\omega/k = v_{phase}$. The straight line shows a constant velocity nature of wave with change in perturbation frequency, and it is one of the characteristics of the IA wave [21,105].

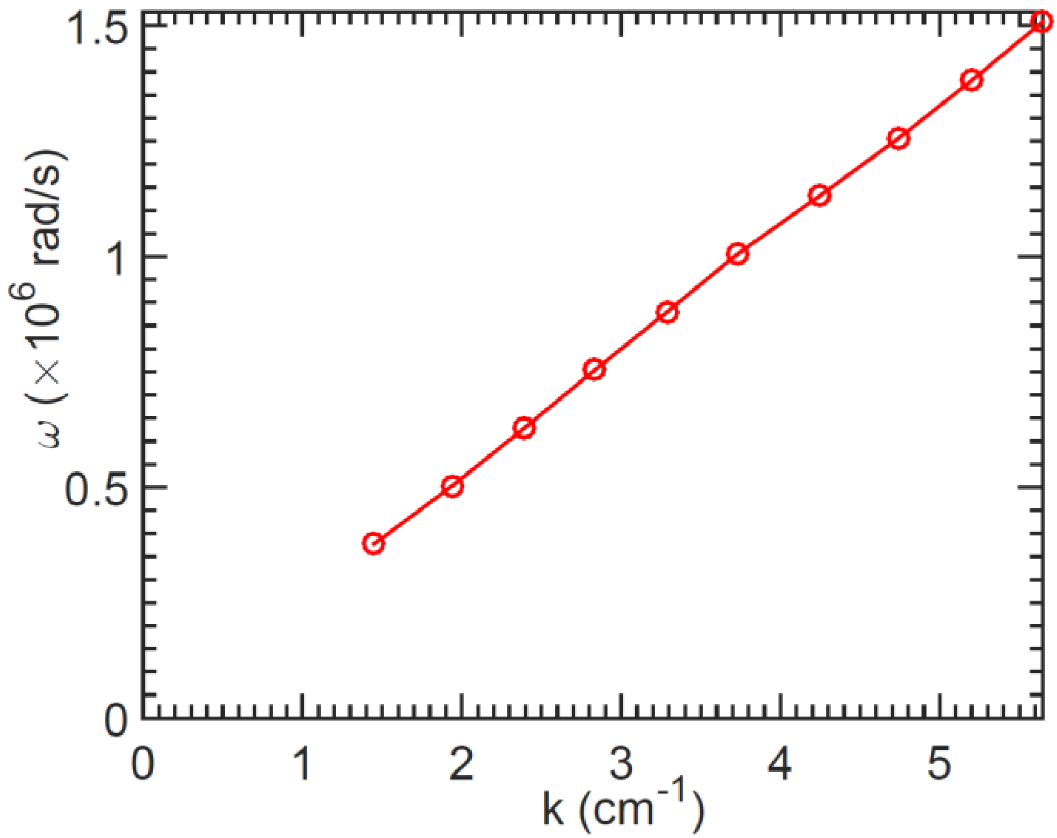

Figure 4.11: Experimentally obtained dispersion curve ($\boldsymbol{\omega}$ vs k) for $\boldsymbol{\omega_{pi}/2\pi = 2 \times 10^6}$ Hz and $\boldsymbol{\lambda_{De} = 0.08}$ mm, when continuous sinusoidal perturbation of 2 $\boldsymbol{V_{p-p}}$ and 100 kHz is excited in plasma.

4.3.3 Phase Relation of Density and Potential for IA wave

For IA wave the relation between plasma density and potential fluctuations, for the linear regime of wave, is given by

$$\frac{\delta n}{n} \sim \frac{e\delta\phi}{T_e}$$

The density fluctuation (δn) is normalized by mean plasma density (n), and potential fluctuation ($\delta\phi$) is normalized by mean electron temperature (T_e). Figure 4.12 shows the temporal characteristic of $e\phi/T_e$, and $\delta n/n$ (for continuous sinusoidal perturbation of 2 V_{p-p} and 100 kHz). As noted, the temporal evolution of both the quantities is in the same phase and has same amplitude.

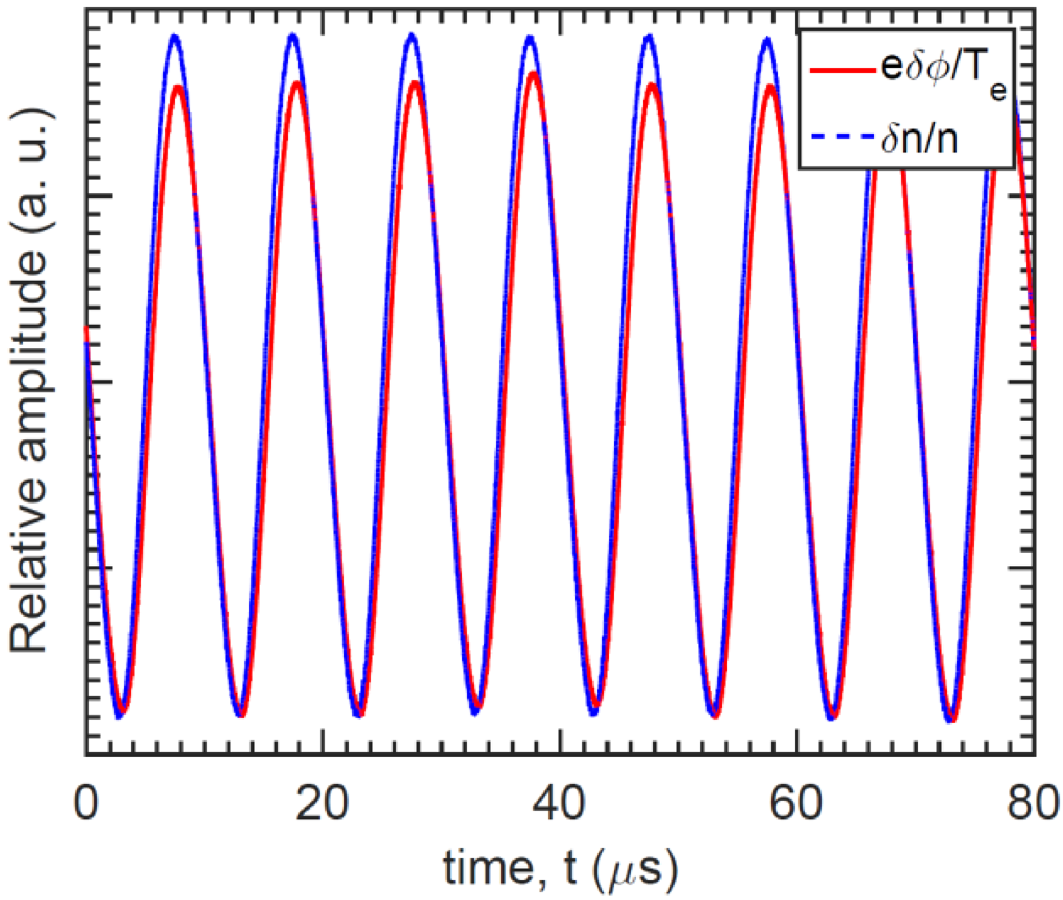

Figure 4.12: Temporal evolution of normalized plasma density, n and potential, $\boldsymbol{\phi}$ *fluctuations when continuous sinusoidal perturbation of 2* $\boldsymbol{V_{p-p}}$ *and 100 kHz is excited in plasma.*

4.3.4 Power Spectral of Excited IA wave

The power spectral analysis is performed to observe the effect of the external perturbation on background plasma fluctuations. The temporal evolution of fluctuation in plasma density for two plasma conditions, without and with the external perturbation of continuous sinusoidal signal of 2 V_{p-p} and 100 kHz, is shown in figure 4.13. The level of fluctuation is low for unperturbed plasma, which is $\leq 0.1\%$ and can be considered as quiescent plasma. The normalized plasma density fluctuations are observed to enhance in the presence of external potential perturbation, as shown in figure 4.13.

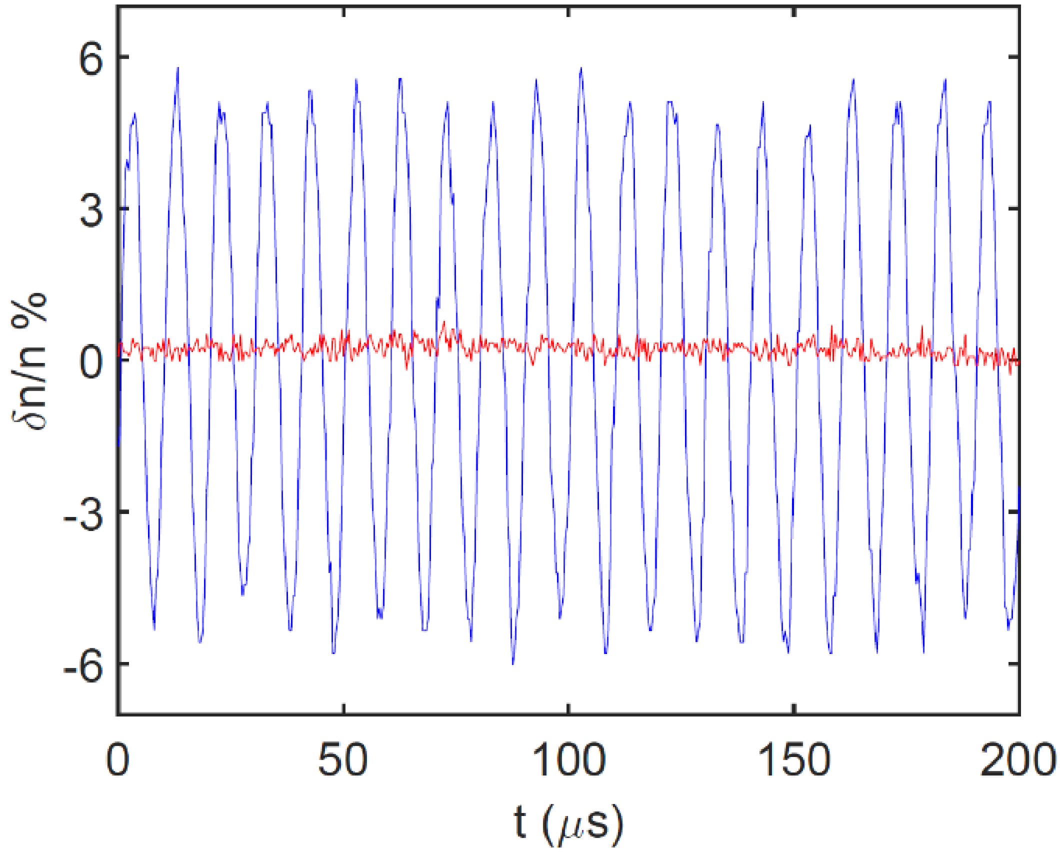

Figure 4.13: Time evolution of normalized density fluctuation, $\boldsymbol{\delta n/n}$, the red trace shows the density fluctuation of quiescent plasma, and blue trace shows the density fluctuation when continuous sinusoidal perturbation of 2$\boldsymbol{V_{p-p}}$ and 100 kHz is excited in plasma.

The power spectrum of both signals is shown in figure 4.14. For quiescent (unperturbed) plasma, absence of any recognizable peak demonstrates the non-existence of power coupling in significant mode. As the perturbation of 100 kHz is excited in the plasma the frequency spectra show a sharp peak at100 kHz along with its harmonics.

From figure 4.14 few more observations can be made such as (i) the propagation frequency of the wave is same as the perturbation frequency; hence, we are exciting the known frequency in plasma, (ii) in presence of perturbation, the maximum power is coupled to the excited IA wave. Hence only the IA wave is excited in plasma with the launched sinusoidal signal, and it is not exciting any other wave in the plasma.

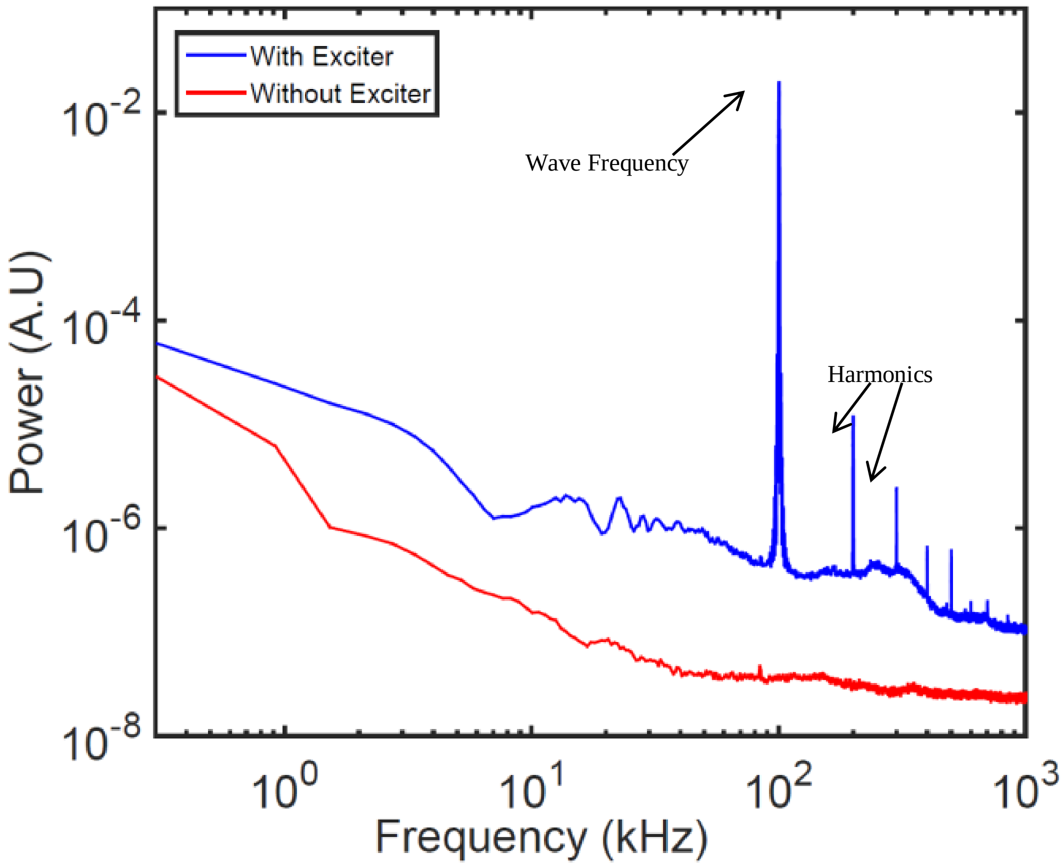

Figure 4.14: The power spectrum of both the signals the lower trace (red) is for quiescent plasma and the upper trace is when the perturbation of 2$\boldsymbol{V_{p-p}}$ and 100 kHz is excited in plasma. The signal is recorded at d = 4.5 cm.

4.3.5 Effect of Perturbation Potential of IA wave

To understand the effect of change in applied exciter potential on IA wave, the applied potential on exciter grid is varied from 1 V_{p-p} to 10 V_{p-p}. The normalized wave amplitude measured by receiver probe at d=3.5 cm is shown in figure 4.15. As the applied potential increases, the amplitude of the excited IA wave increases. Time delay for various applied potential is same, it suggests that wave velocity does not changes with increase in potential. In literature, the pseudowave velocity was found to be increased as the applied voltage amplitude was increased [162,163].

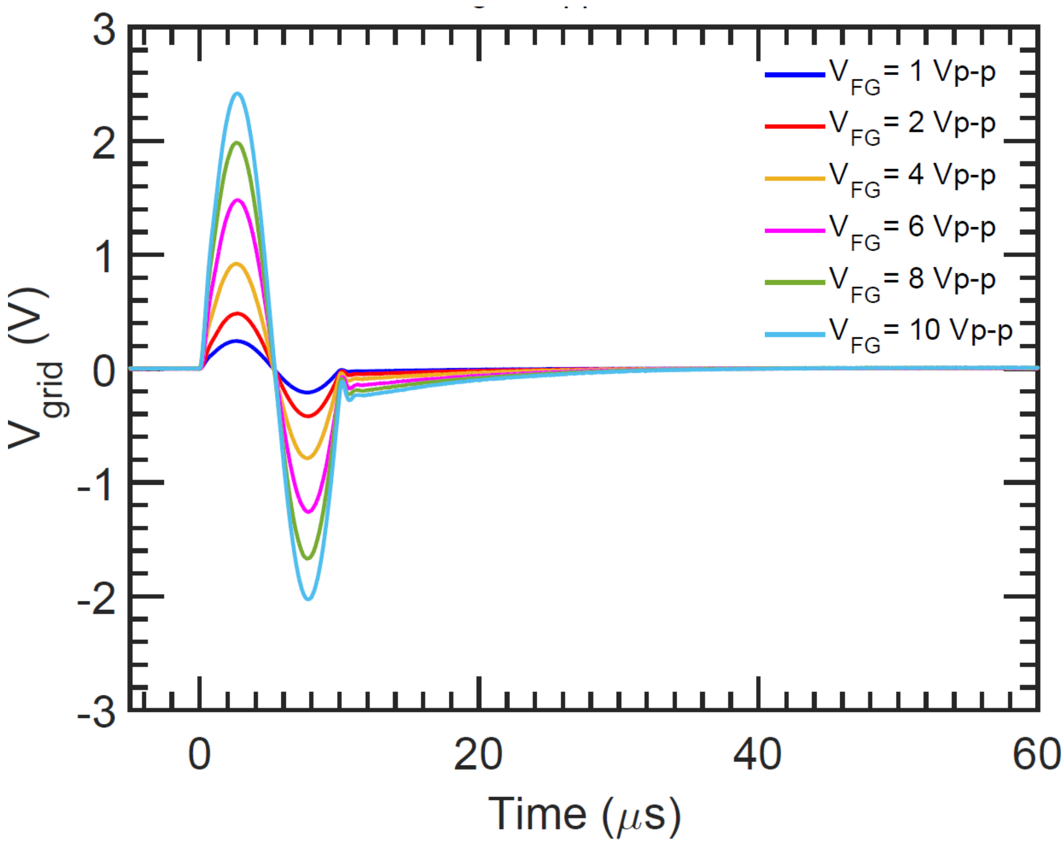

Figure 4.15: temporal evolution of density perturbation ($\boldsymbol{\delta n/n}$) for various perturbation potential when the receiver probe is placed at 3.5 cm away from the exciter grid along the z-axis for 100 kHz perturbation frequency.

With all above studies on excited wave, it is ensured and confirmed that launched sinusoidal signal through grid is exciting IA wave in Plasma.

4.3.6 Spatial Variation of IA Wave Amplitude

As observed in figure 4.8, the wave amplitude ($\delta n/n$) decreases spatially when wave propagates in plasma. The spatial variation of observable propagation length is shown in figure 4.16. The maximum distance away from the exciter, up-to which the wave amplitude can be measured within the resolution of the oscilloscope, is observable propagation length of IA wave for this experimental condition. The signal amplitude measured at all locations is normalized with the amplitude of the signal at 2.5 cm, along the wave propagation axis (Z-axis of cylindrical device).

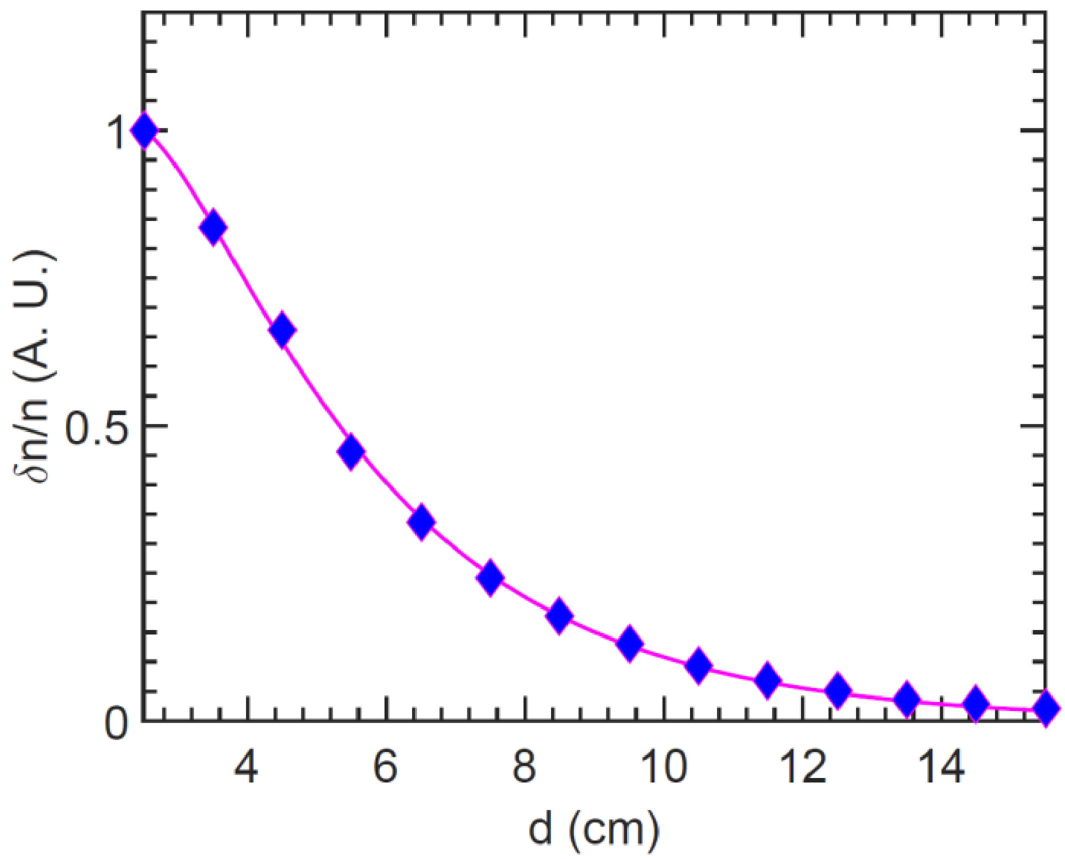

Figure 4.16: The spatial variation of $\boldsymbol{\delta n/n}$ or wave amplitude for $\mathbf{30 \times 10^{-4}}$ mbar neutral pressure. The diamond-shaped markers are experimental data, and the solid lines are an exponential fit to the experimental data.

4.3.7 Damping Mechanisms

Several possible mechanisms can contribute to wave damping phenomena in plasma, such as (1) An amplitude loss due to the geometric spread of the wave. (2) Collisional damping [90,91,104] arises when the ion-neutral collision frequency is a significant fraction of the wave frequency. (3) Landau damping [164,165] arises when particles move near the phase velocity of the wave and there are more slower than faster particles, i.e., the slope of the distribution function is negative at v_{phase}. (4) Plasma density gradient [166] driven damping along the wave propagation axis. (5) Finally, if the wave is scattered by other waves (e.g. in a turbulent plasma) the energy spread in frequency gives rise to an energy loss at the injected signal frequency, hence an amplitude decay. In order to distinguish among the various damping mechanisms, a few basic studies and discussion are taken into consideration as presented in below trailing section.

4.3.7.1 Spatial Damping due to Geometrical Spread of Wave Packet

Plane waves are produced close to a plane grid of dimensions large compared to the wavelength. This partially holds for the present experiments, as the grid diameter, 5 cm is greater than wavelength of IA wave, 3 cm. But, the grid dimension and wave wavelength are not very different, there is a possibility of amplitude loss due to the geometric spread of the wave.

4.3.7.2 Landau Damping

Landau damping is one of the most important and widely studied phenomena predicted by collisionless plasma theory [88,164,165,167,168] and first observed by Wong [71] in 1962 for IA wave. This dissipation-less damping takes place when the energy of the plasma wave transfers to ions moving at nearly equal to the phase velocity of the wave. Both electrons and ions can produce Landau damping. Landau damping is strong when the electron temperature is close to the ion temperature. In our experimental conditions, $T_e > T_i$ ($T_i = T_e/10 = 0.2$) [132], for this the ion thermal speed, $V_{thi} = 700$ m/sec much lower than the wave phase velocity, $\omega/k = 2.8 \times 10^3$ m/sec. Even at high electron temperatures, ion Landau damping is strong near the ion plasma frequency where the phase velocity decreases to the ion thermal velocity. In present experimental study the IA wave is launched much below the ion plasma frequency, $\omega\ (10^5\ Hz) < \omega_{pi}(10^6\ Hz)$. We observe that the wave phase-velocity (2.8×10^3 m/sec), is much less than the electron thermal velocity ($\sim 10^6$ m/sec), and it is greater than the ion thermal velocity (700 m/sec). When $T_i \ll T_e$, then the wave phase-velocity can simultaneously lie on almost flat portions of the ion and electron distribution functions, showing the absence of the negative slope of the distribution function at v_{phase}. It implies that the wave is subject to very little Landau damping. Hence, it may be interpreted that Landau damping, may not be the reason for observed damping.

4.3.7.3 Plasma Density Gradient Driven Damping

The gradient in plasma density along the wave propagation axis can be a source to make the amplitude decrease spatially as discussed by Doucet et al. [166]. To obtain more insight into the spatial decrease in the wave amplitude, we look for the axial (along the propagation axis of the wave) variation of plasma parameters. The axial profile of plasma parameters is measured at center of the device, R=0 cm, for 5×10^{-4} mbar neutral pressure. Electron temperature T_e is nearly constant over the axial length, and plasma density n has a gradient as shown in figure 4.17 (a). In the figure the variation of electron is shown in blue line with diamond shape marker and plasma density is in red line with circular shape marker. The scale length of density is (~30 cm) constant upto Z=95 cm as shown in figure 4.17 (b).

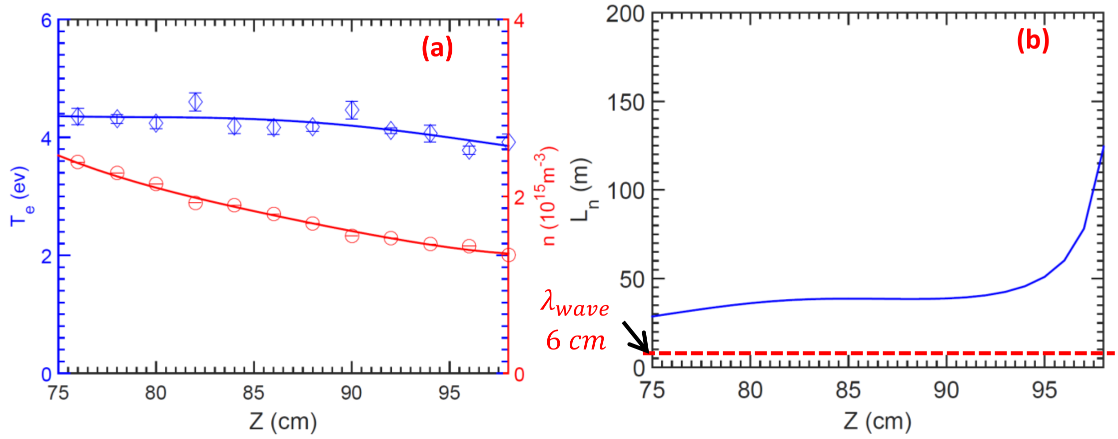

Figure 4.17: Axial variation of (a) electron temperature, $\boldsymbol{T_e}$ (blue line with diamond shape marker), and plasma density, n (red line with circular shape marker), and (b) plasma density scale length, $\boldsymbol{L_n}$ the dotted line shows value of IA wavelength ($\boldsymbol{\lambda_{wave}}$) for -50 V discharge voltage and neutral pressure $\mathbf{5 \times 10^{-4}}$ mbar. The exciter grid is placed at Z=75 cm.

The gradient scale length of density is higher than the wavelength of IA wave ($L_n > \lambda_{wave} \sim 6-3$ cm). Hence the gradient in plasma density cannot be the reason for the spatial wave damping.

Collisional damping can be tested by varying the neutral pressure and this will be discussed in next chapter 5.

4.4 Summary and Discussion

Ion-acoustic wave has been excited in Argon plasma driven by the localized grid, and the basic features of IA wave in plasma have been studied and discussed. The observation of IA wave excitation has been characterized further and validated. To explore the effect of the neutral collision on IA wave the experiment has been performed for various neutral densities. The neutral density is varied by changing the neutral pressure, which in turn allows the change in ion-neutral, and electron-neutral collision mean free path. It is obvious and conventional that as the neutral collision increases the IA wave gets heavily damped in plasma.

Chapter 5

Effect of Neutral collisions on Ion Acoustic wave propagation

5.1 Introduction

Neutral particles are important and integral component of plasma and play a vital role in the characteristics of the plasma. In partially ionized plasmas the influence of neutrals are known to modify the plasma characteristics, like most of the laboratory plasmas. Even in high-temperature plasmas, such as Tokamak, a very small amount of neutrals in the edge is known to affect the overall equilibrium configuration and dynamical behavior of plasma, leading to L to H transition triggered by radial electric field generated via neutral particle ionization [169,170]. The neutral particles move undisturbed until they make a collision with another plasma species, and these collisions affect the particle's motion. The influence of the neutral collision on IA wave is very intriguing, and the details are not fully explored yet in experiments.

An experimental study of Ion Acoustic (IA) wave propagation is performed to investigate the effect of neutral collisions on IA wave for Argon plasma in an unmagnetized linear plasma device MPD. The neutral density is varied by changing the neutral pressure, which in turn allows the change in ion-neutral, electron-neutral collision frequencies and mean free paths. The collisions of plasma species with neutrals are found to modify the IA wave characteristics such as the wave amplitude, velocity, and propagation length. In earlier work, the studies on the effect of neutral collision on the IA wave propagation support the conventional idea that neutrals take away the momentum of wave and render heavy wave damping in collisional regime of plasma [104,105]. The influence of ion-neutral collisions on the ion sound wave has been observed experimentally by HATTA and SATO (1961); DOUCET and GRESILLON (1968); ASKORNKITI, HSUAN and LONGREN (1969); the phase velocity decreases and the damping coefficient increases when the frequency ω is decreased below the ion-neutral collision frequency ν_{in}. Hence, the collisional damping of IA wave is reported in the frequency regime $\omega < \nu_{in}$ (where ω is ion-acoustic mode frequency and ν_{in} is ion-neutral collision frequency). The impression is that effect of neutral collisions on IA wave for frequency regime $\omega \geq \nu_{in}$ is not explored in literature. In the experiments reported in this thesis, the IA wave is excited for $\omega > \nu_{in}$.

5.2 Basic Plasma Parameters

In this chapter all the experiments are performed in un-magnetized plasma. The mean plasma parameters are measured using I-V characteristic of single Langmuir probe (LP).

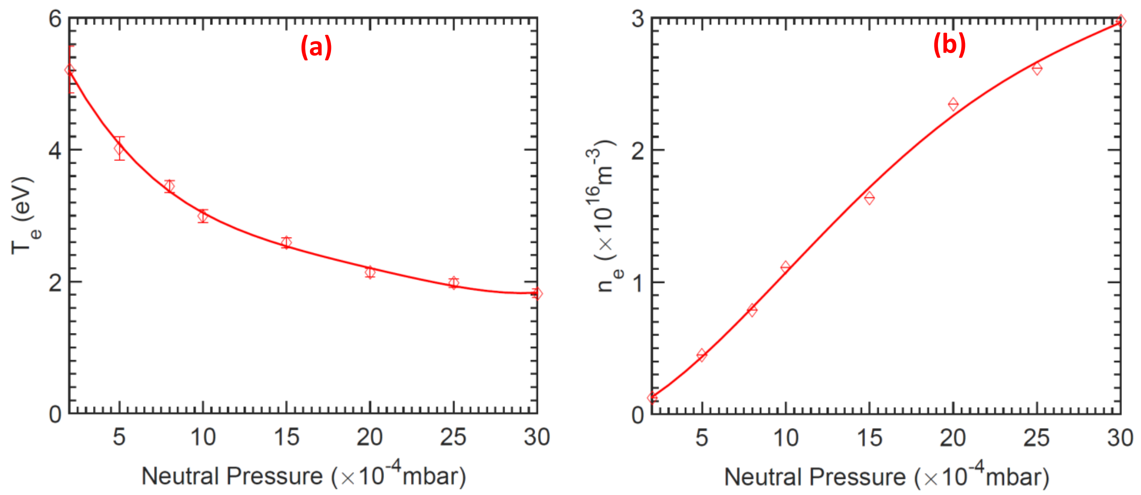

Figure 5.1: Variation of (a) electron temperature, $\boldsymbol{T_e}$, and (b) plasma density, $\boldsymbol{n}$ at $\boldsymbol{R} = \mathbf{0}$ cm, as a function of neutral pressure for -50 V discharge voltage.

A sweep voltage ramp of -80 V to 25 V is applied on the Langmuir probe, to obtain I-V characteristics using I to V converter circuit. The electron current is obtained by subtracting ion saturation current (I_{isat}) from total probe current and the logarithmic slope of electron current provides electron temperature (T_e). The plasma density (n) is calculated by using ion-saturation current and electron temperature. The measured electron temperature (T_e) and plasma density (n) with different Argon gas pressure is shown in figure 5.1.

To identify the effect of neutral density on the evolution of plasma parameters Argon gas pressure is varied from $2 \times 10^{-4} - 30 \times 10^{-4}$ mbar. The plasma parameters are measured at R=0 cm, and Z=75 cm center of the cylindrical device, with -50 V discharge voltage. As the neutral pressure (density) is increased from 2×10^{-4} mbar to 30×10^{-4} mbar the plasma density is found to increase from $1.5 \times 10^{15} - 3 \times 10^{16}$ m^{-3} and electron temperature is found to decrease from $\sim$6 eV to $\sim$2 eV for -50 V discharge voltage. The electron-neutral collision mean free path, $\lambda = 1/n_n\sigma_{en}$, decreases with increase in neutral density (it is shown later in table 5.1), electrons suffer more collisions before they hit the wall of the grounded chamber, and ionization increases as a result. Hence the plasma density enhances with increase in neutral density, and it leads to a decrease in electron temperature. For above background plasma condition, the ion plasma frequency $\omega_{pi/2\pi}$ varies from $1.3 \times 10^{6} - 5.8 \times 10^{6}$ Hz. Therefore, in this work the perturbation frequency to study the IA wave propagation is chosen to be 10^{5} Hz.

The effect of neutral collisions on the IA wave is explored, as described in the following section 5.3. The experiments on IA wave presented in the next section are performed at 100 kHz perturbation frequency and $2V_{p-p}$ perturbation voltage unless specifically stated.

5.3 Effect of neutral density on IA wave

In partially ionized plasma, the presence of neutral is found to modify the IA wave propagation. A detailed experiment is performed for various neutral densities to quantify the effect of neutral density on the IA wave in MPD. The temporal evolution of wave amplitude ($\delta n/n$) is shown in figure 5.2, for two values of Argon gas pressure. The pressure is a representation of neutral density in experimental studies. The wave amplitude shown in the figure is measured at various spatial locations by moving the receiver probe away from the exciter grid and the distance between grid and receiver probe is noted as d.

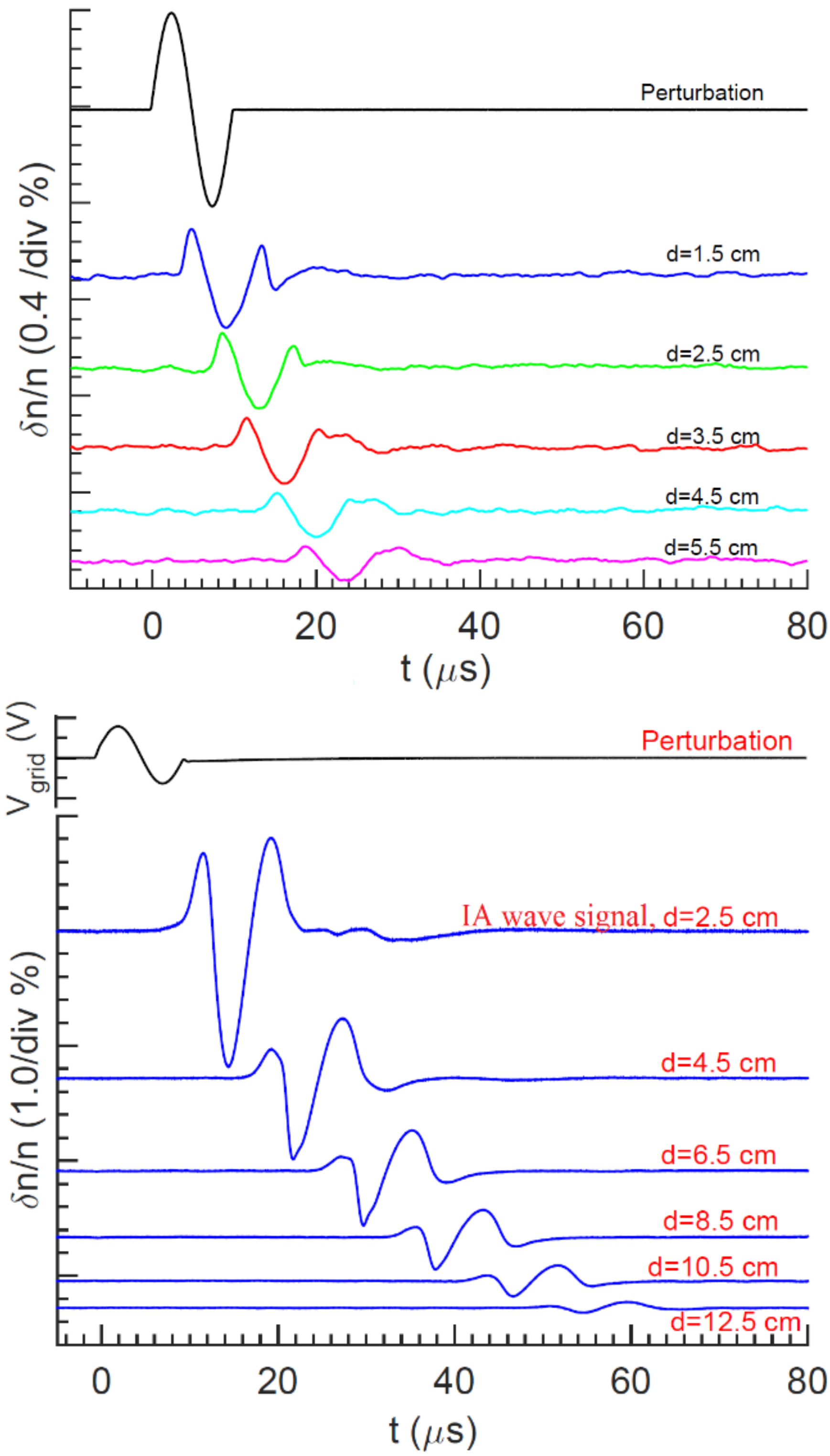

Figure 5.2: Temporal evolution of wave amplitude ($\boldsymbol{\delta n/n}$), for Argon gas pressure (a) $\mathbf{2 \times 10^{-4}}$ mbar, and (b) $\mathbf{20 \times 10^{-4}}$ mbar, 100 kHz perturbation frequency and 2$\boldsymbol{V_{p-p}}$ perturbation voltage.

The wave amplitude ($\delta n/n$) shown in the figure 5.3 is measured at d=2.5 cm, for various pressure values. The horizontal position of each set, obtained for different neutral density, is displaced to avoid overlapping in the figure.

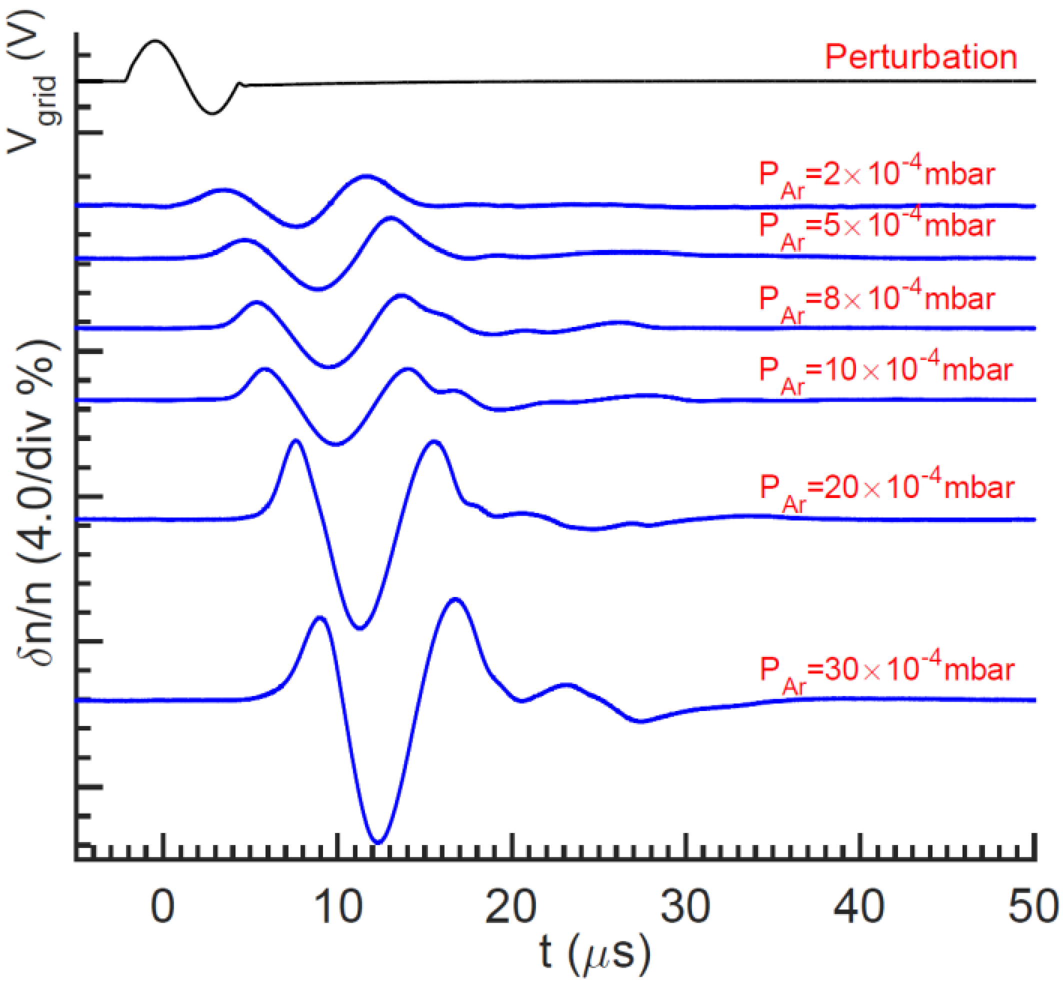

Figure 5.3: Propagation of IA wave for various neutral pressures, the signal of electron saturation current is measured at d=2.5 cm for -50 V discharge voltage, where d is the distance between the exciter grid and receiver probe.

The wave amplitude increases as the neutral pressure increases from 2×10^{-4} mbar to 30×10^{-4} mbar. The spatial variation of wave amplitude measured at d=2.5 cm and the effect of change in neutral density on this spatial variation is discussed further.

As observed in figure 5.2, the wave amplitude $(\delta n/n)$ decreases spatially when wave propagates in plasma. The spatial variation of observable propagation length is shown in figure 5.4. The distance from the exciter up-to which the wave amplitude can be measured within the resolution of the oscilloscope, is called the observable propagation length of IA wave for this experimental condition. The signal amplitude measured at all locations is normalized with the amplitude of the signal at 2.5 cm, along the wave propagation axis (Z-axis of cylindrical device).

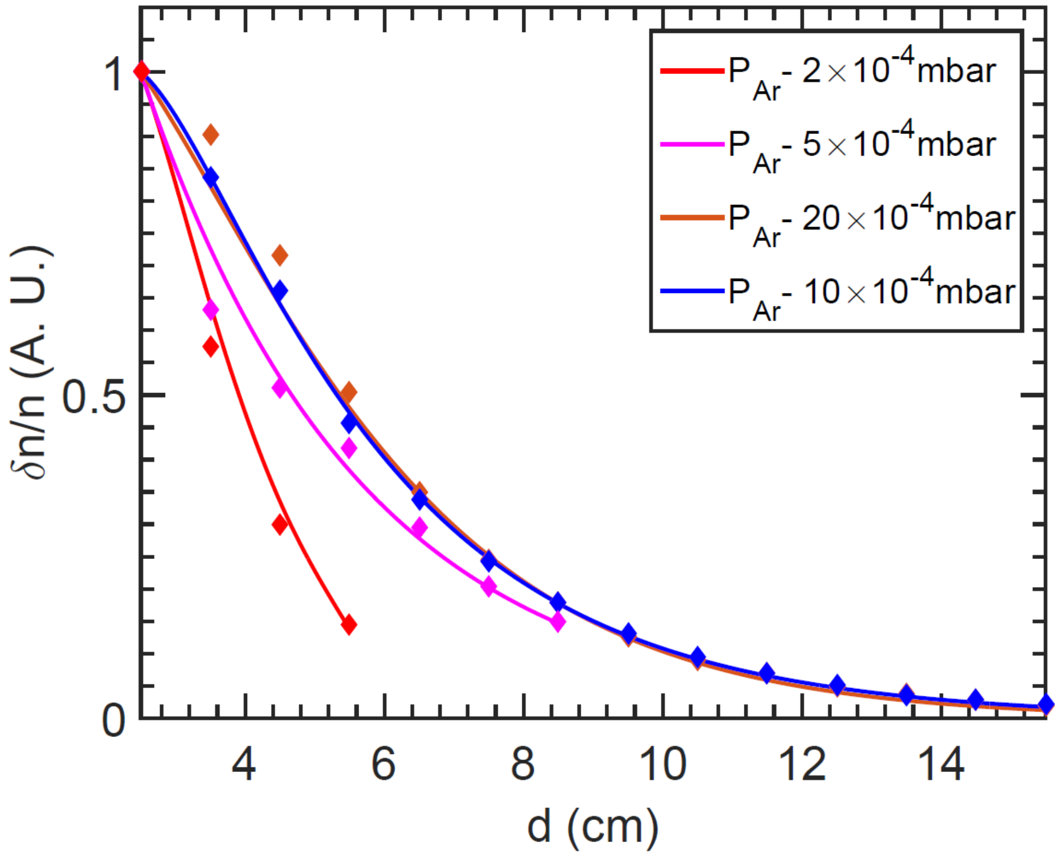

Figure 5.4: The spatial variation of $\boldsymbol{\delta n/n}$ *or wave amplitude for various neutral pressures. The diamond-shaped markers are experimental data, and the solid lines are exponential fits to the experimental data.*

The observable propagation length by varying the neutral pressure within the experimental limit, from 2×10^{-4} mbar to 20×10^{-4} mbar is presented to show the effect of neutral density on wave propagation [Figure 5.4]. It is observed from figure 5.4 that as the neutral pressure increases, the wave propagation length increases from 5 cm to 15 cm. One can also infer from this figure that wave amplitude decreases sharply for low neutral pressure. The observations suggest that wave propagates for longer distances at higher neutral pressure.

The increase in observed propagation length with an increase in neutral density is in contrast to the earlier reported work [104,105]. As the neutral density increases, the collision of neutrals with plasma species also increases, as shown in table 1. As discussed in the literature, the propagation length should decrease with increase in neutral density. In a theoretical work, Vranjes et al. [171] found a region where neutrals do support wave propagation. They argued that for a relatively small number of collisions, the wave is weakly damped because initially neutrals do not participate in the wave motion and do not share the same momentum. However, for much larger collision frequencies, the plasma species drag the neutrals along, and all three components (electrons, ions, and neutrals) move together. For stronger collisions, Vranjes et al. suggested that the propagations lengths will be large. Our experimental observations suggest that we may have hit this parametric space.

Table 5-1: Important plasma characteristics in MPD.

Pressure (mbar)	ω/ω_{pi}	$k\lambda_{de}$	ν_{en} (Hz)	ν_{in} (Hz)	λ_{en} (cm)	λ_{in} (cm)	λ_{wave} (cm)
2×10^{-4}	0.015	0.045	1.5×10^6	3×10^3	62	25.56	6.7
5×10^{-4}	0.0092	0.025	3.4×10^6	6.8×10^3	25	10.22	5.5
10×10^{-4}	0.0039	0.017	5.7×10^6	1.1×10^4	12	5.11	4.2
20×10^{-4}	0.0030	0.014	9.9×10^6	2×10^4	6	2.55	3.1

The parameters described in table 5.1 are discussed as follows: electron Debye length, $\lambda_{de} = \sqrt{\epsilon_0\ k_B T_e/ne^2}$ is calculated using electron temperature, T_e and plasma density n, the ion plasma frequency, ω_{pi} is calculated using the plasma density as shown in figure 5.1, n_n is neutral density, ion temperature is admitted to be $T_i = T_e/10$, ion-neutral collision cross section $\sigma_{in} = 80 \times 10^{-20}\ m^{-2}$, electron-neutral collision cross section $\sigma_{en} = 3.3 \times 10^{-19}\ m^{-2}$ [118], $\lambda_{en} = 1/n_n\sigma_{en}$, $\lambda_{in} = 1/n_n\sigma_{in}$, $\nu_{en} = n_n\sigma_{en}V_{the}$, and $\nu_{in} = n_n\sigma_{in}V_{thi}$ are electron-neutral and ion-neutral collision mean free path and collision frequencies respectively. The experiments are performed for a constant frequency, $f = 100$ kHz, (wave frequency, $\omega = 2\pi f$).

Table 5.1 indicates that IA wave frequency is greater than the ion-neutral collision frequencies, for all the values of neutral pressures at which experiments are performed. It shows that for present work the IA wave experiments are performed for $\omega > \nu_{in}$ regime. Therefore, to understand the experimental observation of enhancement in IA wave propagation length, we look for the dynamics related to the electron-neutral, ion-neutral collision mean free path (λ_{en} and λ_{in} respectively) and wavelength of IA wave (λ_{wave}). Ions and neutrals are comparable in mass and size and electrons are small comparatively, so probability of momentum transfer from ions to neutrals is more than that to electrons. As one can observe from the table 5.1 that for low neutral density, λ_{wave} (6.7 cm) is very small in comparison to λ_{in} (25 cm), in this condition only few collisions will take place between ions and neutrals before the ions hit to wall of the device. It suggests that interaction of the ions with neutrals is negligible, and as a result ions do not impart the IA wave momentum to neutrals. Hence the neutrals do not participate in the wave motion. However, as the neutral pressure increases, λ_{wave} (3.1 cm) becomes comparable to λ_{in} (2.5 cm). Collisions between ions and neutrals will take place more frequently, it increases the interaction of ions with neutrals; hence the ions transfer and share the IA wave momentum with neutrals. The plasma species drag the neutrals along, and all three components (electrons, ions, and neutrals) move together. The neutrals also start to carry the IA wave momentum as ions and electrons do, and it leads to increase in the wave propagation length as the neutral pressure increases.

The above discussion qualitatively can be understood using the analytical work of Doucet et al. [166].

We have extended their solution for IA wave to include collisions between ions and neutrals and the obtained relation for perturbed density (n_1) as:

$$\boldsymbol{n_1} = \boldsymbol{\lambda\sqrt{n_0}\cos kz} \qquad \text{5-1}$$

where,

$$k = \sqrt{k_0^2 + ik_0\frac{\nu_{in}}{c_s} - \frac{1}{\sqrt{n_0}}\frac{d^2(n_0^{1/2})}{dx^2}}$$

Here, n_0 is the mean plasma density, $k_0 = \omega/c_s$, ω is the IA wave frequency, $c_s = \sqrt{k_B T_e/m_i}$, k is wavenumber, ν_{in} is the ion-neutral collision frequency, λ is the arbitrary constant. The detail of the calculation can be found in Appendix A.

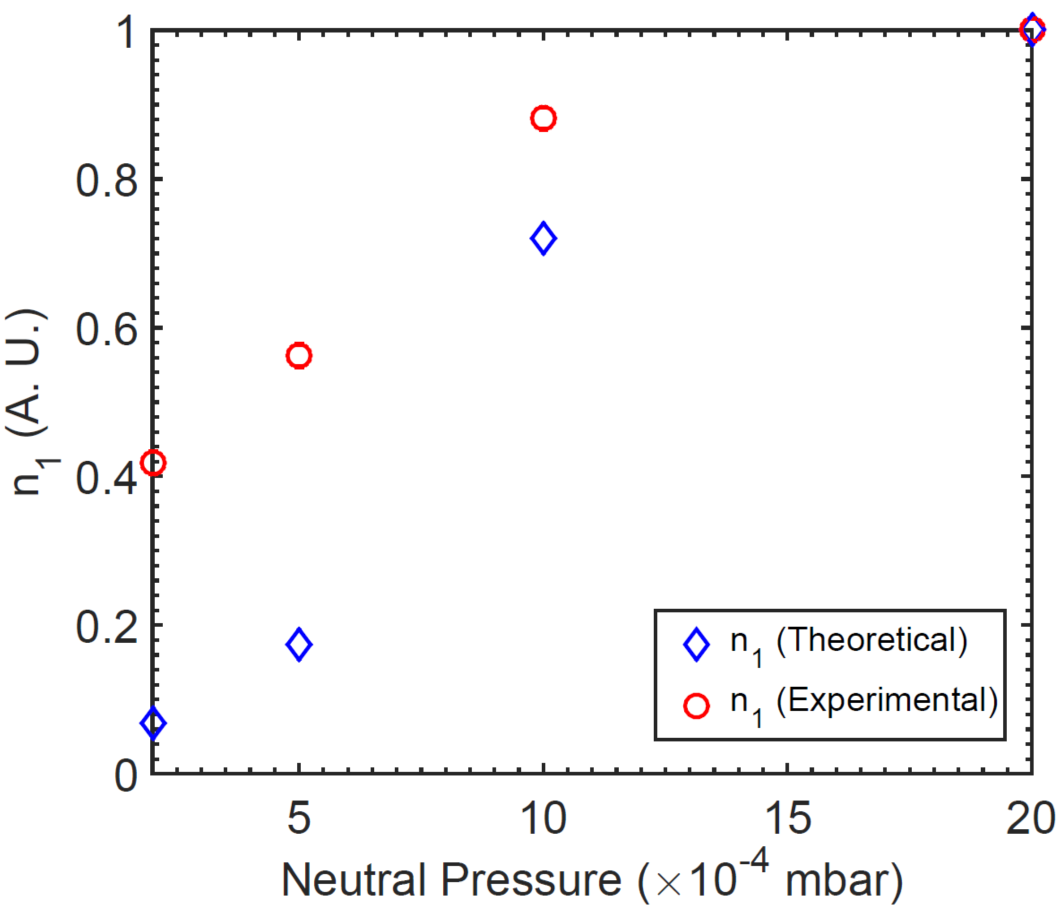

Figure 5.5: Variation of perturbed density amplitude ($\boldsymbol{n_1}$) with neutral pressure, experimental values are shown by circle and theoretically calculated values using eq (1) are shown by diamond marker.

The values of k are calculated by substituting the experimentally obtained parameters and real part of k is used to calculate the perturbed density. Perturbed density amplitude measured experimentally and calculated theoretically shows qualitative match as shown in Figure 5.5.

5.4 Summary and Discussion

The analysis of IA wave presented here shows the importance of collisions in describing the wave behaviour. To explore the effect of the neutral collision on IA wave the experiment has been performed for various neutral densities. The neutral density is varied by changing the neutral pressure, which in turn allows the change in ion-neutral, and electron-neutral collision mean free path. It is obvious and conventional that as the neutral collision increases with the neutral gas pressure and the IA wave gets heavily damped in plasma. Our experimental observation shows rather contrary results: it shows that, the wave amplitude ($\delta n/n$) and observable propagation length of IA wave enhances as the neutral density increases. Increase in neutral density leads to decrease in ion-neutral collision mean path. We observe that collisions support the wave to propagate for larger distances as the neutral density increases. This phenomenon is observed for the first time in IA wave experiments, to the best of our knowledge. For the experiments represented here, the ion-neutral mean free path becomes comparable to the wavelength of IA wave, and ions impart the momentum of IA wave to neutrals. The collisions of electrons and ions make the neutrals to carry and share the IA wave momentum. It makes the wave survive and propagate for larger distances in plasma. Experimental findings are shown to be qualitatively consistent with the estimates from a simple fluid model of collisional IA wave.

Chapter 6

Effect of Cusp Field on IA Wave Propagation

In the previous Chapter, the effect of ion-neutral collision on ion-acoustic wave without magnetic field is described. In our device, cusp magnetic field configuration is adopted for plasma confinement. Application of magnetic field on plasma, changes the plasma characteristic is various expected ways. A detail study of plasma characteristic in cusp magnetic field is described in Chapter 3. The IA is launched in the field free region of cusp magnetic field, where the ions are unmagnetized and hence the IA propagation is expected not to be affected by the magnetic field in the cusp regions. Since, the electrons also participate in the IA wave propagations and the cusp magnetic field affects them, there is a need to study the effect of the cusp magnetic field on the propagation of IA waves. In this chapter, the observed effects of cusp magnetic field on the propagation of IA wave in the field free central region are given in detail along with possible physics explanations as well as the shortcoming for a complete understanding.

6.1 Introduction

Ion waves are low frequency pressure waves in plasma. If the ion plasma frequency (ω_{pi}) greatly exceeds the wave frequency, both the electrons and ions oscillate almost in phase. They are longitudinal in nature and in the propagation of ion waves electrons provide the restoring force for ion inertia. Sound wave propagation in air depends on the particle collisions but in plasma long range electromagnetic forces plays an important role in the propagation of ion acoustic waves. Electrons in plasma tend to move faster than ion species. Electric field induced by a slight charge separation retards the motion of electrons, forcing the two species to propagate together.

Multi-line cusp plasma device (MPD) is used to perform experiments presented in this Chapter. As discussed above, the plasma confined in cusp geometry is extremely quiescent, we found $\delta n/n \leq 1 \times 10^{-3}$. Use of electromagnets to produce multi-line cusp magnetic field is the key that gives an opportunity to vary the cusp field strength to study of the effect of cusp magnetic field on the propagation of IA waves. For this, many IA wave experiments are done with varying field values at the cusp region.

Zakharova and Kuznetsova found that in a longitudinal Magnetic Field (MF) a localized ion-acoustic wave of low frequency mode can propagate parallel to the magnetic field without any deformation [172]. The cusp magnetic field has only r and θ components of the magnetic field and no z-component is present in this configuration and the wave is excited perpendicular to the field lines, along the z-axis. IA wave properties like damping length, amplitude and velocity of the wave have been examined with various cusp magnetic field strength. The effect of two temperature electron population on IA wave has also identified and discussed.

As, discussed in Chapter 3, the twelve pole six magnet (TPSM) Cusp magnetic field geometry is suitable for external perturbation studies. Hence, the TPSM cusp configuration is adopted for further IA wave studies. Multi-line cusp geometry produced using 6 electromagnets, a physical appearance of how the electromagnets are integrated with the main chamber is shown in figure 1 (c). The current direction in electromagnets is kept in such a way that all 6 poles on the inner circumference are North-poles as shown in figure 1(c).

The ion acoustic wave is excited using a circular mesh grid centred at $R = 0$, $Z = 75$ cm, mid- plane (R-Z) of the device. The IA wave is excited by appplying a sinusoidal voltage of 100 kHz to a 50 mm diameter stainless steel (SS304) mesh having a wire of diameter 0.26

mm and 0.9 mm aperture. The propagation of applied perturbation is detected by receiver directional Langmuir probe biased at electron saturation region.

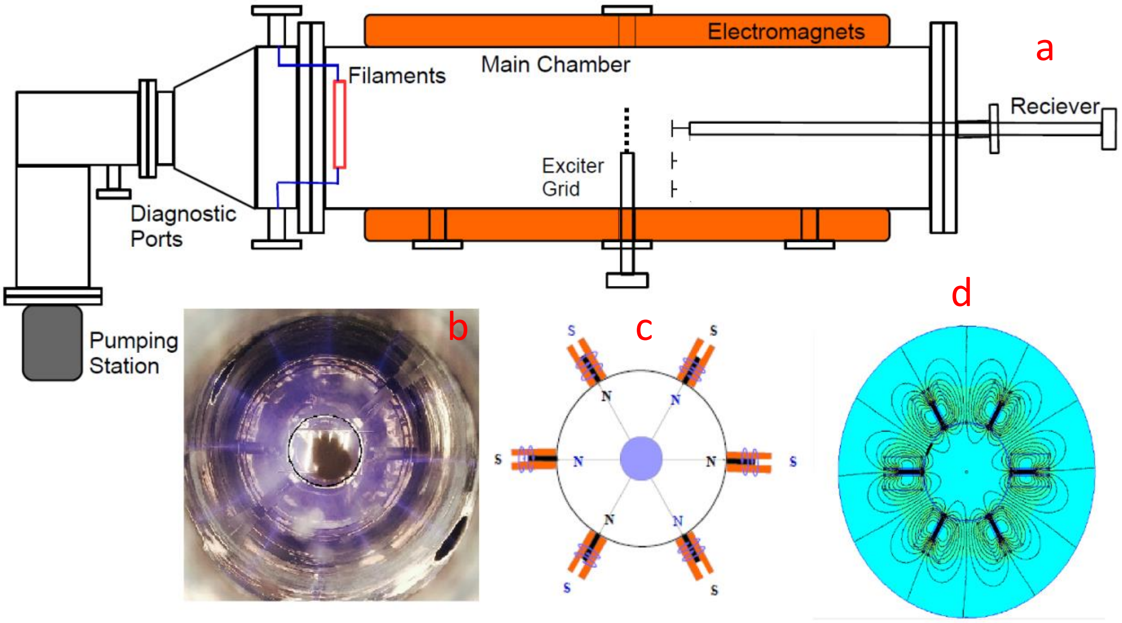

Figure 6.1: (a) Schematic of Multi-line cusp Plasma Device (MPD), (b) Image of plasma confined in BLCC, (c) Cross-sectional view of MPD showing the alignment of electromagnets integrated with device, (d) Cusp Magnetic field profile simulated using FEMM software.

The circuit being used for exciting and detecting ion acoustic wave is shown in Figure 4.4. The data is acquired in 12-bit digitization based Agilent (2024 Model) Oscilloscope and stored at a sampling rate of 250 MSa/sec for further analysis. The details about the excitation of IA wave are described in chapter 4.

6.2 Experimental Observation and Discussion

Quiescent, collisionless and uniform plasma has been produced in MPD by using cusp magnetic field geometry for plasma confinement. Initial characterization of MPD has been carried out in argon plasma using Langmuir probe and described in Chapter 3. The plasma density and temperature has been varied over range of $10^9 - 10^{11}$ cm^{-3} and 1-10 eV respectively by varying operating pressure, filament heating current, discharge voltage, and cusp magnetic field strength. The operating parameters for experiments presented in this chapter are listed as follows:

Operating Parameters:

Argon Pressure, P: 2×10^{-4} mbar

Discharge Voltage, V_D: -50 V

Magnet Current, I_{mag}: 10-35 A (varies on the requirement of experiment)

Perturbation Frequency, f $(\omega/2\pi)$: 100 kHz (10^5 Hz)

Perturbation Voltage: 4 V_{p-p}

Excited at: R=0 cm, Z = 75 cm, middle plane of cylindrical device

6.2.1 Excitation of Ion Acoustic Wave with Cusp Magnetic field

The cusp magnetic field strength tends to fall radially inward and has minimum value at R=0 cm, as shown in figure 3.7. The experiments are performed in this very low cusp magnetic field strength, which is perpendicular to the propagation of excited of IA wave along z-axis of cylinderical chamber as cusp magnetic field have only r and θ components. The initial results of the oscillating potential disturbance, excited as IA wave are shown in figure 6.2. Propagation of ion acoustic wave is measured by moving the disk probe axially away from the exciter, along the z-axis. The data is recorded for different spatial locations noted as d in figure 6.2, is the distance of receiver probe from exciter grid. The figure 6.2 depicts temporal evolution of applied sinusoidal signal and normalized density known as IA wave amplitude, for $B_p = 160$ G (pole cusp magnetic field strength, for $I_{mag} = 20$ A). Normalized density fluctuations are the ratio of density fluctuation to mean density.

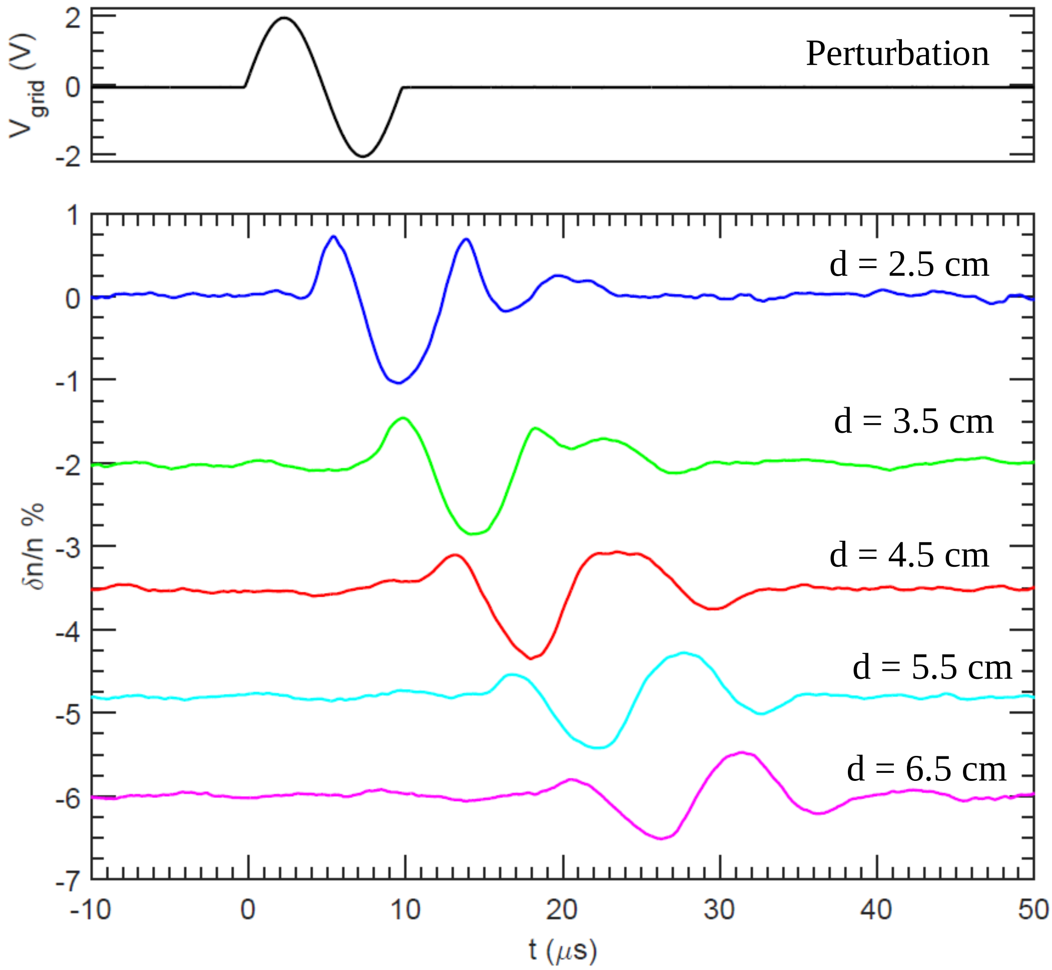

Figure 6.2: Propagation of sinusoidal perturbation at different axial, $\boldsymbol{Z}$ locations, here d is the distance of receiver probe from the exciter grid for $\mathbf{2 \times 10^{-4}}$ mBar Argon pressure, $\boldsymbol{B_p} = \mathbf{0.16}$ kG and discharge voltage, $\boldsymbol{V_D} = \mathbf{-50}$ V.

Upper most trace in figure 6.2 is the applied sinusoidal potential perturbation to exciter grid. The lower traces are detected wave propagation for different spatial locations d, measured by moving the receiver probe axially away from the grid. The spatial variation is meacured to determine propagation velocity and damping length of the wave. Progation velocity of IA wave is calculated by time of flight method for every d, spatial location and found to be $\sim 2.8 \times 10^3$ m/sec. In figure 6.2, one can observe that, the amplitude of IA wave decreases as it propagates in space. To estimate the damping length of the IA wave, the variation of amplitude of the IA wave along the spatial length d is plotted in Figure 6.3.

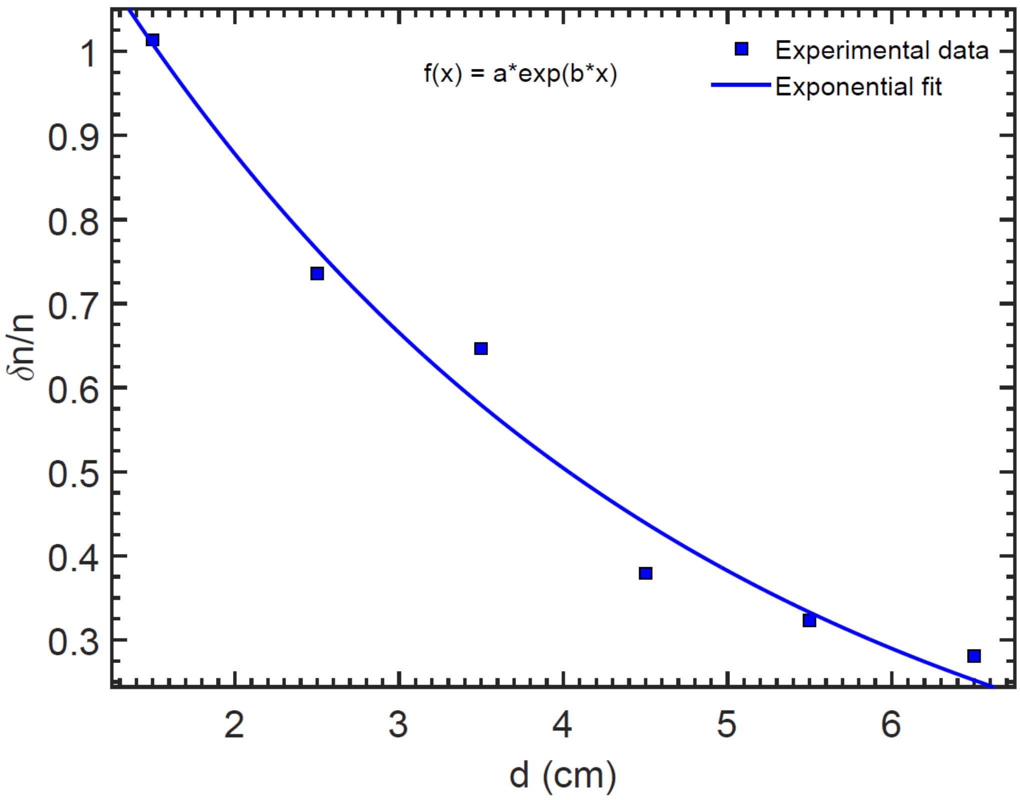

Figure 6.3: Shows variation in the wave amplitude (normalized to the amplitude of first peak of detected signal) for different spatial locations d, distance from the grid, for 160G cusp magnetic field strength, at $\mathbf{2 \times 10^{-4}}$ *mBar Argon pressure and discharge voltage,* $\boldsymbol{V_D = -50}$ *V.*

The square shaped markar (in figure 6.3) shows the actual wave amplitude, experimentally recorded and obtained from figure 6.2. Solid line in the figure 6.3 is an exponential fit to experimental values of amplitude. The damping length of the IA wave is calculated by $1/e$ fold times the maximum amplitude. The maximum amplitude is the amplitude of first peak of the detected signal at d = 1.5 cm. Therefore the damping length of IA wave, estimated from figure 6.3 is approximately 4.3 cm.

6.2.2 Effect of cusp magnetic field

As we know, any phenomenon in plasma depends on various plasma parameters and same applies to IA wave also, so increase in cusp magnetic field strength can also lead to some significant changes in IA wave properties. As earlier has been mentioned, the wave is excited at R=0 cm. The cusp magnetic field strength tends to fall radially inward and it has minimum value at R=0 cm, as shown in figure 3.8. In this section the propagation of IA wave has been examined for various values of cusp magnetic field strength.

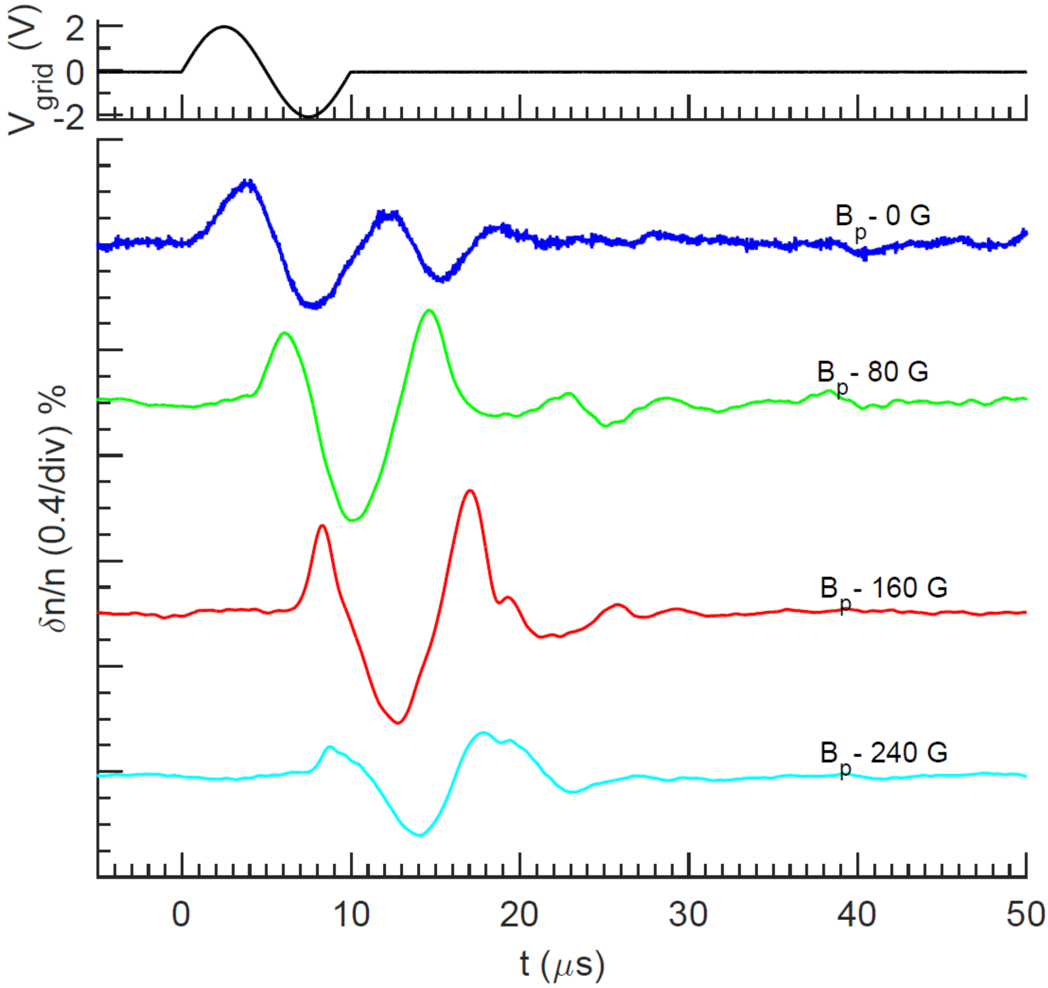

Figure 6.4: Propagation of sinusoidal perturbation at $\boldsymbol{d} = \mathbf{2.5}$ cm, here d is distance of receiver probe from the exciter grid for various values of $\boldsymbol{B_p}$ ($\boldsymbol{I_{mag}}$), at $\mathbf{2} \times \mathbf{10^{-4}}$ mBar Argon pressure and discharge voltage, $\boldsymbol{V_D} = \mathbf{-50}$ V.

The temporal evolution of applied sinusoidal signal and IA wave amplitude with increasing cusp strength is captured in figure 6.4. The upper most trace in figure is the applied sinusoidal disturbance and the lower traces are detected wave propagation for increasing cusp magnetic field strength. Temporal evolution of the propagation of IA wave in plasma is measured by receiver probe at d=2.5 cm. In figure 6.4, the IA wave propagation is shown from $B_p = 0\ G - 240\ G$ ($I_{mag} = 0\ A - 30\ A$). The wave amplitue is plotted only upto 240 G ($I_{mag} = 30$ A) cusp field strength, because the wave gets heavily damped, and its propagation ceases to exist in plasma for higher cusp field strength, $B_p \geq 240$ G ($I_{mag} \geq 30$ A) and no wave is observed afterwards (shown in figure 6.5).

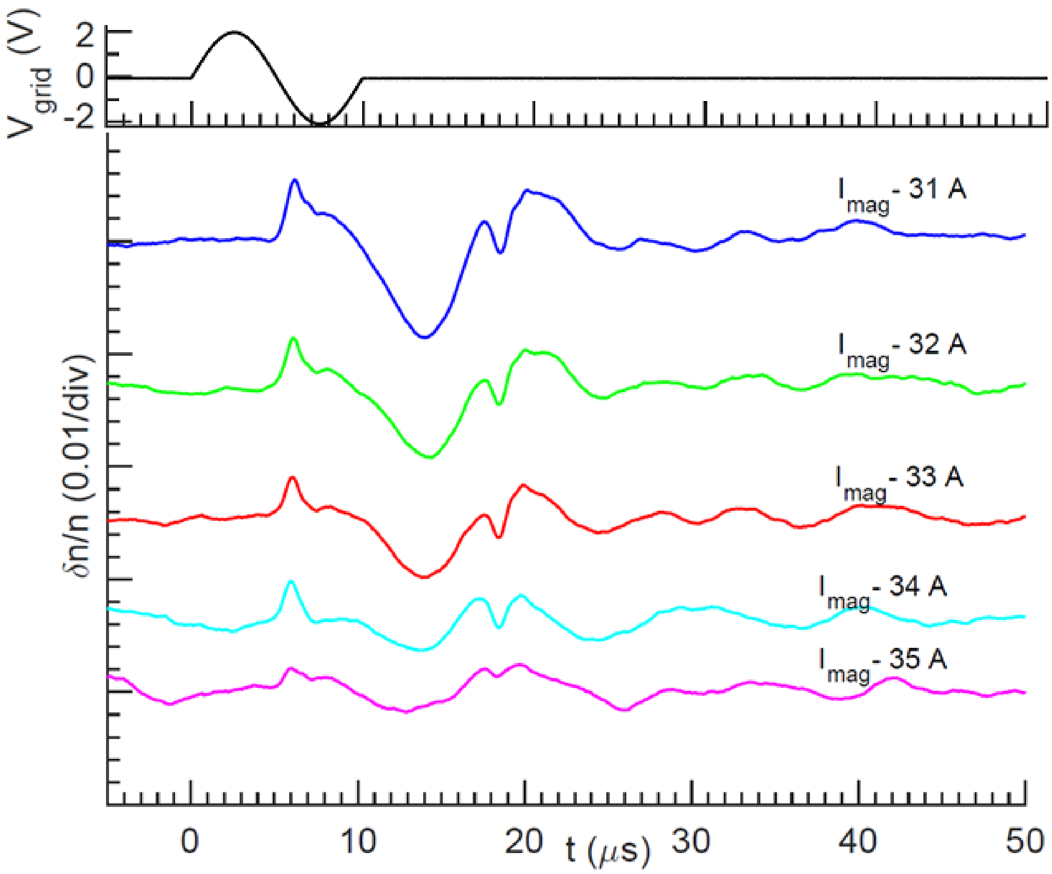

Figure 6.5: Propagation of sinusoidal perturbation at d=2.5 cm, here d is distance of receiver probe from the exciter grid for various values of $\boldsymbol{I_{mag}}$ ($\boldsymbol{B_p}$), at $\mathbf{2 \times 10^{-4}}$ mBar Argon pressure and discharge voltage, $\boldsymbol{V_D}$=-50 V.

The figure 6.5 shows the temporal evolution of IA wave amplitude with increasing cusp magnetic field strength for I_{mag} varies from $31 - 35$ A ($B_p \geq 240$ G). This IA wave amplitude is measured at same spatial location as it measured in figure 6.4, d=2.5 cm. In figure 6.4, one wave can observe a finite wave amplitude for 30 A magnet current ($B_p =$ 240 G. As the magnet current increases above 30 A, the wave deformation starts, it gets heavily damped, and its propagation ceases to exist in plasma, as shown in figure 6.5. As for $I_{mag} > 30$ A, only noisy signal is being recored by receiver probe, observed in figure 6.5.

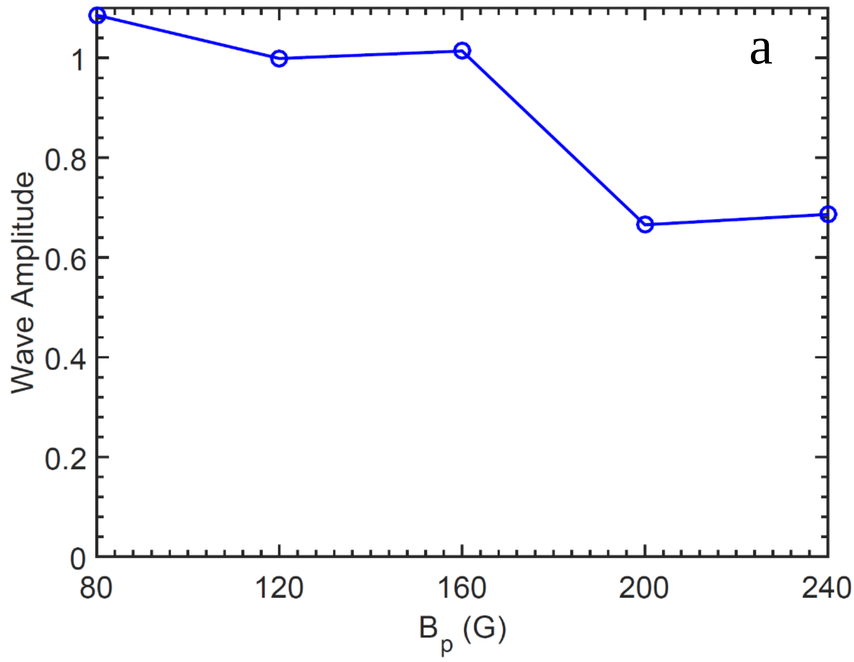

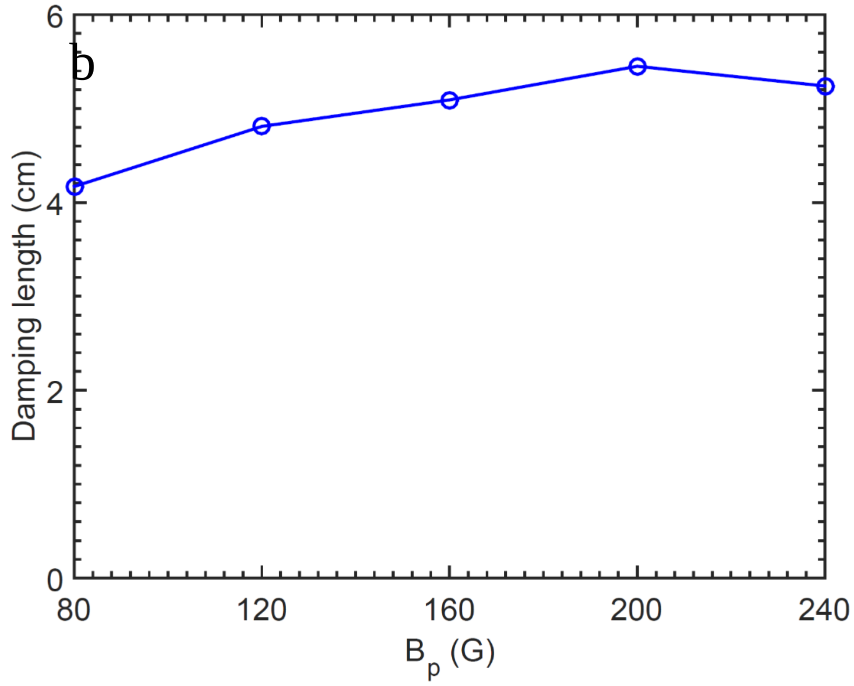

Figure 6.6: (a) Variation of amplitude of first peak of detected normalized signal of IA wave at d=1.5cm, away from the grid, $\boldsymbol{\delta n/n}$ and (b) shows the variation of damping length for increasing cusp magnetic field strength, at $\mathbf{2 \times 10^{-4}}$ mBar Argon pressure and discharge voltage, $\boldsymbol{V_D = -50}$ V.

The cause behind this strong damping of IA wave above a certain cusp magnetic field strength (or magnet current) will be discussed later on.

Increase in the cusp field strength, upto $\boldsymbol{B_P} = 240$ G, leads to change the amplitude, damping length and, propagation velocity of wave, so it will be the next step of discussion.

The variation of normalized wave amplitude with cusp magnetic field strength is shown in figure 6.6 (a). The amplitude and the wave amplitude measured for all field values is normalized by the amplitude measured for $B_p = 80$ G ($I_{mag} = 10$ A). It depicts that wave amplitude is almost constant for $B_p = 80 - 160$ G ($I_{mag} = 10, 15, and\ 20$ A) and shows a deacrease for $B_P = 160 - 200$ G ($I_{mag} = 20 - 25$ A).

The amplitude of IA wave decreases as it propagates in space. The damping distance of this IA wave is calculated by $1/e$ fold times. The damping length of IA wave is shown in figure 6.6(b). The damping length also shows an increase with increasing magnetic field and becomes constant at the higher magnetic fields. The damping length varies from 4.2 cm to 5.5 cm, which can be interpreted so that the damping length of IA wave does not vary significantly with increase in cusp field strength.

6.2.3 Wave Damping

As figure 6.4 and 6.5 shows that, the propagation of IA wave ceases out in plasma for higher cusp field strength, $B_p \geq 240$ G and no wave is observed for further increase in field strength. The IA wave wave propagation in plasma depends on many factors and properties of plasma. Major mechanisms responsible for the damping of the IA wave are described below:

a) Landau damping [71,87]

b) Damping due to geometrical spread of wave packet

c) Collisional damping or gas damping [90]

d) Damping due to plasma density gradient [166]

e) Two-electron temperature plasma [173,174]

f) Magnetic field obliqe to propagation of wave [175]

In MPD $T_e \gg T_i$ so Landau damping do not occur in present experimental scenario. The details about Landau damping are described in Chapter 4, section 4.3.7.2. As discussecd in Chapter 4, the geometrical spread of wave packet affects the spatial propagation and amplitude of wave. This phenomenon mainly depends on geometry of exciter and it is totally independent of magnetic field. Hence, it plays no significant role in heavy damping of IA wave with incereasing cusp field strength.

Low temperature plasmas are partially ionized as MPD Argon plasma and it has three species, electrons, ions, and neutrals. Collisions between these particles can significantly affect the wave propagation. For the curernt experimental conditions the ion neutral collision frequency, $\nu_{in} \sim 10^3$ Hz, $\nu_{in} \ll f$. The ion-neutral collision frequency is less than the perturbation frequency and it do not play a role in the damping. The electron neutral collision frequency, $\nu_{en} \sim 10^6$ Hz and IA wave perturbation frequency, $f = 10^5$ Hz, $\nu_{en} > f$. The electron neutral collision frequency is higher than the perturbation frequency. So, the electron-neutral collisions ($\nu_{en} = n_n \sigma_{en} v_{the}$) should play a role in the damping mechanism. In this chapter, we are discussing the results of experiments performed with the change of cusp magnetic field strength, while the neutral pressure is kept at 2×10^{-4} mbar. As we change the magnetic field strength the neutral density does not change, hence for a constant neutral density the electron neutral collision frequency does not change. Therefore, the role of both of collisions seem to be neglected.

The gradient in plasma density along the wave propagation axis can be a source to make the amplitude decrease spatially as discussed by Doucet et al. [166]. In Chapter 4, the axial plasma density variation is measured without any applied magnetic field. For present case, with applied cusp magnetic field the variation of normalized plasma density is presented in figure 6.7 for both cases without magnetic field (I_{mag} = 0 A) and with cusp magnetic field (I_{mag} = 30 A). The plasma density for both cases is normalized to the density value at z=80 cm, to compare the profile of axial density profile. The axial density is flatter (uniform) for I_{mag} = 30 A compared to density variation for without magnetic field (figure 6.7).

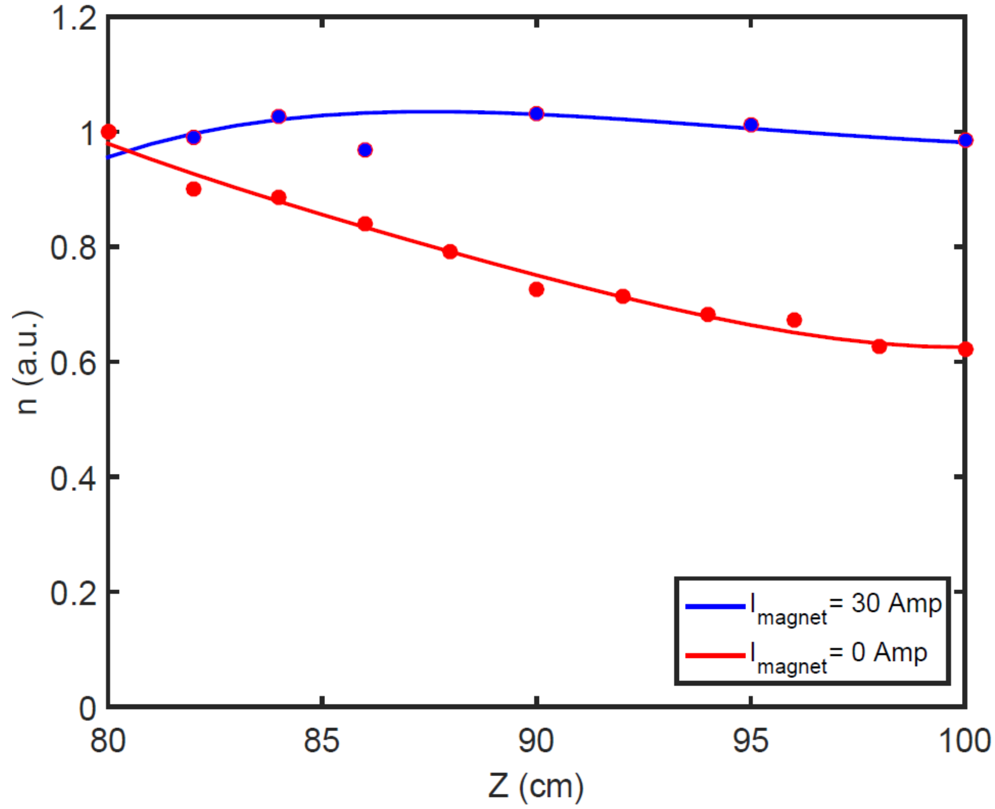

Figure 6.7: Axial variation of (a) plasma density, n, at $\mathbf{2 \times 10^{-4}}$ *mBar Argon pressure and 240 G cusp magnetic field strength.*

Therefore, for any value of cusp magnetic field strength, the density gradient scale length (L_n) will always be greater than 30 cm, as the L_n ~ 30 cm for I_{mag} = 0 A. As discussed in Chapter 4 and shown in figure 4.17, the density gradient scale length for without magnetic field case is much higher than the wavelength of IA wave, along the propagation of IA wave (z-axis). The gradient in plasma density was not the reason for the spatial wave damping for $I_{mag} = 0$ A. Hence, it cannot be a reason of damping in presence of applied cusp magnetic field.

Now the effect of two electron temperature and oblique magnetic field lines are more relevant in current experimental scenerio and hence are discussed in more detail in the following sections

6.2.3.1 Two-electron temperature

The details of variation of plasma parameters at R= 0 cm with increase in cusp field strength (B_p) are described in Chapter 3, section 3.1.1. Still, for the current requirement the variation of plasma density, n and cold electron temperature, T_e is shown in figure 6.8 (a) and (b) respectively. In MPD, the filamentary emission is used for plasma production, therefore, the population of two temperature electron distribution is present here. Confinement of primary electrons is one of the advantage of Cusp magnetic field geometry [67]. An increase in cusp magnetic field strength increases the plasma density as shown in figure 6.8 (a). The enhancement in plasma density is a result of increase in the population of primary electrons with cusp field strength.

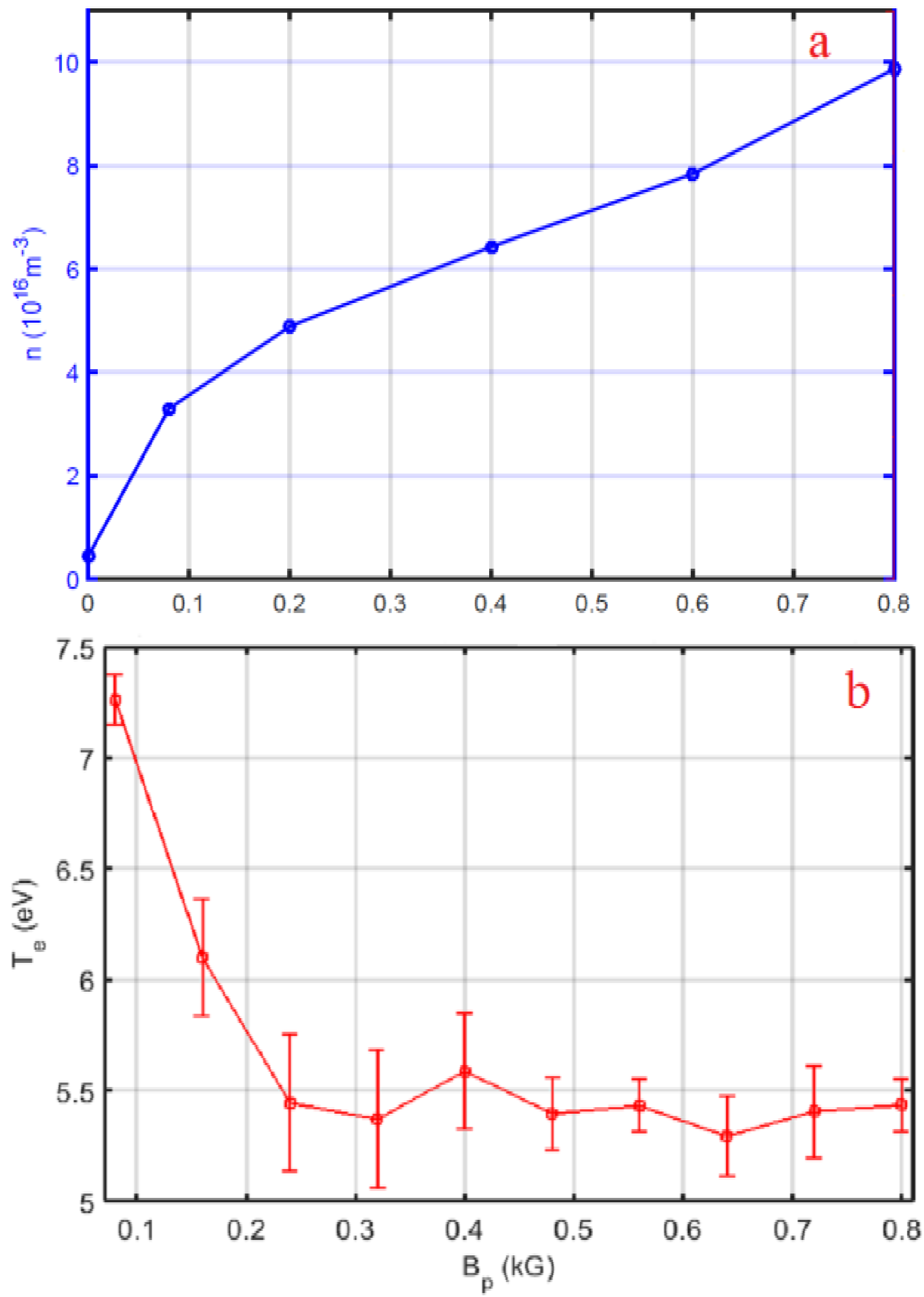

Figure 6.8: Variation of (a) plasma density, $\boldsymbol{n}$ *and (b) electron temperature,* $\boldsymbol{T_e}$ *with cusp magnetic field strength at* $\boldsymbol{R} = \boldsymbol{0}$ *cm for* $\boldsymbol{2} \times \boldsymbol{10^{-4}}$ *mBar Argon pressure and discharge voltage,* $\boldsymbol{V_D} = -\boldsymbol{50}$ *V.*

The experimetally estimated cold electron temperature shows that with an increase in cusp magnetic field the electron temperature reduces utpo 0.24 kG cusp field strength. It becomes constant with further increase in magnetic field, shown in figure 6.8 (b).

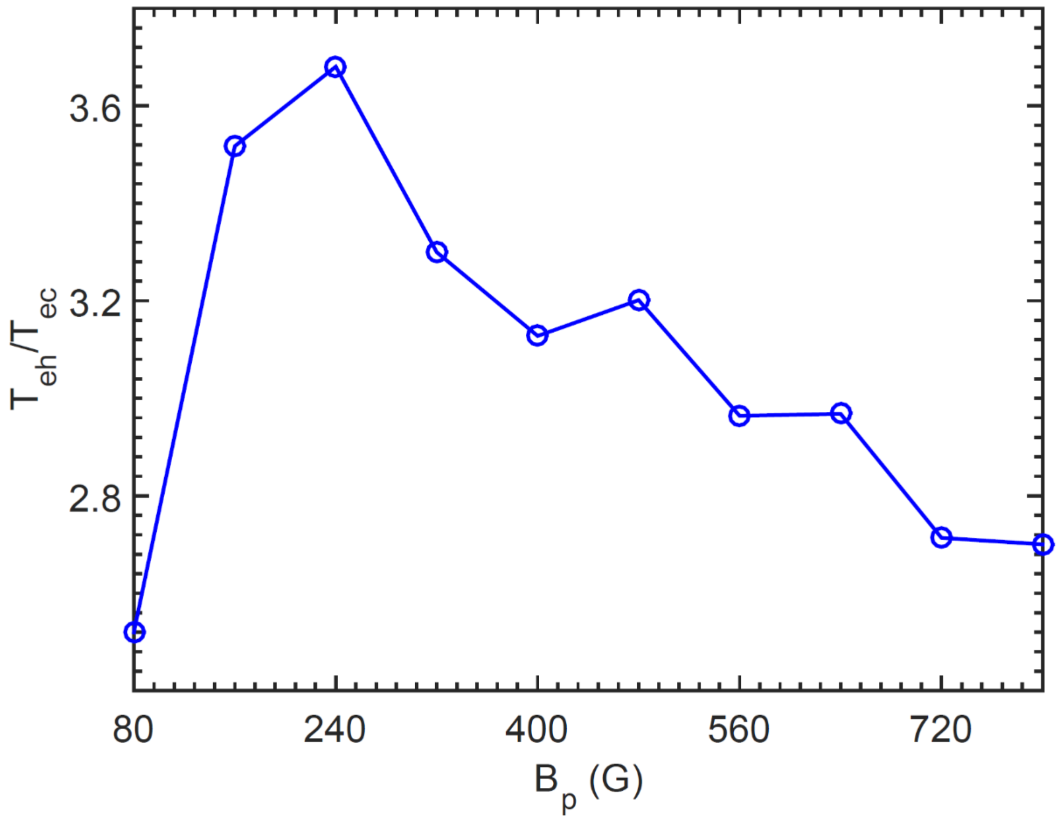

Figure 6.9: Variation of the ratio of high to low electron temperature with cusp magnetic field strength at $\boldsymbol{R = 0}$ *cm for* $\mathbf{2 \times 10^{-4}}$ *mBar Argon pressure and discharge voltage,* $\boldsymbol{V_D = -50}$ *V.*

Figure 6.9 shows the variation of the ratio of high electron temperature, T_{eh} to low electron temperature, T_{el} with increase in cusp magnetic field strength. The figure 6.9 shows a change at 240 G, cusp field value, where the propagation of IA wave ceases away. Initially increase in the ratio of electron temperatures says that difference in the temperatures of both the electrons is increasing. After $B_p > 0.24$ kG, the ration start decreasing, showing the dominance of cold electrons increases over high temperature electrons. As discussed by Jones et al., the increase in dominance of cold electrons can hugely affects the IA wave properties and it can make the damping of wave. The change in the ratio of T_{eh}/T_{el} effects the nature of IA wave propagation as shown in figure 6.9.

6.2.3.2 Magnetic field oblique to propagation of wave

The experimental study of IA wave is performed in the TPSM cusp configuration. In TPSM configuration, the central cylindrical volume (of radius ~ 8 cm and length ~ 100 cm) has very low magnetic field $B < 2$ G for ($B_P = 800$ G). The IA wave is excited in this regime of TPSM cusp magnetic field. For low magnetic field (B ≤ 2 G at R=0 cm), the ion cyclotron frequency, $\Omega_i = eB/m_i < 1$ kHz, the electron cyclotron frequency, $\Omega_e = eB/m_e \sim$ 0.1 GHz. The perturbation frequency for IA excitation is 100 kHz. The IA wave is studied in cusp magnetic field $\omega \gg \Omega_i$, therefore, the ions are unmagnetized for the IA wave. In the presence of IA waves, ions will follow nearly straight lines regardless of the direction of the wave number vector k and magnetic field vector. Ions can behave as unmagnetized in the perturbed plasma also in case of $\nu_i > \Omega_i$ and for short wavelengths $\lambda < \rho_i$, $\rho_i = v_{thi}/\Omega_i$ and $v_{thi} = \sqrt{(kT_i/m_i)}$. Hence, we can say that the ion behavior is not affected by the cusp magnetic field and ions will act same as it was in IA wave without magnetic field. Since, $\omega \ll \Omega_e$, it indicates that electrons are magnetized for excited IA wave in MPD. Therefore, the electrons are bound to follow magnetic field lines and, their perpendicular and parallel (to magnetic field lines) dynamics will be essentially different.

As the cusp field value suppose to be zero (theoretically) at center R=0, where the IA wave is excited. When the magnetic field is measured using hall probe, we observe the non-zero value of magnetic field. We observed that, as the cusp magnetic field at the pole increases, the value of magnetic field at R=0 cm also increases. Hence, the decrease in electron larmor radius ($\rho_e = m_e v_{the}/qB$) at R=0 cm is been predicted and calculated, with increase in cusp magnetic field strength. The wavelength of IA wave, $\lambda_\phi = 3\ cm$, after which it damped in plasma and the larmor radius, $\rho_e \sim 6$ cm. At that cusp magnetic field for $I_{mag} = 30$ A ($B_p \sim 240$ G), and at R=1.0 cm, the magnetic field (B_0) is $\sim$ 0.8 G. Wavelength of IA wave falls in the range of electron larmor radius as the cusp field strength increases. In cusp magnetic field configuration, the net magnetic field B is average of radial and poloidal component of cusp magnetic field B_r and B_θ, the axial z component of magnetic field B_z

being negligible. The IA wave propagation is perpendicular to cusp magnetic field. The magnetized electrons are bound to follow magnetic field lines and magnetic field lines, oblique to wave propagation restricts the motion of electrons along the direction of propagation of IA wave. Therefore the restoring force provided by electrons will become weak and the propagation velocity of IA wave get slows down. As we increase cusp field strength the larmor radius decreases more and more, it reflects in reducing the restoring force of electron and restricting its motion along the propagation of wave. As a result, the wave propagation ceases away in the absence of proper restoring force. The little difference in wavelength and larmor radius where the wave damps out can be due to measurement of electron temperature. In presence of magnetic field electron temperature have two components $T_{e_{\perp}}\ and\ T_{e\parallel}$ and larmor radius depends on $T_{e_{\perp}}$. If the effect of the magnetic field on temperature is incorporated for the estimation of electron temperature, the values of larmore radius and wave's wavelength might come closer.

6.3 Summary and Conclusions

This Chapter, presents the experimental observation on IA wave propagation in Multi-line cusp plasma device at R=0 center of the device. The IA is launched in the field free region where the ions are unmagnetized and hence the IA propagation is expected not to be affected by the magnetic field in the cusp regions. The IA wave properties like amplitude, damping length, and wave velocity are examined with various cusp magnetic field strength. It is observed, above a certain value of cusp magnetic field (certain current value in electromagnets), the IA gets heavily damped, and its propagation ceases to exist in plasma.

Plasma contains two temperature electron species and its temperature and population changes with cusp magnetic field. The change in T_{eh} and T_{ec} is measured to understand the variation of IA wave properties with an increase in B_p. The ratio T_{eh}/T_{ec} first increases with

B_p and at the same values of B_p the amplitude of IA wave increases. For cusp magnetic field $B_p > 0.24$ kG, T_{eh}/T_{ec} starts decreasing with cusp magnetic field strength and the wave amplitude also decreases due to the dominance of low temperature electrons. The effect of two electron temperature is observed and found that the increase in dominance of bulk electron temperature hugely affect the characteristics of IA wave. The oblique cusp magnetic field lines restrict the free motion of electrons along the wave propagation. This make the electron response quasi-adiabatic or effect the electron Boltzmann behavior and the restoring force provided by electrons becomes weak, it makes the IA wave slower than C_s. As the cusp magnetic field strength increases the wave propagation ceases away in absence of proper restoring force of electrons.

The experimentally observed IA wave damping for $B_p \geq 240$ Gauss is a combined effect of two electron temperature and oblique magnetic field. Since the cusp magnetic field confines hot primary electrons by mirror effect, the increase in the cusp field value alters the local plasma parameters before the wave is even launched. Hence the exact segregation of data for comparisons with different cusp field values is not possible. To do this, more diagnostics and control are needed to keep as much as variables (plasma parameters) constant and allow the rest to change for said studies.

References

[1] J. W. Connor, Plasma Physics and Controlled Fusion **37**, A119 (1995).

[2] L. G. Althaus and O. G. Benvenuto, Monthly Notices of the Royal Astronomical Society **278**, 981 (1996).

[3] G. R. Tynan, A. Fujisawa, and G. McKee, Plasma Physics and Controlled Fusion **51**, 113001 (2009).

[4] E. J. D. (Chair T. Physics), W. A. H. (Chair C. Da Modelling), Y. K. (Chair P. and Edge), V. M. (co-C. T. Physics), T. H. O. (co-C. P. and Edge), A. P. (co-C. C. Da Modelling), G. Bateman, J. . Connor, J. G. C. (retired), T. Fujita, X. Garbet, T. . Hahm, L. . Horton, A. . Hubbard, F. Imbeaux, F. Jenko, J. . Kinsey, Y. Kishimoto, J. Li, T. . Luce, Y. Martin, M. Ossipenko, V. Parail, A. Peeters, T. . Rhodes, J. . Rice, C. . Roach, V. Rozhansky, F. Ryter, G. Saibene, R. Sartori, A. C. . Sips, J. . Snipes, M. Sugihara, E. . Synakowski, H. Takenaga, T. Takizuka, K. Thomsen, M. . Wade, H. . Wilson, I. T. P. T. Group, I. C. D. and M. Group, and I. P. and E. T. Group, Nuclear Fusion **47**, S18 (2007).

[5] A. J. Wootton, B. A. Carreras, H. Matsumoto, K. McGuire, W. A. Peebles, C. P. Ritz, P. W. Terry, and S. J. Zweben, Physics of Fluids B: Plasma Physics **2**, 2879 (1990).

[6] B. A. Carreras, C. Hidalgo, E. Sánchez, M. A. Pedrosa, R. Balbín, I. García-Cortés, B. van Milligen, D. E. Newman, and V. E. Lynch, Physics of Plasmas **3**, 2664 (1996).

[7] P. C. Liewer, Nuclear Fusion **25**, 543 (1985).

[8] A. H. Nielsen, H. L. Pécseli, and J. J. Rasmussen, Physica Scripta **51**, 632 (1995).

[9] A. Fasoli, B. Labit, M. McGrath, S. H. Müller, G. Plyushchev, M. Podestà, and F. M. Poli, Physics of Plasmas **13**, (2006).

[10] X. Garbet, L. Garzotti, P. Mantica, H. Nordman, M. Valovic, H. Weisen, and C. Angioni, Physical Review Letters **91**, 035001 (2003).

[11] J. A. Krommes and C.-B. Kim, Physics of Fluids **31**, 869 (1988).

[12] J. D. Callen, C. C. Hegna, and A. J. Cole, Nuclear Fusion **53**, 113015 (2013).

[13] L. Irving and K. H. KINGDON, Proceedings of the Royal Society of London. Series A, Containing Papers of a Mathematical and Physical Character **107**, 61 (1925).

[14] P. J. Paris and N. Rynn, Review of Scientific Instruments **61**, 1095 (1990).

[15] N. Rynn and N. D'Angelo, Review of Scientific Instruments **31**, 1326 (1960).

[16] N. Rynn, Review of Scientific Instruments **35**, 40 (1964).

[17] P. J. Barrett, H. G. Jones, and R. N. Franklin, Plasma Physics **10**, 911 (1968).

[18] H. L. Pecseli, T. Mikkelsen, S. E. Larsen, T. Huld, S. Iizuka, J. H. Misguich, R. Balescu, and H. L. Picseli, Physica Scripta **T2A**, 147 (1982).

[19] N. D'Angelo, H. L. Pécseli, and P. I. Petersen, Review of Scientific Instruments **17**, 1853 (1974).

[20] N. D'Angelo and R. W. Motley, Physics of Fluids **6**, 422 (1963).

[21] F. F. Chen, in *Introduction to Plasma Physics and Controlled Fusion* (Springer International Publishing, Cham, 2018), pp. E1–E1.

[22] M. A. Lieberman and A. J. Lichtenberg, *Principles of Plasma Discharges and Materials Processing* (John Wiley & Sons, Inc., Hoboken, NJ, USA, 2005).

[23] R. J. Taylor, K. R. MacKenzie, and H. Ikezi, Review of Scientific Instruments **43**, 1675 (1972).

[24] M. G. Haines, Nuclear Fusion **17**, 811 (1977).

[25] M. G. Haines, Nuclear Fusion **17**, 811 (1977).

[26] M. G. Haines, K. N. Leung, R. D. Collier, L. B. Marshall, T. N. Gallaher, W. H. Ingham, R. E. Kribel, G. R. Taylor, R. J. Taylor, K. R. MacKenzie, and H. Ikezi, Review of Scientific Instruments **49**, 321 (1978).

[27] T. K. Allen and I. J. Spalding, The Physics of Fluids **8**, 2032 (1965).

[28] M. Sadowski, Physics Letters A **25**, 695 (1967).

[29] M. Sadowski, Physics Letters A **27**, 435 (1968).

[30] M. Sadowski, Physics Letters A **28**, 626 (1969).

[31] K. N. Leung, N. Hershkowitz, and T. Romesser, Physics Letters A **53**, 264 (1975).

[32] R. Limpaecher and K. R. MacKenzie, Review of Scientific Instruments **44**, 726 (1973).

[33] S. M., Journal of Plasma Physics **4**, 1 (1970).

[34] M. Sadowski, Review of Scientific Instruments **40**, 1545 (1969).

[35] M. Q. Tran, Physics Letters A **48**, 447 (1974).

[36] K. N. Leung, T. K. Samec, and A. Lamm, Physics Letters A **51**, 490 (1975).

[37] K. N. Leung, G. R. Taylor, J. M. Barrick, S. L. Paul, and R. E. Kribel, Physics Letters A **57**, 145 (1976).

[38] S. Bhattacharjee and H. Amemiya, Rev. Sci. Instrum. **70**, 3332 (1999).

[39] M. Pathak, V. K. Senecha, R. Kumar, and D. V. Ghodke, Nuclear Instruments and Methods in Physics Research Section A: Accelerators, Spectrometers, Detectors and

Associated Equipment **838**, 96 (2016).

[40] M. Kuriyama, N. Akino, M. Araki, N. Ebisawa, M. Hanada, T. Inoue, M. Kawai, M. Kazawa, J. Koizumi, T. Kunieda, M. Matsuoka, K. Miyamoto, M. Mizuno, K. Mogaki, Y. Ohara, T. Ohga, Y. Okumura, H. Oohara, F. Satoh, T. Suzuki, S. Takahashi, T. Takayasu, H. Usami, K. Usui, K. Watanabe, M. Yamamoto, and T. Yamazaki, Fusion Engineering and Design **26**, 445 (1995).

[41] D. M. Goebel and I. Katz, *Fundamentals of Electric Propulasion* (John Wiley & Sons, Inc., Hoboken, NJ, USA, 2008).

[42] V. N. Tondare, Journal of Vacuum Science & Technology A: Vacuum, Surfaces, and Films **23**, 1498 (2005).

[43] H. Conrads and M. Schmidt, Plasma Sources Science and Technology **9**, 441 (2000).

[44] W. L. Stirling, P. M. Ryan, C. C. Tsai, and K. N. Leung, Review of Scientific Instruments **50**, 102 (1979).

[45] S. Mukherjee and P. I. John, Surface and Coatings Technology **93**, 188 (1997).

[46] R. Günzel, E. Wieser, E. Richter, and J. Steffen, Journal of Vacuum Science & Technology B: Microelectronics and Nanometer Structures Processing, Measurement, and Phenomen **12**, 927 (1994).

[47] T. E. Wicker and T. D. Mantei, Journal of Applied Physics **57**, 1638 (1985).

[48] Y. Wang and T. W. Coyle, Journal of Thermal Spray Technology **16**, 898 (2007).

[49] S. Takamura, IEEJ Transactions on Electrical and Electronic Engineering **7**, 1 (2012).

[50] L. S. Combes, C. C. Gallagher, and M. A. Levine, Physics of Fluids **5**, 1070 (1962).

[51] T. J. Mcguire, **1**, (2014).

[52] G. Knorr and R. L. Merlino, Plasma Physics and Controlled Fusion **26**, 433 (1984).

[53] N. Hershkowitz, J. R. DeKock, P. Coakley, and S. L. Cartier, Review of Scientific Instruments **51**, 64 (1980).

[54] B. Dankongkakul, S. J. Araki, and R. E. Wirz, Physics of Plasmas **21**, 043506 (2014).

[55] J. S. and J. L. H. J. M. BUZZI, Physics Letters A **54**, 4 (1975).

[56] A. A. Hubble and J. E. Foster, Journal of Vacuum Science & Technology A: Vacuum, Surfaces, and Films **30**, 011301 (2012).

[57] M. Hosseinzadeh and H. Afarideh, Nuclear Inst. and Methods in Physics Research, A **735**, 416 (2014).

[58] A. D. Patel, M. Sharma, N. Ramasubramanian, J. Ghosh, and P. K. Chattopadhyay, Physica Scripta **95**, 035602 (2020).

[59] S. T. K. and L. A. Leung, K. N., Physics Letters A **51**, 490 (1975).

[60] J. H. Kim, Physics Procedia **66**, 498 (2015).

[61] J. S. Sovey, Journal of Spacecraft and Rockets **19**, 257 (1982).

[62] A. Kitsunezaki, Physics of Fluids **17**, 1895 (1974).

[63] T. Christensen and N. Hershkowitz, IEEE Transactions on Plasma Science **PS-5**, 23 (1977).

[64] and T. R. Noah Hershkowitz, K. N. Leung, Physical Review Letters **35**, 277 (1975).

[65] H. Kozima, S. Kawamoto, and K. Yamagiwa, Physics Letters A **86**, 373 (1981).

[66] R. Jones, Plasma Physics **21**, 505 (1979).

[67] A. D. Patel, M. Sharma, N. Ramasubramanian, R. Ganesh, and P. K. Chattopadhyay, Review of Scientific Instruments **89**, 043510 (2018).

[68] A. D. Patel, M. Sharma, N. Ramasubramanian, J. Ghosh, and P. K. Chattopadhyay, Physica Scripta 0 (2019).

[69] L. Tonks and I. Langmuir, Physical Review **33**, 195 (1929).

[70] R. W. Revans, Physical Review **44**, 798 (1933).

[71] A. Y. Wong, N. D'Angelo, and R. W. Motley, Physical Review Letters **9**, 415 (1962).

[72] P. J. Barrett and P. F. Little, Physical Review Letters **14**, 356 (1965).

[73] I. Alexeff and R. V. Neidigh, Physical Review **129**, 516 (1963).

[74] G. M. Sessler, Physical Review Letters **17**, 243 (1966).

[75] H. Tanaca, M. Koganei, and A. Hirose, Physical Review Letters **16**, 1079 (1966).

[76] H. Ikezi, R. J. Taylor, and D. R. Baker, Physical Review Letters **25**, 11 (1970).

[77] R. J. Taylor, K. R. MacKenzie, and H. Ikezi, Review of Scientific Instruments **43**, 1675 (1972).

[78] H. Ikezi, Physics of Fluids **16**, 1668 (1973).

[79] M. Q. Tran, Physica Scripta **20**, 317 (1979).

[80] Y. Nakamura and T. Ogino, Plasma Physics **24**, 1295 (1982).

[81] S. Watanabe, Journal of Plasma Physics **14**, 353 (1975).

[82] I. B. Bernstein, Physics of Fluids **14**, 628 (1971).

[83] J. L. Hirshfield, Physics of Fluids **14**, 615 (1971).

[84] T. Christensen and N. Hershkowitz, Physics of Fluids **20**, 840 (1977).

[85] O. Ishihara, I. Alexeff, H. J. Doucet, and W. D. Jones, Physics of Fluids **21**, 2211 (1978).

[86] R. P. Dahiya, P. I. John, and Y. C. Saxena, Physics Letters A **65**, (1978).

[87] I. Alexeff, Physics of Fluids **11**, 167 (1968).

[88] I. Alexeff, W. D. Jones, and D. Montgomery, Physical Review Letters **19**, 422 (1967).

[89] R. J. Armstrong, W. J. Weber, and J. Trulsen, **74**, 319 (1979).

[90] R. L. Berger and E. J. Valeo, Physics of Plasmas **12**, 032104 (2005).

[91] R. W. Short and A. Simon, Physics of Plasmas **9**, 3245 (2002).

[92] A. M. Hala and N. Hershkowitz, Review of Scientific Instruments **72**, 2279 (2001).

[93] J. L. Cooney, D. W. Aossey, J. E. Williams, M. T. Gavin, H. S. Kim, Y.-C. Hsu, A. Scheller, and K. E. Lonngren, Plasma Sources Science and Technology **2**, 73 (1993).

[94] L. St-Onge, J. Margot, and M. Chaker, Applied Physics Letters **72**, 290 (1998).

[95] H. Amemiya, Journal of Physics D: Applied Physics **23**, 999 (1990).

[96] M. Shindo, S. Uchino, R. Ichiki, S. Yoshimura, and Y. Kawai, Review of Scientific Instruments **72**, 2288 (2001).

[97] L. Oksuz, D. Lee, and N. Hershkowitz, Plasma Sources Science and Technology **17**, 015012 (2008).

[98] D. Lee, N. Hershkowitz, and G. D. Severn, Applied Physics Letters **91**, 041505 (2007).

[99] D. A. Gurnett, E. Marsch, W. Pilipp, R. Schwenn, and H. Rosenbauer, Journal of Geophysical Research **84**, 2029 (1979).

[100] K. Annou, Astrophysics and Space Science **357**, 163 (2015).

[101] F. Haas, K. A. Pascoal, and J. T. Mendonça, Physics of Plasmas **24**, 052115 (2017).

[102] F. Haas, K. A. Pascoal, and J. T. Mendonça, Physical Review E **95**, 013207 (2017).

[103] M. Shindo, S. Uchino, R. Ichiki, S. Yoshimura, and Y. Kawai, Review of Scientific Instruments **72**, 2288 (2001).

[104] J. Virmont, Plasma Physics **16**, 201 (1974).

[105] W. D. Jones, H. J. Doucet, and J. M. Buzzi, *An Introduction to the Linear Theories and Methods of Electrostatic Waves in Plasmas* (Springer US, Boston, MA, 1985).

[106] K. Nagashima, A. Sakasai, and T. Fukuda, Nuclear Fusion **33**, 1677 (1993).

[107] C. Wersal and P. Ricci, Nuclear Fusion **57**, 116018 (2017).

[108] E. E. Scime and A. M. Keesee, Frontiers in Astronomy and Space Sciences **6**, 1 (2019).

[109] E. Scime and A. Zaniewski, Review of Scientific Instruments **75**, 3526 (2004).

[110] M. Gruntman, Review of Scientific Instruments **68**, 3617 (1997).

[111] H.-J. Fahr, H. Fichtner, and K. Scherer, Reviews of Geophysics **45**, 1 (2007).

[112] J. H. Westlake, D. G. Mitchell, P. C. so. Brandt, B. G. Andrews, and G. Clark, Journal of Geophysical Research: Space Physics **121**, 8228 (2016).

[113] S. Ma, W. Yan, and L. Xu, Journal of Geophysical Research: Space Physics **120**, 9334 (2015).

[114] N. Sergis, E. J. Bunce, J. F. Carbary, S. W. H. Cowley, X. Jia, D. C. Hamilton, S. M. Krimigis, D. G. Mitchell, and M. K. Dougherty, in *Electric Currents in Geospace and Beyond* (2018), pp. 139–154.

[115] A. PATEL, STUDY OF PLASMA IN A MULTI-POLE LINE CUSP MAGNETIC FIELD, 2019.

[116] H. M. Mott-Smith and I. Langmuir, Physical Review **28**, 727 (1926).

[117] R. C. Davidson, in *Pure and Applied Physics* (1972), p. ii.

[118] Yuri P. Raizer, *Gas Discharge Physics* (1991).

[119] T. Pierre, G. Leclert, and F. Braun, Review of Scientific Instruments **58**, 6 (1987).

[120] I. G. Brown, Physics of Fluids **14**, 1377 (1971).

[121] L. D. Landau, Journal of Physics **10**, 25 (1946).

[122] R. L. Merlino, American Journal of Physics **75**, 1078 (2007).

[123] M. Umair Siddiqui and N. Hershkowitz, Physics of Plasmas **21**, 020707 (2014).

[124] I. Choi, C. Chung, and S. Youn Moon, Physics of Plasmas **20**, 083508 (2013).

[125] F. F. Chen, Plasma Sources Science and Technology **18**, 035012 (2009).

[126] S. Bose, M. Kaur, P. K. Chattopadhyay, J. Ghosh, Y. C. Saxena, and R. Pal, Journal of Plasma Physics **83**, 615830201 (2017).

[127] I. D. Sudit and R. C. Woods, Journal of Applied Physics **76**, 4488 (1994).

[128] U. Kumar, S. G. Thatipamula, R. Ganesh, Y. C. Saxena, and D. Raju, Physics of Plasmas **23**, 102301 (2016).

[129] M. Hudis and L. M. Lidsky, Journal of Applied Physics **41**, 5011 (1970).

[130] B. J. Peterson, J. N. Talmadge, D. T. Anderson, F. S. B. Anderson, and J. L. Shohet, Review of Scientific Instruments **65**, 2599 (1994).

[131] I. Langmuir, Journal of the Franklin Institute **196**, 751 (1923).

[132] J. P. Sheehan, Y. Raitses, N. Hershkowitz, I. Kaganovich, and N. J. Fisch, Physics of Plasmas **18**, 073501 (2011).

[133] R. F. Kemp and J. M. Sellen, Review of Scientific Instruments **37**, 455 (1966).

[134] J. W. Bradley, S. Thompson, and Y. A. Gonzalvo, in *IEEE Conference Record - Abstracts. PPPS-2001 Pulsed Power Plasma Science 2001. 28th IEEE International Conference on Plasma Science and 13th IEEE International Pulsed Power Conference (Cat. No.01CH37255)* (IEEE, 2001), p. 376.

[135] P. C. Stangeby, Physics of Fluids **27**, 2699 (1984).

[136] I. H. Hutchinson, *Principles_of_Plasma_Diagnostics* (n.d.).

[137] I. H. Hutchinson, Physical Review A **37**, 4358 (1988).

[138] L. Patacchini and I. H. Hutchinson, Physical Review E **80**, 036403 (2009).

[139] K. Nagaoka, A. Okamoto, S. Yoshimura, and M. Y. Tanaka, Journal of the Physics Society of Japan **70**, 131 (2001).

[140] J. M. Beall, Y. C. Kim, and E. J. Powers, Journal of Applied Physics **53**, 3933 (1982).

[141] Y. C. Kim and E. J. Powers, IEEE Transactions on Plasma Science **7**, 120 (1979).

[142] A. D. Patel, M. Sharma, R. Ganesh, N. Ramasubramanian, and P. K. Chattopadhyay, Physics of Plasmas **25**, 112114 (2018).

[143] D. Lee, Y. Ting, L. Oksuz, and N. Hershkowitz, Plasma Sources Science and Technology **15**, 873 (2006).

[144] L. Oksuz and N. Hershkowitz, Plasma Sources Science and Technology **13**, 263 (2004).

[145] K. S. Chung, Plasma Sources Science and Technology **21**, (2012).

[146] K. N. Leung, N. Hershkowitz, and K. R. Mackenzie, The Physics of Fluids **1045**, 1045 (1976).

[147] M. Martínez-Sánchez and E. Ahedo, Physics of Plasmas **18**, 033509 (2011).

[148] R. A. Bosch and R. L. Merlino, Journal of Applied Physics **60**, 3056 (1986).

[149] R. A. Bosch and R. M. Gilgenbach, Physics Letters A **128**, 437 (1988).

[150] S. K. Singh, P. K. Srivastava, L. M. Awasthi, S. K. Mattoo, A. K. Sanyasi, R. Singh, and P. K. Kaw, Review of Scientific Instruments **85**, 033507 (2014).

[151] K. W. Ehlers and K. N. Leung, Citation: Review of Scientific Instruments **52**, (1981).

[152] K. N. Leung and R. E. Kribel, Physics Letters A **66**, 112 (1978).

[153] A. J. T. Holmes, Citation: Review of Scientific Instruments **53**, (1982).

[154] R. A. Bosch and R. L. Merlino, Review of Scientific Instruments **57**, 2940 (1986).

[155] H. Kozima, S. Kawamoto, and K. Yamagiwa, Physics Letters A **86**, 373 (1981).

[156] K. N. Leung, R. E. Kribel, A. P. H. Goede, and T. S. Green, Physics Letters A **66**, 112 (1978).

[157] R. Limpaecher, K. R. MacKenzie, Rudolf Limpaecher and K. R. MacKenzie, R. Limpaecher, and K. R. MacKenzie, Review of Scientific Instruments **44**, 726 (1973).

[158] A. Lang and N. Hershkowitz, Journal of Applied Physics **49**, 4707 (1978).

[159] K. N. Leung, T. K. Samec, and A. Lamm, PHYSICS LETTERS **51 A**, 490 (1975).

[160] R. A. Bosch and R. L. Merlino, Physics of Fluids **29**, 1998 (1986).

[161] H. Lin, R. D. Bengtson, and C. P. Ritz, Physics of Fluids B: Plasma Physics **1**, 2027 (1989).

[162] I. Alexeff, W. D. Jones, and K. Lonngren, Physical Review Letters **21**, 878 (1968).

[163] N. Hershkowitz and Y.-C. Ghim (Kim), Plasma Sources Science and Technology **18**, 014018 (2009).

[164] A. Hirose, I. Alexeff, W. D. Jones, N. A. Krall, and D. Montgomery, Physics Letters A **29**, 31 (1969).

[165] A. Y. Wong, R. W. Motley, and N. D'Angelo, Physical Review **133**, A436 (1964).

[166] H. J. Doucet, W. D. Jones, and I. Aiexeff, Physics of Fluids **17**, 1738 (1974).

[167] I. Alexeff, Physics of Fluids **11**, 167 (1968).

[168] A. Hirose, Physics of Fluids **13**, 1290 (1970).

[169] B. J. Ding, E. H. Kong, M. H. Li, L. Zhang, W. Wei, M. Wang, H. D. Xu, Y. C. Li, B. L. Ling, Q. Zang, G. S. Xu, X. F. Han, H. L. Zhao, L. Zhang, L. M. Zhao, H. C. Hu, Y. Yang, L. Liu, A. Ekedahl, M. Goniche, R. Cesario, Y. Peysson, J. Decker, V. Basiuk, P. Huynh, J. Artaud, F. Imbeaux, J. F. Shan, F. K. Liu, Y. P. Zhao, X. Z. Gong, L. Q. Hu, X. Gao, H. Y. Guo, B. N. Wan, and J. G. Li, Nuclear Fusion **53**, 113027 (2013).

[170] A. R. Field, P. G. Carolan, R. J. Akers, E. R. Arends, K. Axon, R. J. Buttery, N. J. Conway, G. F. Counsell, G. Cunningham, S. J. Fielding, M. Gryaznevich, A. Kirk, I. P. Lehane, B. Lloyd, M. A. McGrath, H. Meyer, C. Ribeiro, A. Sykes, A. Tabasso, M. R. Tournianski, M. Valovic, M. J. Walsh, H. R. Wilson, T. MAST, and N. Teams, Plasma Physics and Controlled Fusion **44**, 307 (2002).

[171] J. Vranjes and S. Poedts, Physics of Plasmas **17**, 022104 (2010).

[172] V. E. Zakharov, **39**, 1973 (1975).

[173] W. D. Jones, A. Lee, S. M. Gleman, and H. J. Doucet, Physical Review Letters **35**, 1349 (1975).

[174] I. Alexeff, Physics of Fluids **11**, 167 (1968).

[175] A. Hirose, K. E. Lonngren, H. M. Skarsgard, and S. H. M. Hirose, A, Lonngren K. E., Physical Review Letters **28**, 270 (1972).

[176] M. Podestà, A. Fasoli, B. Labit, M. McGrath, S. H. Müller, and F. M. Poli, Plasma Physics and Controlled Fusion **47**, 1989 (2005).

[177] R. A. Bosch and R. L. Merlino, Physics of Fluids **29**, 1998 (1986).

[178] W. L. Stirling, P. M. Ryan, C. C. Tsai, and K. N. Leung, Review of Scientific Instruments **50**, 102 (1979).

Thesis Highligh

Name of the Student: Meenakshee Sharma

Name of the CI/OCC: **Enrolment No.: PHYS06201304002**

Thesis Title: Perturbation Studies In A Plasma Confined By Multi-Pole Line-Cusp Magnetic Field

Discipline: eg. Physical Sciences **Sub-Area of Discipline: Experimental Plasma Physics**

Date of viva voce: March 12th 2021

The highlight of thesis is as follows:

- Perturbation studies need field free and quiescent plasma because the presence of magnetic fields triggers Drift waves, many other instabilities, and fluctuations.
- Plasma confined in Multi-pole line-cusp magnetic field has field free region. This region is characterized in this thesis and found to be quiescent as well.
- In a quest for more quiescent plasma, experiments were done with two different configurations of the Multi-pole line-cusp field using the electromagnets of the device.
- The Twelve Pole Six Magnet (TPSM) configuration is identified to confine the larger volume of quiescent and uniform for perturbation study in Multi-pole line-cusp Plasma Device (MPD).
- The Ion Acoustic (IA) wave is successfully exited in MPD; its basic characteristics and dispersion relation is established and validated experimentally.
- The effect of neutrals on IA wave is observed to enhance the propagation length of IA wave as with increasing neutral density; the neutrals also carry the momentum of IA wave and help in the increase in propagation length.
- The experimental result of effect of cusp magnetic field on the IA wave propagation is presented. The role of oblige cusp magnetic field and two electron temperature on wave damping with increasing magnetic field strength is discussed.

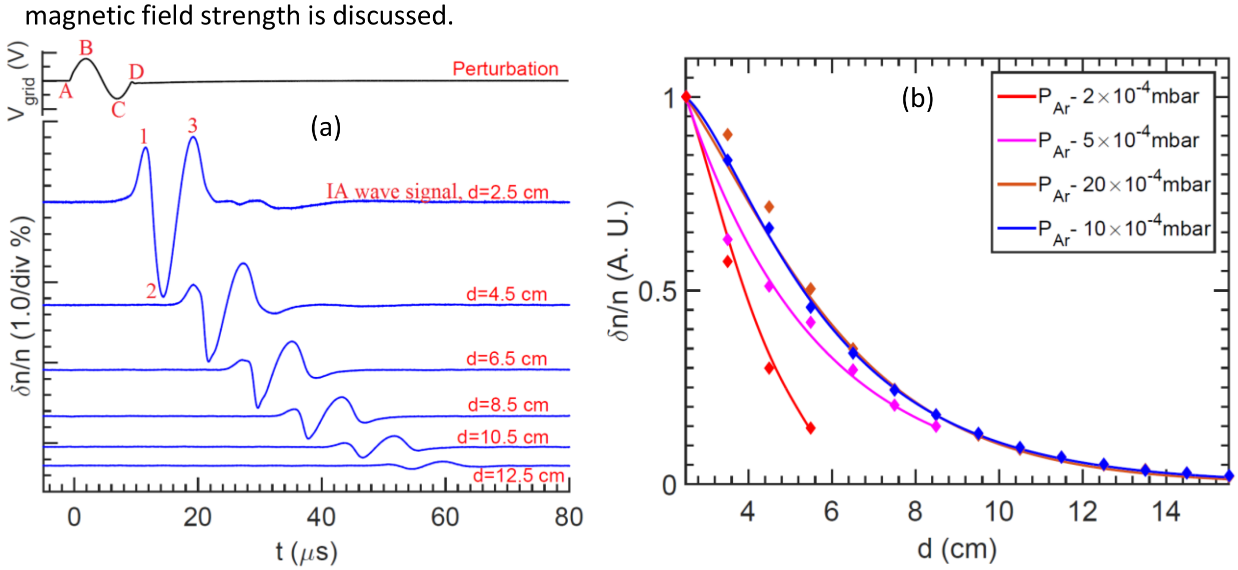

Figure 1: (a) Shows a temporal evolution of density perturbation ($\delta n/n$) at different axial locations as the receiver probe moves away from the exciter grid along the z-axis for -50 V discharge voltage, 20×10^{-4} mbar neutral pressure, and 100 kHz perturbation frequency, here d is the distance between exciter grid and receiver probe, (b) The spatial variation of $\delta n/n$ or wave amplitude for various neutral pressures. The diamond-shaped markers are experimental data, and the solid lines are exponential fits to the experimental data.